Setting the Scale: Photometric and Dynamical Properties of High-Redshift Early-Type Galaxies

Setting the Scale: Photometric and Dynamical Properties of High-Redshift Early-Type Galaxies

Proefschrift

ter verkrijging van
de graad van Doctor aan de Universiteit Leiden,
op gezag van de Rector Magnificus Dr. D. D. Breimer,
hoogleraar in de faculteit der Wiskunde en
Natuurwetenschappen en die der Geneeskunde,
volgens besluit van het College voor Promoties
te verdedigen op donderdag 29 september 2005
te klokke 16.15 uur

door

Arjen van der Wel
geboren te Benthuizen, Nederland
in 1978

Promotiecommissie

Promotores:	Prof. dr. M. Franx Prof. dr. P. G. van Dokkum (Yale University)
Referent:	Dr. S. Trager (Rijksuniversiteit Groningen)
Overige leden:	Prof. dr. K. H. Kuijken Prof. dr. G. K. Miley Prof. dr. P. T. de Zeeuw

Voor mijn opa en oma's

Photographic material for cover by:
Alex te Pas and Mevr. H. te Pas-Snijders
Inti Pelupessy
NASA, *ESA*, S. Beckwith (STScI) and the *HUDF* Team

Printed by: Optima Grafische Communicatie, Rotterdam

Contents

Chapter 1

Introduction

1.1 Early-Type Galaxies

Galaxies are referred to as the building blocks of the universe. They are broadly divided into two different types. Late-type galaxies, a class to which also the Milky Way belongs. are visually dominated by an exponential disk of stars and gas with spiral arms. Spiral arms appear in different degrees of prominence. The bulge at the center, a roundish and smooth distribution of stars that are on average older than the stars in the disk, is a minor component compared to the disk. Early-type galaxies are dominated by a smooth and ellipsoidal distribution of stars with little gas and dust. In complete absence of a disk, such galaxies are called ellipticals. If a faint disk is present, they are qualified as lenticulars. Late-type galaxies greatly outnumber early-type galaxies, but the latter are on average brighter and more massive than the former: $50\% - 75\%$ of all the stars are thought to reside in early-type galaxies (e.g., Bell et al., 2003). Other sub-classes are irregular and peculiar galaxies. The former are generally small galaxies; the latter are mostly mergers. These contribute less to the stellar mass in the universe.

Between the 1920s and the 1940s, astronomers realized that the Milky Way consists of different stellar components, distinguished, for example, by their metal-content and spatial distribution. These results and their interpretation culminated in a paper by Eggen, Lynden-Bell & Sandage (1962). They suggest that one component (the metal-poor stars that are found in the bulge and the halo) has formed long ago (~ 10 billion years) in a quickly radially collapsing gas cloud. The second component (the metal-rich stars that are found in the disk) would be formed later, and on longer time scales, by accretion of gas onto a disk. This idea is still alive, Eggen's paper being cited on average more than four times per week over the past decade.

Early-type galaxies, which do not contain prominent populations of young stars, consist only of metal-poor stars. In Eggen's picture of 'monolithic collapse', these galaxies formed very early, and have not rejuvenated their stellar populations ever since: for some reason the accretion of gas at later stages did not occur. Hence the nomenclature invented by Hubble (1930), who thought that early-type galaxies are older than late-type galaxies.

Between the 1960s and 1980s it was discovered that there are strong relations with small scatter between a broad range of photometric and spectroscopic parameters of early-type galaxies. This started with Minkowski (1962) who found a relation between velocity dispersion and luminosity. This work was extended by Faber & Jackson (1976), which turned out to be the basis of the discovery of the fundamental plane (FP, Djorgovski & Davis, 1987; Dressler et al., 1987) wherein the three parameters of size, surface brightness and central velocity dispersion are narrowly correlated.

The relation between the strength of the Mg_2-line and velocity dispersion (Burstein et al., 1987) and the color-magnitude-relation (Sandage & Visvanathan, 1978; Bower, Lucy & Ellis, 1992) suggest that the physical parameters of early-type galaxies, such as their mass, are related to their stellar populations.

One would think that taking together the ideas of Eggen et al. and scaling relations like the FP can provide a relatively simple and physical theory for the formation of galaxies. However, nothing is ever as easy as it seems.

1.2 Galaxy Formation in a Cosmological Framework

The description of galaxy formation becomes far more complicated if one realizes that a galaxy is not an isolated island universe. Galaxies are parts of groups, clusters, and super-clusters, and their properties correlate with the environment they live in. Late-type galaxies prefer regions where the galaxy density is low, whereas early-type galaxies prefer denser areas, i.e., the centers of clusters (see also Dressler, 1980). The existence of peculiar galaxies, and the lack of spiral galaxies in dense environments, led to the idea that spirals merge into ellipticals (Toomre & Toomre, 1972). In terms of assembly time, early-type galaxies are younger than late-type galaxies, not older as their stellar populations suggest.

The answer to the question how galaxies were formed and how the environment affects this process is thus clearly linked to the question how large-scale structure, i.e., clusters and super-clusters, was formed. The cosmological models that are used to describe the emergence of large-scale structure (pioneered by Press & Schechter, 1974) are used as a framework to describe the formation of stars and galaxies out of collapsing gas clouds (first implemented by White & Rees, 1978). Smaller building blocks are formed first, which subsequently merge into progressively larger galaxies and clusters. Merging is therefore a self-evident feature of these models.

The main reason for the popularity of this model for galaxy formation is that it successfully explains large-scale structure in the universe. The prediction of the levels and scales of clustering only depends on the cosmological model and gravity. Given the predictive power of a wide range of observational properties of large-scale structure, and the small number of parameters, this model is believable.

However, as soon as it is used as a framework within which properties of the galaxy population are calculated, the predictions become much more uncertain, since there is no physically motivated prescription for star formation, the role of feedback from active galactic nuclei (AGNs) and supernovae, and the role of magnetic fields and turbulence. The problem at hand is very complex, and the models have many degrees of freedom. Phenomenological models are necessary to understand the formation of galaxies and the role of the environment in which they reside.

Using the currently available telescopes and instruments it is possible to constrain the evolution of galaxies. Studying relatively nearby galaxies alone is not sufficient, because this only provides a snapshot of the universe at its current age of ~ 13.7 billion years. In order to construct a picture that describes the temporal evolution of the galaxy population throughout the history of the universe, galaxies over a wide range of cosmological distances, i.e., redshifts, should be studied, making use of billions of years of look-back time. The direct measurement of the evolution of the galaxy population provides strong constraints on the formation models.

1.3 Masses of High-Redshift Galaxies

The question to be answered in order to obtain an observationally driven picture of the formation and evolution of galaxies may be summarized as follows:

How do the numbers of different types of galaxies and their stellar populations change with redshift?

The trick is to interpret the light of distant galaxies and infer their physical properties. Only then can local galaxies be quantitatively compared with distant galaxies. The most basic properties of a galaxy are its mass, size, luminosity, and morphology. The latter three are relatively easy to infer from imaging; mass requires a little more work.

In principle, if one knows of each of the ~ 100 billion stars in a galaxy where it is and how fast it moves in what direction, one can precisely infer the gravitational potential, and thus the mass of the galaxy. In practice, one can study with integral field spectroscopy how the dynamical structure varies over the projected surface of the galaxy and then infer a model of the potential (e.g., de Zeeuw et al., 2002).

Such methods, requiring high signal-to-noise observations at high spatial resolution, can generally only be used for relatively nearby galaxies. For distant galaxies, which are mostly too small and faint, this cannot be done, and one can only infer the overall velocity dispersion, σ. It can be obtained by measuring the width of absorption lines originating in the atmospheres of stars. The second basic parameter that carries information about the mass of a galaxy is its size. The virial theorem implies that the mass of a galaxy, M, is proportional to $r\sigma^2$.

By comparing the masses, color, and luminosities of local and distant galaxies, an evolutionary picture can be constructed. Specifically for early-type galaxies, a quantitative measurement of their luminosity evolution and the ages of their stellar populations can be done. This tool is provided by the FP. Jørgensen, Franx & Kjærgaard (1996) found that for cluster early-type galaxies the FP is described by

$$r_{\rm eff,B} \propto \sigma_c^{1.2} I_{\rm eff,B}^{0.83},$$

where $r_{\rm eff,B}$ is the effective radius measured in the B-band, σ_c is the central velocity dispersion, and $I_{\rm eff,B}$ is the B-band surface brightness at the effective radius. The FP is very narrow, i.e., the scatter is very small (less than 10% in $r_{\rm eff,B}$).

Since the luminosity, L, of a galaxy is proportional to Ir^2, re-ordering the above expression reveals that the FP is, in fact, a relation between luminosity and mass for

early-type galaxies:

$$M/L_B \propto M^{0.28}.$$

The mass-to-light ratio, M/L, is the holy grail for observing high-redshift galaxies, because it tells you how to convert the detected light into mass.

The FP can be used as a powerful tool to directly measure the evolution of M/L with redshift. Because early-type galaxies consist of very old stellar populations, it is reasonable to assume that their stellar populations have been evolving passively over many billions of years. This implies fading of galaxies with time. By measuring the three FP quantities of high-redshift galaxies, the offset from the local FP is inferred which is purely due to luminosity evolution: the mass of the galaxy does not change. Hence, the evolution of M/L with redshift is directly measured with good accuracy because of the small scatter in the FP. Since the rate of M/L-evolution is linked to the age of a stellar population, the formation epoch can be constrained.

This method was proposed by Franx (1993) and has been applied successfully over the past decade. The spectroscopic observations needed to measure σ are very hard to obtain: they demand the use of the largest telescopes in the world, and then still many hours of integration are needed to obtain spectra with the necessary signal-to-noise ratios.

The maximum redshift for galaxies in clusters with dynamically measured masses has been increasing steadily from $z = 0.6$ (van Dokkum & Franx, 1996) to $z = 1.27$ (van Dokkum & Stanford, 2003). These results have shown that massive cluster early-type galaxies have become fainter by about 1 magnitude in the B-band between $z = 1$ and the present, which implies that their stars must have formed at redshifts well beyond $z = 2$. This is consistent with the old stellar populations of large local early-types.

One caveat, however, is that the early-type galaxy population at $z \sim 1$ might be only a sub-component of the local early-type galaxy population, due to morphological evolution and/or the formation of new galaxies. This causes us to overestimate the formation redshift of the local early-type galaxy population. This concept called 'progenitor bias', inspired by the observation that even today spiral galaxies merge into elliptical galaxies, was modeled by van Dokkum & Franx (2001). They show that, even taking a maximum bias into account, the formation redshift of early-type cluster galaxies is still $z \sim 2$.

One important prediction made by galaxy formation models is that early-type galaxies in low-density environments (referred to as field galaxies) have younger stellar populations than early-type galaxies in high-density environments (e.g., Diaferio et al., 2001). Several groups have measured the M/L-evolution of field early-type galaxies, which, if the model prediction is correct, should be faster than the M/L-evolution of cluster galaxies.

The question whether field galaxies are younger, however, remains unanswered, because the results so far are contradictory: Kochanek et al. (2000), Treu et al. (2001) and van Dokkum & Franx (2001) find that field galaxies evolve as slowly as cluster galaxies; van de Ven, van Dokkum & Franx (2003), Rusin et al. (2003), and van Dokkum & Ellis (2003) find a mix between fast and slow evolution within their samples; Treu et al. (2002) and Gebhardt et al. (2003) report faster evolution for field galaxies than for cluster galaxies.

The question remained unanswered so far because the required observations are so hard to obtain. The first of the two main questions addressed in this thesis is: **Are field early-type galaxies younger than cluster early-type galaxies?** The mystery of the field galaxies is the topic of Chapters 2 through 5, where we describe the acquisition of uniquely deep spectra, solving the controversy.

The second main question relates to the first through the M/L. Measuring σ can only be done up to $z = 1.3$ with the current instruments, and for a limited number of objects. To construct a picture of the high-redshift galaxy population as a whole, and to determine galaxy masses at redshifts higher than $z = 1.3$, alternative mass estimators have to be used.

Evolutionary models for stellar populations, predicting their luminosities, colors, and M/L (e.g., Vazdekis et al., 1996; Bruzual & Charlot, 2003) are used to convert galaxy colors into M/L. However, the relation between color and M/L depends on many parameters, such as the shape of the stellar mass-function, metal- and dust-content, and star-formation history.

Furthermore, models differ in their predictions, even for the same set of parameters. Hence, the conversion of color into M/L suffers from systematic uncertainties, and needs to be calibrated by dynamical measurements at high redshift, which are provided in Chapter 4.

The advance of the *Spitzer Space Telescope* (SST) allows to easily measure near-infrared luminosities of distant galaxies. The infrared is less attenuated by dust than the UV and optical. Furtermore, it is generally assumed that the infrared luminosity of a galaxy is more representative of its stellar mass than its UV or optical luminosity. Therefore, SST imaging of high-redshift galaxies is anticipated to play an important role in estimating their stellar masses. The robustness of mass estimates based on near-infrared properties of galaxies are addressed in Chapters 6 and 7.

Thus, the second main question addressed in this thesis is: **How accurately can stellar masses of high-redshift galaxies be inferred from their colors?**

1.4 This Thesis

Chapter 2

In this Chapter we describe the measurement of M/L of 4 early-type galaxies in the RDCS 1252.9-2927 cluster at $z = 1.24$. We use deep *Hubble Space Telescope* (HST) imaging to measure $r_{\rm eff}$, and $I_{\rm eff}$ and spectra from the *Very Large Telescope* (VLT) to determine σ. The spectra have integration times of 24 hours, which yields unprecedentedly deep spectra. In Figure 1.1 I show a beautiful example.

All four galaxies are massive: $M > 10^{11} M_{\odot}$. We combine this sample with 3 galaxies in the RDCS 0848+4453 cluster at $z = 1.27$ with measured M/L (van Dokkum & Stanford, 2003) The offset of the local FP shows that the luminosity evolution in the rest-frame B-band is ~ 1 mag for galaxies with $M > 3 \times 10^{11} M_{\odot}$. This implies a characteristic age of ~ 3 Gyr for their stellar populations, and a formation redshift of $z \sim 3.4$. The two galaxies with lower masses, also have lower M/L and bluer colors, implying more recent star formation.

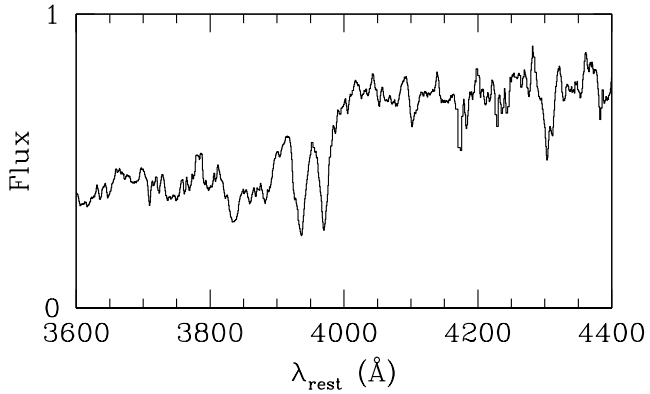

Figure 1.1: Example of a VLT spectrum of a cluster early-type galaxy at $z = 1.24$. The integration time is ~ 24 hours, resulting in an unprecedented data quality, revealing many absorption features characteristic of an evolved stellar population.

Chapters 3 and 4

In these chapters we describe and analyze the FP of high-redshift field galaxies. Chapter 3 contains pilot-results, based on a sub-sample of 6 galaxies that were observed earliest, in 2002. In Chapter 4 we describe the entire sample of 27 field early-type galaxies, observed in 2002 and 2003. Here we address the question whether or not field galaxies are younger than cluster galaxies.

We have obtained very deep spectra from the VLT (with integration times of typically ~ 12 hours) for 27 field early-types that were selected by color and morphology. HST imaging is used to measure effective radii and surface brightnesses. This sample removes the difference in data quality between the older field and cluster samples.

The offset of this field sample from the local FP implies fading in the B-band by almost 2 magnitudes between $z = 1$ and the present. This is much more than for cluster galaxies (see Chapter 2). There is a large spread in M/L. This spread is proved to be real and due to differences among the stellar populations of the galaxies by a strong correlation between M/L and color.

Furthermore, the amount of evolution in M/L correlates with galaxy mass. If we only consider galaxies more massive than $M > 2 \times 10^{11} M_{\odot}$, we find slow evolution (1.3 magnitudes), which is similar to what is found for cluster galaxies in the same mass range (1.2 magnitudes). Answering the first question posed in this thesis, **we conclude that massive field and cluster galaxies do not have very different ages.** The similarity of massive field and cluster galaxies is at odds with the model predictions.

We demonstrate that the observed mass-dependent evolution of M/L_B is partially caused by selection effects: low-mass galaxies with high M/L are too faint to measure σ for, and are not included in the sample. Still, if we take this into account, we provide evidence for an intrinsic difference between low- and high-mass galaxies. Low-mass galaxies seem to be younger, on average, than high-mass galaxies. Individual properties of galaxies seem to determine the ages of their stellar populations,

more so than large-scale environment.

We demonstrate that the controversy in the literature so far is largely caused by the differences between the methods used to calculate the evolution, but are also due to the small samples, low redshifts, and poor data quality.

Finally, five of the early-type galaxies in our sample have AGN. There is tentative evidence that the stellar populations in these galaxies are younger than those of galaxies without AGN.

Chapter 5

In this chapter we measure the evolution of the color-magnitude relation (CMR) of field galaxies. Together with the relation between M/L and color, discovered in Chapter 4, this puts a constraint the intrinsic mass-dependence of the evolution of M/L, also discovered in Chapter 4.

We compile from the literature 270 redshifts of galaxies in the range $0.55 < z < 1.15$. Quantitative morphological classifications are derived from HST imaging. This allows us to compare the zero-point, slope, and scatter of the high-z CMR with the local CMR. We find no significant evolution of the slope and the scatter, whereas the zero-point in $B-I$ becomes bluer by 0.44 magnitudes from $z=0$ to $z=1$. These results are very similar to the results of cluster galaxies.

Because of the empirical relation between dynamically determined M/L and color of early-type galaxies at $z \sim 1$, the absent or slow evolution of the slope of the CMR suggests that the tilt of the FP also evolves at most slowly. The observed steep relation between M and M/L at $z \sim 1$, found by FP studies, is therefore most likely mainly caused by selection effects, and not intrinsic.

Furthermore, due to this bias, the true evolution of M/L_B may be $30-40\%$ slower than observed. The scatter in the relation between color and M/L is the main source of uncertainty in this analysis. Dynamical mass measurements of low-luminosity early-type galaxies are required to quantitatively measure the tilt of the FP at $z=1$.

Chapter 6

In this chapter we measure the evolution of the rest-frame K-band FP from $z=1$ to the present. SST imaging is used to measure M/L_K for our sample of $z \sim 1$ early-type galaxies.

We find that M/L_K evolves by 1.3 magnitudes between $z=1$ and the present, and a similar dependence on galaxy mass as M/L_B. This is somewhat slower than the evolution in the B-band of the same sample (1.6 magnitudes), agreeing qualitatively with stellar population models. Various models, however, differ significantly in their prediction of the evolution of M/L_K compared to M/L_B. Contrary to the Maraston (2004) stellar population model, the Bruzual & Charlot (2003) model does not fit well to our results unless the IMF is assumed to be top-heavy.

These results show that the interpretation of rest-frame near-IR photometry is severely hampered by model uncertainties and therefore that the determination of galaxy masses from rest-frame near-IR photometry may be harder than was previously thought.

Chapter 7

We compare dynamical masses of samples of distant ($z \sim 1$) and local early-type galaxies with stellar masses inferred from their broadband spectral energy distributions (SEDs), ranging from the rest-frame UV to the rest-frame near-infrared.

We find that the relation between dynamical mass and inferred stellar mass has significant scatter and a zero-point which is highly model-dependent. Furthermore, if including the rest-frame infrared in the fits, the zero-point of the relation is generally different for galaxies at different redshifts.

In particular, "standard" Bruzual & Charlot (2003) models imply larger stellar masses for the distant galaxies relative to the stellar masses of the local galaxies. The discrepancy is as large as a factor of $\sim 2-3$ for models with Solar metallicity and a Salpeter IMF. If using the Maraston (2004) stellar population model with the same parameters, we find no such discrepancy.

If the rest-frame near-infrared is excluded from the fits, the systematic difference between the zero-points of high- and low-redshift galaxy masses is close to zero for all models. This implies that the bias and systematic uncertainties originate in the near-infrared. We also show that including the rest-frame UV and allowing the star-formation history and dust content to vary as free parameters do not change the photometric mass estimates significantly.

Our results have far-reaching implications: determinations of the evolution of the stellar mass-density based on the Bruzual-Charlot model and rest-frame near-infrared photometry will underestimate the real evolution, and the systematic uncertainty is of the same order (a factor of $\gtrsim 2$) as the evolution of the mass-density from $z = 1$ to the present.

Answering the second main question posed in this thesis, **we conclude that mass estimates based on near-infrared are systematically uncertain at the level of a factor of 3; optical colors provide a more accurate estimate.**

References

Bell, E. F., McIntosh, D. H., Katz, N., & Weinberg, M. D. 2003, *ApJS* **149**, 289

Bower, R. G., Lucey, J. R., & Ellis, R. S. 1992, *MNRAS* **254**, 601

Bruzual, G. & Charlot, S. 2003, *MNRAS* **344**, 1000

Burstein, D., Davies, R. L., Dressler, A., Faber, S. M., Stone, R. P. S., Lynden-Bell, D., Terlevich, R. J., & Wegner, G. 1987, *ApJS* **64**, 601

de Zeeuw, P. T. et al. 2002, *MNRAS* **329**, 513

Diaferio, A., Kauffmann, G., Balogh, M. L., White, S. D. M., Schade, D., & Ellingson, E. 2001, *MNRAS* **323**, 999

Djorgovski, S. & Davis, M. 1987, *ApJ* **313**, 59

Dressler, A. 1980, *ApJ* **236**, 351

Dressler, A., Lynden-Bell, D., Burstein, D., Davies, R. L., Faber, S. M., Terlevich, R., & Wegner, G. 1987, *ApJ* **313**, 42

Eggen, O. J., Lynden-Bell, D., & Sandage, A. R. 1962, *ApJ* **136**, 748

Faber, S. M. & Jackson, R. E. 1976, *ApJ* **204**, 668

Franx, M. 1993, *PASP* **105**, 1058
Gebhardt, K. et al. 2003, *ApJ* **597**, 239
Hubble, E. P. 1930, *ApJ* **71**, 231
Jørgensen, I., Franx, M., & Kjærgaard, P. 1996, *MNRAS* **280**, 167
Kochanek, C. S. et al. 2000, *ApJ* **543**, 131
Maraston, C. 2004, *MNRAS* submitted, astro-ph/0410207
Minkowski, R. 1962, in *IAU Symp. 15: Problems of Extra-Galactic Research*, p.112
Perlmutter, S. et al. 1999, *ApJ* **517**, 565
Press, W. H. & Schechter, P. 1974, *ApJ* **187**, 425
Riess, A. G. et al. 1998, *AJ* **116**, 1009
Rosati, P. et al. 2004, *AJ* **127**, 230
Rusin, D. et al. 2003, *ApJ* **587**, 143
Sandage, A. & Visvanathan, N. 1978, *ApJ* **223**, 707
Spergel, D. N. et al. 2003, *ApJS* **148**, 175
Toomre, A. & Toomre, J. 1972, *ApJ* **178**, 623
Treu, T., Stiavelli, M., Bertin, G., Casertano, S., & Møller, P. 2001, *MNRAS* **326**, 237
Treu, T., Stiavelli, M., Casertano, S., Møller, P., & Bertin, G. 2002, *ApJ* **564**, L13
van de Ven, G., van Dokkum, P. G., & Franx, M. 2003, *MNRAS* **344**, 924
van Dokkum, P. G. & Ellis, R. S. 2003, *ApJ* **592**, L53
van Dokkum, P. G. & Franx, M. 1996, *MNRAS* **281**, 985
van Dokkum, P. G. & Franx, M. 2001, *ApJ* **553**, 90
van Dokkum, P. G. & Stanford, S. A. 2003, *ApJ* **585**, 78
Vazdekis, A., Casuso, E., Peletier, R. F., & Beckman, J. E. 1996, *ApJS* **106**, 307
White, S. D. M. & Rees, M. J. 1978, *MNRAS* **183**, 341
Zwicky, F. 1937, *ApJ* **86**, 217

Chapter 2

The Fundamental Plane of Cluster Ellipticals at $z = 1.25$

Abstract

Using deep *Hubble Space Telescope* Advanced Camera for Survey imaging and Very Large Telescope FOcal Reducer/low dispersion Spectrograph 2 spectra, we determined the velocity dispersions, effective radii, and surface brightnesses for four early-type galaxies in the $z = 1.237$ cluster RDCS 1252.9-2927. All four galaxies are massive, greater than $10^{11} M_{\odot}$. These four galaxies, combined with three from RDCS 0848+4453 at $z = 1.276$, establish the fundamental plane of massive early-type cluster galaxies at $\bar{z} = 1.25$. The offset of the fundamental plane shows that the luminosity evolution in rest-frame B is $\Delta \ln M/L_B = (-0.98 \pm 0.06)z$ for galaxies with $M > 10^{11.5} M_{\odot}$. To reproduce the observed mass-to-light ratio (M/L) evolution, we determine the characteristic age of the stars in these $M > 10^{11.5} M_{\odot}$ galaxies to be $3.0^{+0.3}_{-0.3}$ Gyr; i.e., $z_* = 3.4^{+0.5}_{-0.4}$. Including selection effects caused by morphological bias (the "progenitor bias"), we estimate an age of $2.1^{+0.2}_{-0.2}$ Gyr, or $z_* = 2.3^{+0.2}_{-0.2}$ for the elliptical galaxy population. Massive cluster early-type galaxies appear to have a large fraction of stars that formed early in the history of the universe. However, there is a large scatter in the derived M/L values, which is confirmed by the spread in the galaxies' colors. Two lower mass galaxies in our $\bar{z} = 1.25$ sample have much lower M/L values, implying significant star formation close to the epoch of observation. Thus, even in the centers of massive clusters, there appears to have been significant star formation in some massive, $M \simeq 10^{11} M_{\odot}$, galaxies at $z \simeq 1.5$.

Holden, B.P., van der Wel, A., Franx, M., Illingworth, G.D., Blakeslee, J.P., van Dokkum, P.G., Ford, H., Magee, D., Postman, M., Rix, H.-W. & Rosati, P.
The Astrphysical Journal Letters, **620**, 83 (2005)

2.1 Introduction

The fundamental plane (FP) allows one to directly measure the mass and the mass-to-light ratio, M/L, of early-type galaxies. The FP combines three variables: the effective radius ($r_{\rm e}$), the average surface brightness within the effective radius ($I_{\rm e}$), and the velocity dispersion (σ). These data are combined into the relation $\sigma^{1.20} \propto r_{\rm e} I_{\rm e}^{0.83}$ for the rest-frame B band (Jørgensen, Franx & Kjærgaard, 1996). With such quantities, we can measure $M/L \propto \sigma^2/(r_{\rm e} I_{\rm e})$ and how it depends on mass, proportional to $r_{\rm e}\sigma^2$. Massive galaxies out to $z \simeq 1$ appear to evolve as $\Delta \ln M/L_B \simeq z$ for both clusters (Kelson et al., 2000b; van Dokkum & Franx, 2001; Wuyts et al., 2004) and in some field samples, although there is a larger scatter for the latter (van Dokkum et al., 2001; Gebhardt et al., 2003; van Dokkum & Ellis, 2003; van de Ven, van Dokkum & Franx, 2003; van der Wel et al., 2004). This slow rate of evolution implies an early epoch of formation, $z_f \simeq 3$, for the stars in early-type galaxies assuming passively evolving simple stellar populations. However, at $z \simeq 1.25$, only $\sim 50\%$ of stellar mass we observe today has been formed (e.g., Madau, Pozzetti & Dickinson, 1998; Steidel et al., 1999; Rudnick et al., 2003). This implies that the majority of stars in cluster early-type galaxies formed long before the average star in the universe. Observations determining the luminosity-weighted age of galaxies close to $z = 1.25$ will test this, and there are only three galaxies with FP measurements to date at these redshifts (van Dokkum & Stanford, 2003).

We observed four luminous early-type galaxies in the $z = 1.237$ rich, massive, and X-ray luminous cluster of galaxies RDCS 1252.9-2927 (Rosati et al., 2004) using a combination of the Very Large Telescope (VLT) Focal Reducer/low dispersion Spectrograph 2 (FORS2) and the Advanced Camera for Surveys (ACS) on the *Hubble Space Telescope* (HST). RDCS 1252.9-2927 is the most massive cluster found to date at $z > 1$, thus it contains a number of luminous and, likely, massive galaxies. We use the FP to constrain the M/L evolution and set the mass scale for four galaxies in RDCS 1252.9-2927. These results, combined with van Dokkum & Stanford (2003), measure the ages of the stellar populations in early-type galaxies at $\bar{z} = 1.25$. We assume a $\Omega_m = 0.3$, $\Omega_\Lambda = 0.7$ and $\rm H_o = 70\ km\ s^{-1}\ Mpc^{-1}$. All observed magnitudes are in the AB system. However, for comparison with previous work, we convert observed magnitudes into rest-frame Johnson B using the Vega zeropoint.

2.2 RDCS 1252.9-2927 Fundamental Plane Data

Four galaxies in RDCS 1252.9-2927 were selected from among the nine known cluster members (Demarco et al., 2005; Lidman et al., 2004) with $z_{850} < 22.5$ mag that fit into a single multislit mask. These are the first, second, third and fifth brightest cluster members. An image of each is shown in Figure 2.1 along with the spectra, in descending order of brightness. Below we discuss the measurement of $r_{\rm e}$ and $I_{\rm e}$ from the ACS data, the σ from the FORS2 spectra, and the conversion to the rest-frame Johnson B.

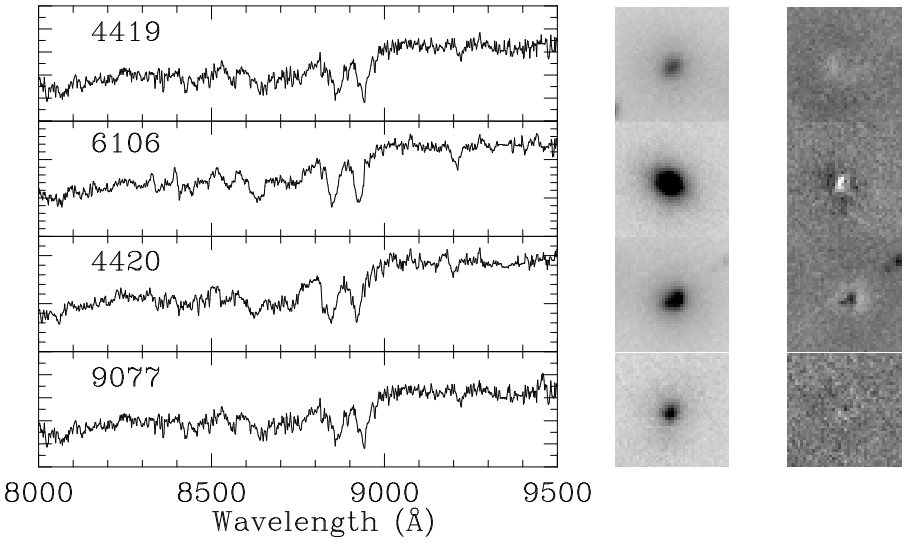

Figure 2.1: Mosaic showing, from left to right, the observed spectra near 4000Å in the rest frame of the cluster, galaxy images and images of the residuals. Each image is 2"0 on a side with 0"05 pixels from the z_{850} ACS data, corresponding to roughly rest-frame Johnson B. The fit results are listed in Table 2.1. The absolute value of flux in the residuals is $\leq$10% of the flux in the original data. For galaxies 4419 and 4420, the residuals have an "S" shape which is interpreted as a sign of interaction (Blakeslee et al., 2003). The residuals for galaxy 6106 show an over subtraction in the center; it is likely that the $r^{1/4}$ law is too steep; in this case, the best fitting profile is proportional to $r^{1/3}$.

Table 2.1: de Vaucouleurs Model Parameters and Velocity Dispersion

Galaxy	$r_{\rm e,z}$ arcsec	$\mu_{\rm e}^a$ mag arcsec^{-2}	S/N^b Å^{-1}	σ km s^{-1}	$(i-J)_{2r_{\rm e}}$ mag	$\log M$ $M_\odot$	$\log M/L_B$ $M_\odot/L_{\odot,B}$
4419	2.806	24.899	24	302 ± 24	2.09	12.40	0.81
6106	0.487	21.573	57	294 ± 10	2.07	11.61	0.22
4420	1.016	23.279	29	323 ± 21	2.11	12.01	0.66
9077	1.008	23.529	24	130 ± 14	1.90	11.22	0.01

[a] All magnitudes are AB

[b] Spectra have a resolution of 3.7Å (FWHM)

2.2.1 HST ACS Imaging

As described in Blakeslee et al. (2003), the ACS imaged RDCS 1252.9-2927 with four overlapping pointings. Each pointing has three orbits in the F775W filter, or i_{775}, and five orbits in the F850LP filter, or z_{850}. A de Vaucouleurs, or $r^{1/4}$ model, was fit to each of the individual z_{850} images using the method of van Dokkum & Franx (1996). Each galaxy in each image had a unique point spread function generated using the `TinyTIM v6.2` package (Krist, 1995). The two galaxies at the middle of the cluster, referred to as 4419 and 4420 in Table 2.1, were fit simultaneously. Table 2.1 contains the average of the best-fitting parameters for each image with the galaxies listed in order of decreasing z_{850} flux. We plot in Figure 2.1 a mean image, corrected for the ACS distortion, of all the z_{850} images for each galaxy along with the average residuals from the fits.

The product $r_{\rm e}I_{\rm e}^{0.83}$ is used to measure the evolution in M/L. Because of the strong anti-correlation between the error for $\mu_{\rm e}$ and the error for r_e (Jørgensen, Franx & Kjærgaard, 1993), the uncertainties on this product for all four galaxies is small at $\simeq$5%.

2.2.2 VLT FORS2 Spectra

The four galaxies in Table 2.1 were observed using FORS2, on the VLT, through slit masks with the 600z grism in conjunction with the OG590 order separation filter. The observations were done in service mode with a series of exposures, dithered over four positions, for a total integration time of 24 hours. The resulting signal-to-noise (S/N) ratios at 4100Å rest-frame are listed in Table 2.1. Details concerning the data reduction are described in van der Wel et al. (2005).

The high spectral resolution, $80\ {\rm km\ s^{-1}}$ per pixel, resulted in accurate internal velocity dispersions for the four cluster members (see Table 2.1). The spectra were fit, by the method of van Dokkum & Franx (1996), with stellar spectra (Valdes et al., 2004) with a wide range in spectral type and metallicity. For more details concerning the usage of the templates and the derivation of velocity dispersions, see van der Wel et al. (2005).

The velocity dispersions were aperture corrected to a $1.7\ {\rm kpc}$ circular aperture at the distance of Coma, as described in Jørgensen et al. (1996). The listed errors include a statistical error derived from the χ^2 value of the fit and a systematic error estimated to be at most 5% for the spectra with the lowest S/N ratio.

2.2.3 Rest-frame Magnitudes

In order to compare with other FP results in the literature, the observed z_{850} magnitudes must be converted into $B_{\rm rest}$, the equivalent of observing the galaxies with a rest-frame Johnson B filter (Bessell, 1990) in the Vega system. The z_{850} filter is centered at 4058Å in the rest-frame of the galaxies in RDCS 1252.9-2927. This filter is close to the central wavelength of Johnson B at 4350Å, but even the modest wavelength difference means that the conversion between z_{850} at $z = 1.237$ and the Johnson B will depend on the color of the galaxy. To compute this conversion, we redshifted the Sbc and E templates from Coleman, Wu & Weedman (1980) to $z = 1.237$

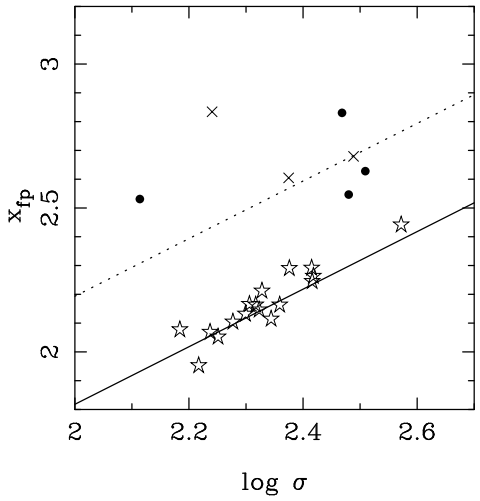

Figure 2.2: Projection of the FP for our sample and Coma. The results for RDCS 1252.9-2927 (z=1.237) are plotted as filled circles, the crosses are from RDCS 0848+4453 (van Dokkum & Stanford, 2003, $z = 1.276$), and the open stars are from Coma (Jørgensen et al., 1996, $z = 0.023$). The y-axis is $x_{\rm fp} = 0.83 \log r_{\rm e} + 0.69 \log I_{\rm e}$, one of the projections of the FP. The solid line is the FP for Coma while the dotted line has the same slope but is shifted $\Delta M/L_B = -0.98$ for the five massive galaxies at $\bar{z} = 1.25$.

and calculated the $B_{\rm rest}$ magnitude as a function the observed z_{850} and $i_{775} - J$ color, yielding $B_{\rm rest} = z_{850} - 0.45(i_{775} - J) + 1.68$. This approach is slightly different than that used in Kelson et al. (2000a) or van Dokkum & Stanford (2003), but yields results that differ in the mean by ≤ 0.02 magnitudes, with an error of only $\leq 5\%$ (see Holden et al., 2004). The J, along with K_s, photometry comes from the VLT ISAAC and New Technology Telescope SOFI observations discussed in Lidman et al. (2004). We will also use this data to examine the rest-frame optical $B - I$ colors below. All colors were measured within an aperture of two effective radii. The ACS imaging was smoothed to match the seeing in the ISAAC data to measure this color.

The statistical errors on the FP are dominated by the error on the velocity dispersions, which are around 10% including an estimate of the systematic error. Because this error dominates the error budget, we will take the error on σ to be the FP error for the rest of the Letter.

2.3 The Fundamental Plane at $\bar{z} = 1.25$

The most straightforward way to measure the evolution in M/L_B is to compute the offsets for the seven galaxies at $\bar{z} = 1.25$ from the FP of the Coma cluster (Jørgensen et al., 1996). In Figure 2.2, we plot our data, along with the FP for Coma, using the rest-frame B. We show the average offset for the five most massive galaxies out of the total of seven in our sample. We will discuss below why we remove those two lower mass galaxies. Measuring the offset from the FP ensures that we measuring $\Delta M/L_B$

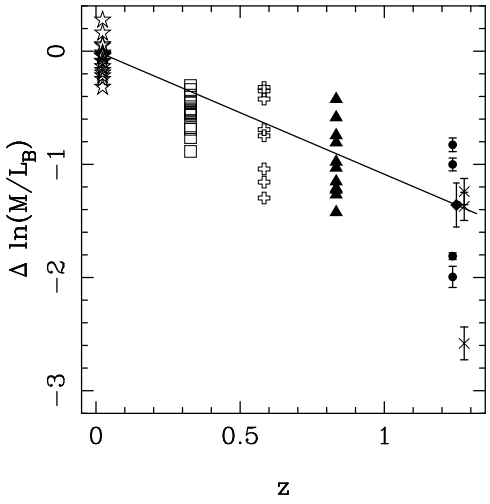

Figure 2.3: Change in M/L_B for early types as a function of redshift. We use the same symbols as Figure 2.2 with the addition of open squares for MS 1358+62 (Kelson et al., 2000b, $z = 0.328$), open plus signs from MS 2053-04 ($z = 0.583$) and the filled triangles are from MS 1054-03 ($z = 0.832$), both from Wuyts et al. (2004). The resulting evolution, with respect to the Coma FP, is shown as a line with the form $\Delta \ln M/L_B \propto (-0.98 \pm 0.06)z$.

for galaxies at the same part of the FP or roughly the same mass. The offset $\Delta M/L$ and rate of M/L_B evolution is readily apparent in Figure 2.3. We find $\overline{\Delta M/L_B} = -1.23 \pm 0.08$ for five $\bar{z} = 1.25$ early-type galaxies, three from RDCS 1252.9-2927 and two from RDCS 0848+4453 with masses $M > 10^{11.5} M_\odot$. This corresponds to an evolution in $\Delta \ln M/L_B \propto (-0.98 \pm 0.06)z$, a small deviation from the $\Delta \ln M/L_B \propto (-1.06 \pm 0.09)z$ of van Dokkum & Stanford (2003) and the $\Delta \ln M/L_B \propto -1.08z$ of Wuyts et al. (2004).

There is a large scatter seen in Figure 2.3 in $\Delta \ln M/L_B$, $\sigma[\ln(M/L_B)] = 0.32$ for the seven $\bar{z} = 1.25$, early-type galaxies. This scatter is twice the size of the scatter in Coma or MS 1358+62, regardless of whether the scatter is computed for all galaxies, or only the seven most luminous galaxies in either MS 1358+62or the Coma Cluster sample. A large part of this scatter comes from the two lower mass galaxies in the sample. The five galaxies with $M > 10^{11.5} M_\odot$ show $\sigma[\ln(M/L_B)] = 0.22$, which is not statistically different from the Coma or MS 1358+62 value. There is an obvious selection effect towards low M/L galaxies in a luminosity-selected sample. This may both increase the scatter and bias the mean change in the M/L ratio; hence, we remove the two low mass galaxies from our sample.

The M/L_B values for the $M > 10^{11.5} M_\odot$ galaxies at $\bar{z} = 1.25$ correlate with the rest-frame $B - I$ colors, as seen in Figure 2.4. Both the colors and the M/L_B track a rapidly declining star-formation rate model from Bruzual & Charlot (2003). As this relatively simple stellar population reproduces most of the observations, the observed scatter in M/L_B is then likely the result of a spread in the luminosity-weighted ages.

At lower redshifts, the M/L is a function of the total mass (Jørgensen et al., 1996). Such a trend is observed at $\bar{z} = 1.25$ (see Figure 2.5) where lower mass galaxies have

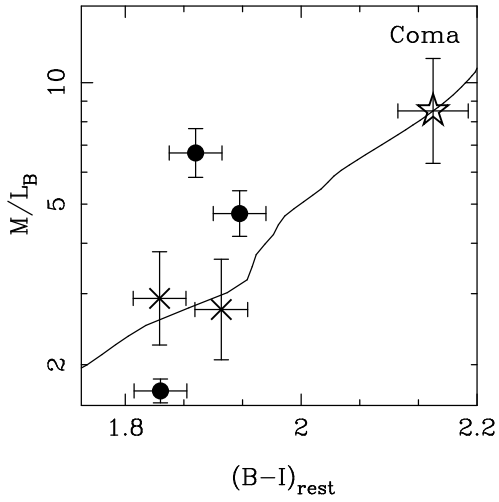

Figure 2.4: Values of M/L_B as a function of the rest-frame Vega $B-I$ color for galaxies with $M > 10^{11.5} M_\odot$. The average Coma values are represented as a star symbol, while the three galaxies from RDCS 1252.9-2927 are filled circles and the two galaxyes from RDCS 0848+4453 are crosses. The line shows the trajectory of a solar metallicity model with an exponentially declining, $\tau = 200$ Myr, star formation rate Bruzual & Charlot (2003) model normalized to the average Coma Cluster observations. The highest M/L_B is galaxy 4419, the brightest cluster galaxy. The colors of galaxy 4419 are significantly bluer than predicted for its observed M/L_B, ruling out the offset being a result of dust or metallicity effects. The lowest mass galaxy in RDCS 0848+4453 is excluded (see text).

lower M/L_B and, therefore, bluer colors (see Figure 2.4.) The slope of the mass-M/L relation appears to steepen at higher redshifts. This is expected for a population where the spread in the M/L comes from the spread in age. As a stellar population becomes younger, the M/L changes more quickly, so the spread in M/L will grow as observations probe closer to the epoch of formation. However, this trend will be exaggerated by the selection of galaxies at a fixed luminosity, as the sample selection will prefer lower M/L galaxies. Lower mass galaxies with larger values for M/L_B will not appear in this sample because of our magnitude limit, effectively $L_B \simeq 10^{11} L_\odot$.

2.4 Implications for the Evolution of Early-type Cluster Galaxies

The rate of the M/L evolution can be used to constrain the luminosity-weighted age for early-type galaxies. The most straightforward estimate is to assume all galaxies formed at one epoch and find the age of the galaxies that will produce the observed change in M/L from $z = 0.023$ to $\bar{z} = 1.25$ using population synthesis models. For our sample of five $M > 10^{11.5} M_\odot$ galaxies, the mean age is $\tau_* = 3.0^{+0.3}_{-0.3}$ Gyr before the time of the observations, or a formation redshift of $z_* = 3.4^{+0.5}_{-0.4}$ using the same models as van Dokkum & Stanford (2003), namely, Worthey (1994). This agrees

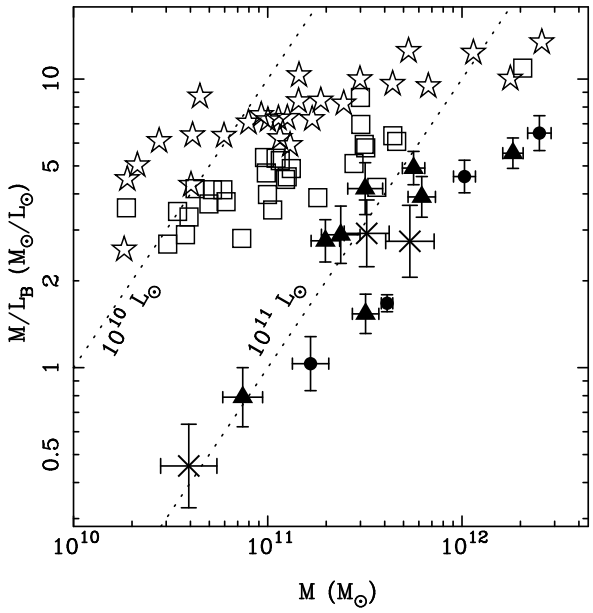

Figure 2.5: Values of M/L_B as a function of mass, using the same symbols as Figure 2.3 but not including the results for MS 2053-04. The lower redshift trend of higher M/L_B at higher masses appears to be preserved at $\bar{z} = 1.25$, even when we ignore the lowest mass galaxy in RDCS 0848+4453. The dotted lines represent $L_B = 10^{11}$ and $10^{10}\,L_\odot$. Our $z_{850} = 22.5$ selection limit corresponds to $L_B \simeq 10^{10.9} L_\odot$ for a galaxy with the colors of a Coma elliptical galaxy.

with the results from the high-mass sample of Wuyts et al. (2004), who found $z_* = 2.95^{+0.81}_{-0.46}$ for galaxies regardless of morphology.

When computing the age for the early-type galaxy population, there is an overestimate of the age of a population caused by young galaxies not being counted as part of the early-type population, even if those young galaxies will evolve into early types after the epoch of observation. This "progenitor bias" depresses the rate of observed evolution in M/L by up to 20% (van Dokkum & Franx, 2001). Using this same assumption, namely, that the true evolution is $\Delta \ln M/L_B \propto (-1.18 \pm 0.06)z$, we instead find $\tau_* = 2.1^{+0.2}_{-0.2}$ Gyr before $\bar{z} = 1.25$, or a formation redshift of $z_* = 2.3^{+0.2}_{-0.2}$. Blakeslee et al. (2003) and Lidman et al. (2004) both find a mean age of ≥ 2.6 Gyr using the colors of the galaxies in RDCS 1252.9-2927. Blakeslee et al. (2003) removed the "progenitor bias" with simulations, whereas Lidman et al. (2004) uses all galaxies, regardless of morphology, to similar effect.

The above results imply that the stars that formed these massive galaxies were created at redshifts of $z_* \simeq 2 - 3$, at which time less than $1/3$ of today's observed stellar mass was formed (e.g., Bell, 2005). However, there is a large spread in the M/L_B for all of the early-type galaxies at $z \simeq 1.25$, larger than at lower redshifts. Using colors confirms the spread, which can be interpreted as an underlying spread in the age of the populations. Thus, although $z_* \simeq 2.5$ for the most massive galaxies,

some early-typegalaxies show much lower M/L values and corresponding younger ages. In fact, the lowest M/L galaxy in Figure 2.3 was tentatively classified by van Dokkum & Stanford (2003) as having a recent starburst based on the spectrum. Such younger appearing galaxies have lower masses than the high M/L galaxies in our sample, but are still massive galaxies with $\log M/M_{\odot} \simeq 11$. The implication of all these results is that a significant fraction of the stars in the most massive galaxies appear to have formed very early in the history of the universe, before the majority of stars present today. The massive cluster galaxies appear to follow the same low-redshift trend of the higher mass systems having higher M/L_B. However, the larger spread at $\bar{z} = 1.25$ in the M/L_B indicates that we have identified some massive, $M \simeq 10^{11} M_{\odot}$, galaxies whose last burst of star formation occurred in the relatively recent past, $z \simeq 1.5$.

ACS was developed under NASA contract NAS5-32865, and this research was supported by NASA grant NAG5-7697. B.P.H. would like to thank Daniel Kelson for useful discussions on the fundamental plane. The authors would also like to thank the referee for many useful suggestions.

References

Bell, E. 2005, *in Planets to Cosmology: Essential Science in Hubble's Final Years, ed. M Livio (Cambridge: Cambridge University Press)* in press, astro-ph/0408023

Bessell, M. S. 1990, *PASP* **102**, 1181

Blakeslee, J. P. et al. 2003, *ApJ* **596**, L143

Bruzual, G. & Charlot, S. 2003, *MNRAS* **344**, 1000

Coleman, G. D., Wu, C.-C., & Weedman, D. W. 1980, *ApJS* **43**, 393

Demarco, R. et al. 2005, *A&A* **432**, 381

Gebhardt, K. et al. 2003, *ApJ* **597**, 239

Holden, B. P., Stanford, S. A., Eisenhardt, P., & Dickinson, M. 2004, *AJ* **127**, 2484

Jørgensen, I., Franx, M., & Kjærgaard, P. 1993, *ApJ* **411**, 34

Jørgensen, I., Franx, M., & Kjærgaard, P. 1996, *MNRAS* **280**, 167

Kelson, D. D., Illingworth, G. D., van Dokkum, P. G., & Franx, M. 2000a, *ApJ* **531**, 137

Kelson, D. D., Illingworth, G. D., van Dokkum, P. G., & Franx, M. 2000b, *ApJ* **531**, 184

Krist, J. 1995, in *ASP Conf. Ser. 77: Astronomical Data Analysis Software and Systems IV*, p.349

Lidman, C., Rosati, P., Demarco, R., Nonino, M., Mainieri, V., Stanford, S. A., & Toft, S. 2004, *A&A* **416**, 829

Madau, P., Pozzetti, L., & Dickinson, M. 1998, *ApJ* **498**, 106

Rosati, P. et al.2004, *AJ* **127**, 230

Rudnick, G. et al. 2003, *ApJ* **599**, 847

Steidel, C. C., Adelberger, K. L., Giavalisco, M., Dickinson, M., & Pettini, M. 1999, *ApJ* **519**, 1

Valdes, F., Gupta, R., Rose, J. A., Singh, H. P., & Bell, D. J. 2004, *ApJS* **152**, 251

van de Ven, G., van Dokkum, P. G., & Franx, M. 2003, *MNRAS* **344**, 924

van der Wel, A., Franx, M., van Dokkum, P. G., & Rix, H.-W. 2004, *ApJ* **601**, L5 (Chapter 3)

van der Wel, A., Franx, M., van Dokkum, P. G., Rix, H.-W., Illingworth, G., & Rosati, P. 2005, *ApJ* in press, astro-ph/0502228 (Chapter 4)

van Dokkum, P. G. & Ellis, R. S. 2003, *ApJ* **592**, L53

van Dokkum, P. G. & Franx, M. 1996, *MNRAS* **281**, 985

van Dokkum, P. G. & Franx, M. 2001, *ApJ* **553**, 90

van Dokkum, P. G., Franx, M., Kelson, D. D., & Illingworth, G. D. 2001, *ApJ* **553**, L39

van Dokkum, P. G. & Stanford, S. A. 2003, *ApJ* **585**, 78

Worthey, G. 1994, *ApJS* **95**, 107

Wuyts, S., van Dokkum, P. G., Kelson, D. D., Franx, M., & Illingworth, G. D. 2004, *ApJ* **605**, 677

Chapter 3

The Fundamental Plane of Field Early Type Galaxies at $z = 1$

Abstract

We present deep VLT spectra of early-type galaxies at $z \approx 1$ in the Chandra Deep Field South, from which we derive velocity dispersions. Together with structural parameters from *Hubble Space Telescope* imaging, we can study the Fundamental Plane for field early type galaxies at that epoch. We determine accurate mass-to-light ratios (M/L) and colors for four field early type galaxies in the redshift range $0.96 < z < 1.14$, and two with $0.65 < z < 0.70$. The galaxies were selected by color and morphology, and have generally red colors. Their velocity dispersions show, however, that they have a considerable spread in M/L (a factor of 3). We find that the colors and directly measured M/L correlate well, demonstrating that the spread in M/L is real and reflects variations in stellar populations. The most massive galaxies have M/L comparable to massive cluster galaxies at similar redshift, and therefore have stellar populations which formed at high redshift ($z > 2$). The lower mass galaxies at $z \approx 1$ have a lower average M/L, and one is a genuine 'E+A' galaxy. The M/L indicate that their luminosity-weighted ages are a factor of 3 younger at the epoch of observation, because of either a late formation redshift or late bursts of star formation contributing 20 - 30% of the mass.

van der Wel, A., Franx, M., van Dokkum, P.G. & Rix, H.-W.
The Astrphysical Journal Letters, **601**, 5 (2004)

3.1 Introduction

Good understanding of the formation and evolution of early-type galaxies is one of the major challenges for current structure-formation models. Models of hierarchical structure generally predict that field early type galaxies form relatively late (e.g., Diaferio et al., 2001). One of the prime diagnostics of the formation history of early-type galaxies is the evolution of the M/L as measured from the fundamental plane (FP Franx, 1993). Studies of the evolution of the luminosity function together with the evolution of M/L, quantify the evolution of the mass function. Previous studies of the evolution of the M/L have produced consistent results for the evolution of massive cluster early-type galaxies: the evolution is slow, consistent with star formation redshifts $z \approx 2$ (e.g., van Dokkum & Stanford, 2003).

On the other hand, studies of the evolution of field galaxies have yielded more contradictory results: whereas early studies found slow evolution (e.g., van Dokkum et al., 2001; Treu et al., 2001; Kochanek et al., 2000), more recently, evidence for much faster evolution was found by Treu et al. (2002) and Gebhardt et al. (2003); and yet other authors found that the majority of field early-types evolve slowly, with a relatively small fraction of fast-evolving galaxies (e.g., Rusin et al., 2003; van Dokkum & Ellis, 2003; van de Ven, van Dokkum & Franx, 2003; Bell et al., 2004).

These previous measurements suffered from several uncertainties: The signal-to-noise ratios (S/N) of the spectra were generally quite low, much lower than usual for nearby studies of the FP (e.g., Faber et al., 1989; Jørgensen, Franx & Kjærgaard, 1996). Those studies based on lensing galaxies used stellar velocity dispersions derived from image separations.

In this Letter, we present high-S/N spectra and accurate measurements of the M/L of four field elliptical galaxies $z =\sim 1 - 1.14$ and two at $z \sim 0.7$ in the Chandra Deep Field-South (CDF-S). The S/N are comparable to those obtained for nearby galaxies. Together with accurate multiband photometry available for the CDF-S, we have measured the accurate M/L and rest frame optical colors at $z \sim 1$.

Throughout this Letter we use Vega magnitudes, and assume a Λ-dominated cosmology ($[\Omega_M, \Omega_\Lambda] = [0.3, 0.7]$), with a Hubble constant of $H_0 = 70\ \mathrm{km\ s^{-1}\ Mpc^{-1}}$.

3.2 Spectroscopy

3.2.1 Sample selection and Observations

The galaxies were selected from the COMBO17 catalog (see Wolf et al., 2003), and imaging obtained by the Great Observatories Origin Deep Survey (GOODS[1], data release v0.5) from the Advanced Camera for Surveys (ACS) on the *Hubble Space Telescope*. We selected compact, regularly shaped galaxies with photometric redshifts higher than 0.8 and $I - z \geq (I - z)_{\mathrm{Sbc}},\ z < 22$. $(I - z)_{\mathrm{Sbc}}$ denotes the color of the Sbc template of Coleman, Wu & Weedman (1980) at the photometric redshift. This template has $(U - V)_{\mathrm{z=0}} = 0.95$. The typical uncertainty in the color is 0.1 mag. Lower priority galaxies were included with either lower redshifts or later types.

[1] http://www.stsci.edu/science/goods/

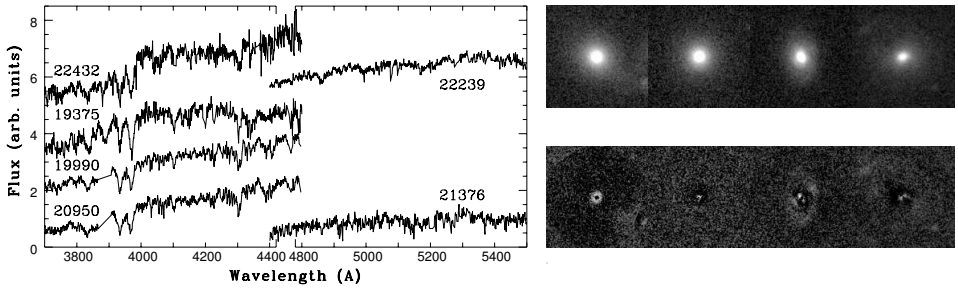

Figure 3.1: *Left*: Unsmoothed rest-frame spectra of the six objects with velocity dispersions. Regions with bright sky lines are interpolated. The wavelength scale is interrupted at $\lambda = 4500\text{Å}$. *Right*: ACS images (F850LP) of the four galaxies at $z \sim 1$, and the residual images from the $r^{1/4}$ fit. *From left to right*: 20950, 19990, 19375, 22432.

The CDF-S was observed in MXU mode with FORS2 on VLT-UT4 during three runs from 2002 September through 2003 February, for a total of 14 hours. The 600 z grism (central wavelength 9010Å, resolution 5.1Å or $\sigma_{\rm instr} = 72\ {\rm km\ s^{-1}}$) was used. During the observations toward the CDF-S the seeing varied between 0"7 and 1"5, with a median seeing of about $1''$. The sky was clear all the time.

3.2.2 Velocity Dispersions

It turned out that 10 out of the 11 high-priority objects at $z_{\rm phot} \sim 1$ have the spectrum of a quiescent galaxy; the other one has a bright OII emission line. The brightest four ($z \lesssim 21.0$, independent of the color) had sufficient S/N to perform reliable dispersion measurements. The rest-frame spectra of these four galaxies are shown in Figure 3.1. They all show a strong 4000Å break and Ca lines. Balmer lines (especially the $H\delta$ line) are also present, though varying in strength from object to object (see Table 3.2). Object 19375 is an "E+A" galaxy, according to the criteria used by Fisher et al. (1998). For two ellipticals with $0.65 < z < 0.70$ we also have sufficient signal to determine a velocity dispersion.

Dispersions were measured by convolving a template star spectrum to fit the galaxy spectrum as outlined by van Dokkum & Franx (1996). We tested this procedure extensively, using different template stars and masking various spectral regions. The final values (see Table 3.2) for the velocity dispersions were obtained by masking the Ca H and K and Balmer lines and using the best-fitting template spectrum, which was a high-resolution solar model spectrum[2] smoothed and rebinned to match the resolution of the galaxy spectra. The Ca lines were not included in the fit because this greatly reduced the dependence of the measured velocity dispersions on template type. The tests using different templates and different masking of the Ca lines indicate that the systematic uncertainty is $\sim 5\%$.

In order for the results to be comparable to previous studies, an aperture cor-

[2]http://bass2000.obspm.fr

Table 3.1: Photometric and Spectroscopic Properties

ID	α arcsec	δ arcsec	$z_{\rm spec}$	i	$v-i$	$i-z$	$\log(r_{\rm eff})$ kpc	$\mu_{\rm eff}$
19375	0	-50	1.089	21.72	1.71	1.04	-0.410±0.012	21.75±0.05
19990	-32	-35	0.964	21.32	1.89	1.00	-0.388±0.007	21.45±0.03
20950	-73	-6	0.964	21.18	2.07	1.07	0.0085±0.026	22.95±0.08
22432	83	41	1.135	22.38	2.00	1.42	-0.109±0.040	23.35±0.13
21376	129	10	0.685	21.46	1.77	0.58	-0.447±0.001	22.16±0.04
22239	236	35	0.660	20.67	1.67	0.50	-0.842±0.002	19.83±0.03

ID	S/N Å^{-1}	σ km s^{-1}	(H_γ+H_δ)/2 Å	[OII] Å
19375	26	198±25	4.1	-4.6
19990	49	159±14	2.5	>-1
20950	39	261±23	<1	>-1
22432	21	217±20	<1	-4.4
21376	27	156±24	–	–
22239	40	177±19	–	–

Table 3.2: Coordinates are in in arcseconds east and north of R.A.$= 03^h32^m25^s$, decl.$= -27^\circ54'00''$. Errors in the magnitudes and colors are, respectively, 0.03 and 0.05 mag. Effective radii and surface brightnesses (mag/arcsec^2 at $r_{\rm e}$) are measured in the z-band for objects 19375, 19990, 20950 and 22432, and in the i-band for objects 21376 and 22239. The listed errors in the velocity dispersions are fitting errors, and do not include a 5% systematic error.

rection as described by Jorgensen, Franx & Kjærgaard (1995) was applied to obtain velocity dispersions within a circular aperture with a radius of 1"7 at the distance of the Coma cluster. This correction is $\sim 7\%$.

This is the first extensive sample of such objects at $z > 0.9$ with high S/N. (see van Dokkum & Ellis, 2003; Treu et al., 2002; Gebhardt et al., 2003, for other spectroscopic studies).

3.3 Photometry

Photometry and structural parameters were determined from the GOODS ACS images (data release v1.0). Images are available in four filters (F435W, F606W, F775W, F850LP), which we refer to as b, v, i, and z, respectively.

For each object, the effective radius ($r_{\rm e}$) and the surface brightness at the effective radius ($\mu_{\rm e}$) were obtained by fitting an $r^{1/4}$ profile, convolved by the point-spread function (PSF van Dokkum & Franx, 1996); z-band images were used for the $z \sim 1$ objects, and i-band images for the $z \sim 0.7$ objects. Stars were used as the PSF. The resulting values for $r_{\rm e}$ and $\mu_{\rm e}$ vary by $\approx 10\%$ when using different stars, but also correlate such that the error is almost parallel to the FP (van Dokkum & Franx,

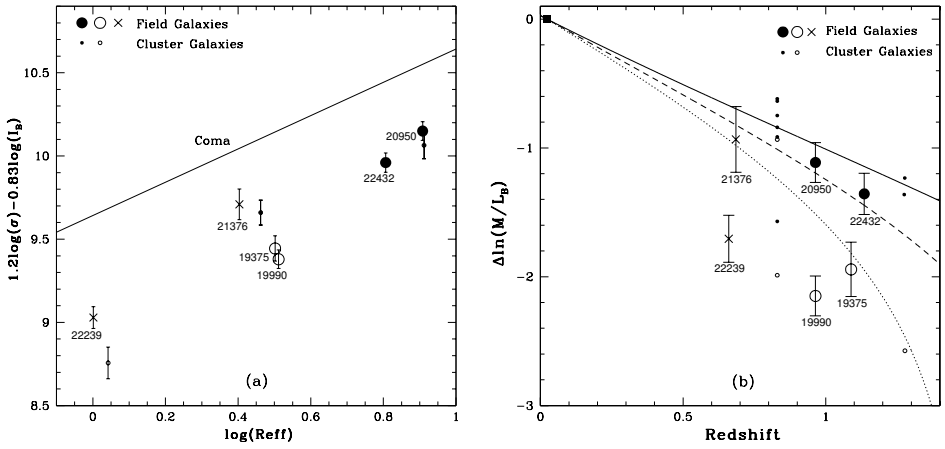

Figure 3.2: (*a*) FP points of the field galaxies presented in this paper (errors include a 5% systematic effect in the velocity dispersions), the FP points of cluster galaxies at $z = 1.27$ (van Dokkum & Standford 2003), and the FP of the Coma Cluster (Jørgensen et al. 1996). (*b*) Offsets in M/L_B from the Coma Cluster FP (*square*; derived from Jørgensen et al. 1996). Besides the $z = 1.27$ cluster, this figure also contains the data from van Dokkum et al. (1998) on the MS 1054 cluster at $z = 0.83$. The full, dashed and dotted curves are the model predictions for a single burst of starformation with a Salpeter (1955) initial mass function for redshifts 3, 2, and 1.5, respectively. Filled symbols indicate galaxies with masses $M > 3 \times 10^{11} M_{\odot}$; other symbols indicate galaxies less massive than that. Crosses and squares distinguish between galaxies at $z < 0.8$ and $z > 0.8$, respectively. All galaxies occupying the region below the $z = 1.5$ model curve are "E+A" galaxies, except 19990, and have masses less than $3 \times 10^{11} M_{\odot}$. The more massive galaxies have significantly older stellar populations.

1996). Therefore, the errors in our results are dominated by the errors in the velocity dispersions. The results are listed in Table 3.2. The images of the $z \sim 1$ objects and the residuals of the fits are shown in Figure 3.1.

To determine the $i-z$ and $v-i$ colors, fluxes were calculated from the $r^{1/4}$ model within the measured effective radius. To this model flux we added the flux within the same radius in the residual images. We corrected for Galactic extinction based on the extinction maps from Schlegel, Finkbeiner & Davis (1998). The correction is extremely small: $E(B-V) = 0.007$.

Restframe B-band surface brightnesses and restframe $U-V$ colors were obtained by transforming observed flux densities in two filters to a restframe flux density exactly as outlined by van Dokkum & Franx (1996). The spectral energy distribution used to calculate the transformations is the early-type spectrum from Coleman et al. (1980). We found the same results for other template spectra. The results are listed in Table 3.2.

3.4 Mass-to-Light Ratios from the FP

Figure 3.2a shows the Fundamental Plane for the six field galaxies described above, and the FP for Coma derived by Jørgensen et al. (1996). Additionally, we show the results from van Dokkum & Stanford (2003) on three cluster galaxies at $z = 1.27$. The offsets of the high-redshift galaxies from the Coma FP are a measure of the evolution of M/L. We show the evolution of M/L in Figure 3.2b as a function of redshift.

Obviously, the field galaxies at $z > 0.6$ span a wide range in offsets, by a factor of approximately 3 in M/L. The error bars on the individual points are much smaller than the offsets. A model with a single formation redshift can be ruled out at the 99% confidence level, as measured from the χ^2-method. The restframe colors of the galaxies confirm the reality of the variations in the M/L. As shown in Figure 3.3, a very strong correlation exists between the colors and the M/L, in the direction predicted by population sysnthesis models. The good correlation demonstrates that colors can be used to estimate the M/L, as applied, for example, by Bell et al. (2004) to a large sample of field early-type galaxies.

We note that galaxies in our study lie fairly close to the red sequence, and were characterised by Bell et al. (2004) to have red colors. The overall spread in colors of field galaxies is much larger (1.5 mag) compared to the spread found here (0.3 mag).

3.5 Discussion

On the basis of our high-S/N spectra we have found a rather wide range in M/L for early-type galaxies at $z = 1$, indicating a range in star formation histories. The M/L and colors are well correlated, as expected from stellar population models. Hence the scatter in M/L is real.

The results agree surprisingly well with earlier results based on lensing galaxies. Rusin et al. (2003) and van de Ven et al. (2003) found a range in M/L, and van de Ven et al. (2003) found a similar correlation between restframe colors and M/L. Other authors found either low M/L (e.g., Treu et al., 2002; Gebhardt et al., 2003), or high M/L (e.g., van Dokkum & Ellis, 2003), and this is most likely due to (still unexplained) sample selection effects. The last authors found that galaxies with residuals from the $r^{1/4}$ profile had young ages. However, we find no such relation in our sample.

Stellar population models indicate that the low M/L of the blue $z \approx 1$ galaxies may be due to an age difference of a factor of 3. Alternatively, bursts involving $20 - 30\%$ of the mass can produce similar offsets. The current sample is too small to determine the fraction of young early-type galaxies at $z \approx 1$ reliably. Large, mass selected samples are needed for this, as current samples are generally optically selected and therefore biased towards galaxies with lower M/L.

It is striking that the most massive galaxies have modest evolution in M/L, similar to what van Dokkum & Stanford (2003) found for massive cluster galaxies. The evolution of the galaxies with $M = 6.07\, r_{\rm e}\sigma^2 \geq 3 \times 10^{11} M_\odot$ (Jørgensen et al., 1996) in our sample is $\Delta \ln M/L_B = -1.17 \pm 0.14\, z$. The implied formation redshift is above 2, ignoring effects of progenitor bias (van Dokkum & Franx, 2001). The mass limit is comparable to the M_* mass of an early-type galaxy: if we take the σ_* of early-

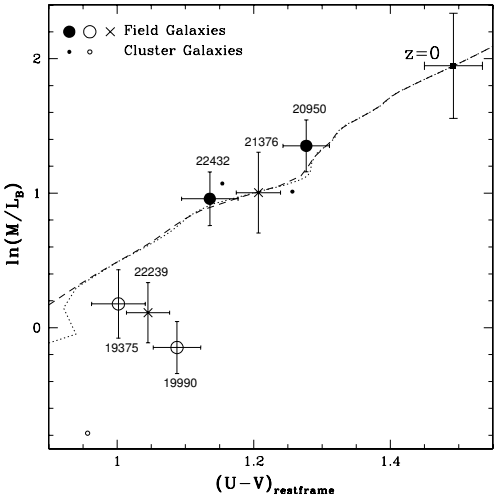

Figure 3.3: Restframe $U-V$ color vs. M/L_B in solar units. Filled symbols are objects more massive than $M > 3 \times 10^{11} M_\odot$; open symbols represent the less massive ones. The cluster galaxies are the $z = 1.27$ galaxies from Figure 3.2. The redshift zero datapoint is the average for galaxies with $\sigma > 150$ km s^{-1} in the clusters Abell 194 and DC2345-28 (Jørgensen et al. 1995). The lines are solar metallicity Bruzual & Charlot (2003) models with constant star formation during the first 200 Myr (*dotted line*) and exponentially decaying star formation on the same time scale (*dashed line*).

type galaxies derived by Kochanek (1994) of 225 km s^{-1}, we derive a typical mass of $M_* = 3.1 \times 10^{11} M_\odot$ based on the sample measured by Faber et al. (1989). The sample as a whole evolves as $\Delta \ln M/L_B = -1.64 \pm 0.45\, z$, whereas the sample with masses smaller than $3 \times 10^{11} M_\odot$ evolves as $\Delta \ln M/L_B = -1.95 \pm 0.29\, z$.

The results are therefore consistent with little or no (recent) star formation in massive early-type galaxies out to $z = 1$, and younger populations in less massive galaxies, possibly caused by bursts involving up to 30% of the stellar mass. Since these less massive galaxies have much more regular stellar populations at $z < 0.5$ without signs of recent star formation, these results are consistent with the downsizing seen in the field population (Cowie et al., 1996): at progressively higher redshifts, more and more massive galaxies are undergoing strong star formation.

It remains to be seen how this trend continues out to even higher redshifts. The biases inherent in studies of galaxies at $z = 2$ and higher make it very hard to perform similar studies: the optical light has shifted to the near-IR, and spectroscopy is extremely hard at those wavelengths.

More studies at redshift $z \approx 1$ are needed to determine the distribution of colors and M/L of the progenitors of field early-types. Such a determination should be based on mass-selected samples. Further studies of spectral energy distributions extending to the rest-frame infrared will be very useful to better constrain the star formation histories of the bluer galaxies.

We thank the ESO staff for their support during the observations. We thank C. Wolf for making available the COMBO17 catalog.

References

Bell, E. F. et al. 2004, *ApJ* **608**, 752

Coleman, G. D., Wu, C.-C., & Weedman, D. W. 1980, *ApJS* **43**, 393

Cowie, L. L., Songaila, A., Hu, E. M., & Cohen, J. G. 1996, *AJ* **112**, 839

Diaferio, A., Kauffmann, G., Balogh, M. L., White, S. D. M., Schade, D., & Ellingson, E. 2001, *MNRAS* **323**, 999

Faber, S. M., Wegner, G., Burstein, D., Davies, R. L., Dressler, A., Lynden-Bell, D., & Terlevich, R. J. 1989, *ApJS* **69**, 763

Fisher, D., Fabricant, D., Franx, M., & van Dokkum, P. 1998, *ApJ* **498**, 195

Franx, M. 1993, *PASP* **105**, 1058

Gebhardt, K. et al. 2003, *ApJ* **597**, 239

Jørgensen, I., Franx, M., & Kjærgaard, P. 1996, *MNRAS* **280**, 167

Jorgensen, I., Franx, M., & Kjærgaard, P. 1995, *MNRAS* **276**, 1341

Kochanek, C. S. 1994, *ApJ* **436**, 56

Kochanek, C. S. et al. 2000, *ApJ* **543**, 131

Rusin, D. et al. 2003, *ApJ* **587**, 143

Schlegel, D. J., Finkbeiner, D. P., & Davis, M. 1998, *ApJ* **500**, 525

Treu, T., Stiavelli, M., Bertin, G., Casertano, S., & Møller, P. 2001, *MNRAS* **326**, 237

Treu, T., Stiavelli, M., Casertano, S., Møller, P., & Bertin, G. 2002, *ApJ* **564**, L13

van de Ven, G., van Dokkum, P. G., & Franx, M. 2003, *MNRAS* **344**, 924

van Dokkum, P. G. & Ellis, R. S. 2003, *ApJ* **592**, L53

van Dokkum, P. G. & Franx, M. 1996, *MNRAS* **281**, 985

van Dokkum, P. G. & Franx, M. 2001, *ApJ* **553**, 90

van Dokkum, P. G., Franx, M., Kelson, D. D., & Illingworth, G. D. 2001, *ApJ* **553**, L39

van Dokkum, P. G. & Stanford, S. A. 2003, *ApJ* **585**, 78

Wolf, C., Meisenheimer, K., Rix, H.-W., Borch, A., Dye, S., & Kleinheinrich, M. 2003, *A&A* **401**, 73

Chapter 4

Mass-to-Light Ratios of Field Early-Type Galaxies at $z \sim 1$ from Ultra-Deep Spectroscopy: Evidence for Mass-dependent Evolution

Abstract

We present an analysis of the Fundamental Plane for a sample of 27 field early-type galaxies in the redshift range $0.6 < z < 1.15$ in the Chandra Deep Field-South and the field of the background cluster RDCS 1252.9-2927. Sixteen of the galaxies are at $z > 0.95$. The galaxies in this sample have high signal-to-noise spectra obtained at the Very Large Telescope and high resolution imaging from the HST Advanced Camera for Surveys. From comparison with lower redshift data, we find that the mean evolution of the mass-to-light ratio (M/L) of our sample is $\Delta \ln (M/L_B) = (-1.74 \pm 0.16)z$, with a large galaxy-to-galaxy scatter. The strong correlation between M/L and rest-frame color indicates that the observed scatter is not due to measurement errors, but due to intrinsic differences between the stellar populations of the galaxies, such that our results can be used as a calibration for converting luminosities of high redshift galaxies into masses. This pace of evolution is much faster than the evolution of cluster galaxies. However, we find that the measured M/L evolution strongly depends on galaxy mass. For galaxies with masses $M > 2 \times 10^{11} M_{\odot}$, we find no significant difference between the evolution of field and cluster galaxies: $\Delta \ln (M/L_B) = (-1.20 \pm 0.18)z$ for field galaxies and $\Delta \ln (M/L_B) = (-1.12 \pm 0.06)z$ for cluster galaxies. The relation between the measured M/L evolution and mass is partially due to selection effects, as the galaxies are selected by luminosity, not mass. We calculate the magnitude of this effect for the sub-sample of galaxies with masses higher than $M = 6 \times 10^{10} M_{\odot}$: the uncorrected value of the evolution is $\Delta \ln (M/L_B) = (-1.54 \pm 0.16)z$, whereas the corrected value is $(-1.43 \pm 0.16)z$. However, even when taking selection effects into account, we still find a relation between M/L evolution and mass, which is most likely caused by a lower mean age and a larger intrinsic scatter for low mass galaxies. Results from lensing early-type galaxies, which are mass-selected, show a very similar trend with mass. This, combined with our findings, provides evidence for down-sizing, i.e., for the proposition that low mass galaxies are younger than high mass galaxies. Previous studies of the rate of evolution of field early-type galaxies found a large range of mutually exclusive values. We show that these differences are largely caused by the differences between fitting methods: most literature studies are consistent with our result and with one another when using the same method. Finally, five of the early-type galaxies in our sample have AGN. There is tentative evidence that the stellar populations in these galaxies are younger than those of galaxies without AGN.

van der Wel, A., Franx, M., van Dokkum, P.G., Rix, H.-W., Illingworth, G.D. & Rosati, P.
The Astrphysical Journal, in press

4.1 Introduction

Understanding the formation and evolution of early-type galaxies is a key issue when addressing the mass assembly and star formation history of the galaxy population as a whole and the formation of structure in the universe, as 50% or more of all stars in the present day universe are in early-type galaxies and bulges (see, e.g., Bell et al., 2003).

In hierarchical galaxy formation theories (e.g., Cole et al., 2000), massive galaxies assemble late, such that strong evolution of the mass density from $z = 1$ to the present day is expected (see, e.g., Kauffmann & Charlot, 1998). Measuring the mass density requires a measurement of the luminosity density, and an accurate determination of the M/L. M/L can be estimated from models (see, e.g., Bell et al., 2004), but these estimates are uncertain due to the age/metallicity degeneracy and the unknown IMF of the stellar populations of the galaxies (Bruzual & Charlot, 2003).

The Fundamental Plane (Djorgovski & Davis, 1987; Dressler et al., 1987) provides a tool to measure the evolution of M/L without model uncertainties. The M/L offset of high redshift galaxies from the local FP can be used to calibrate high redshift galaxy masses and to estimate the age of their stellar populations (Franx, 1993). This technique has been used successfully to measure the luminosity weighted ages of massive cluster galaxies, which have formed most of their stars at redshifts $z \geq 2$ (see, e.g., van Dokkum & Franx, 1996; van Dokkum & Stanford, 2003; Holden et al., 2005). However, it is not clear whether galaxies in the general field evolve in the same way. In fact, in the hierarchical picture the formation redshift of galaxies with a given mass depends on environment (Diaferio et al., 2001). This would lead to substantial age differences between field and cluster galaxies at any redshift (van Dokkum et al., 2001). Since this is a generic property of all hierarchical formation models, measuring this difference is a critical test for those theories.

Various authors have measured the M/L evolution of field early- type galaxies through deep spectroscopy of magnitude limited samples. The results are much less conclusive than the results from cluster studies and the comparison between field and cluster has proved to be very hard. Some authors claim much faster evolution for field galaxies than for cluster galaxies (Treu et al., 2001; Gebhardt et al., 2003), but others find that field and cluster galaxies evolve at comparable rates (van Dokkum et al., 2001; van Dokkum & Ellis, 2003; van der Wel et al., 2004). Studies involving lensing galaxies (Kochanek et al., 2000; Rusin et al., 2003; van de Ven, van Dokkum & Franx, 2003), indicate the presence of a mix of fast and slowly evolving galaxies. It is unclear whether the differences between the various results are caused by selection effects, measurement errors due to low signal-to-noise spectra, low number statistics, or contamination by late-type galaxies.

This paper describes a study of early-type galaxies at $z \sim 1$ using much higher quality data than in previous studies. The substantially large number of objects with very high signal-to-noise spectra enables us to accurately measure the M/L evolution of the field early-type galaxy population, to compare the cluster and field populations, to study correlations between M/L, M, and rest-frame color, and to describe the possible effects of biases. Also, we carefully compare the samples and results from previous studies and this study in order to verify previous claims about the evolution of field galaxies, and to see whether previous results are in fact consistent with each

Table 4.1: Coordinates of the Galaxy Sample

	α	δ		α	δ
ID	J2000	J2000	ID	J2000	J2000
CL1252-1	12:52:45.8899	-29:29:04.5780	CL1252-2	12:52:42.3588	-29:27:47.3112
CL1252-3	12:52:42.4793	-29:27:03.5892	CL1252-4	12:52:48.5594	-29:27:23.2452
CL1252-5	12:52:58.5202	-29:28:39.5256	CL1252-6	12:52:56.3846	-29:26:22.7868
CL1252-7	12:53:03.6396	-29:27:42.5916	CL1252-8	12:53:05.1228	-29:26:29.8680
CL1252-9	12:53:05.6213	-29:26:32.5608	CDFS-1	03:32:25.1597	-27:54:50.1332
CDFS-2	03:32:22.9265	-27:54:34.3429	CDFS-3	03:32:26.2940	-27:54:05.0411
CDFS-4	03:32:19.2880	-27:54:06.1445	CDFS-5	03:32:34.8486	-27:53:50.0705
CDFS-6	03:32:42.8569	-27:53:24.7700	CDFS-7	03:32:31.3700	-27:53:19.1519
CDFS-8	03:32:23.6062	-27:53:06.3463	CDFS-9	03:32:17.4796	-27:52:48.0004
CDFS-10	03:32:20.2801	-27:52:33.0150	CDFS-11	03:32:19.3006	-27:52:19.3400
CDFS-12	03:32:45.1488	-27:49:39.9558	CDFS-13	03:32:39.5987	-27:49:09.6024
CDFS-14	03:32:54.2299	-27:49:03.7722	CDFS-15	03:32:41.4049	-27:47:17.1409
CDFS-16	03:32:29.2152	-27:47:07.5718	CDFS-17	03:32:38.4940	-27:47:02.3640
CDFS-18	03:32:37.1944	-27:46:08.0663	CDFS-19	03:32:32.7124	-27:45:47.4617
CDFS-20	03:32:10.0387	-27:43:33.1237	CDFS-21	03:32:19.5922	-27:43:03.7848
CDFS-22	03:32:09.7051	-27:42:48.1090	CDFS-23	03:32:17.9117	-27:41:22.6795
CDFS-24	03:32:32.9855	-27:41:17.0102	CDFS-25	03:32:27.7000	-27:40:43.6865
CDFS-26	03:32:19.1468	-27:40:40.2190	CDFS-27	03:32:21.3600	-27:40:26.0861
CDFS-28	03:32:24.5444	-27:40:10.4322	CDFS-29	03:32:30.1945	-27:39:30.2407

other and these new results.

In Section 2 we describe the sample selection, the spectroscopic observations and data reduction, and the measurement of velocity dispersions. Section 3 describes the measurement of the structural parameters, colors, morphologies, and the available X-ray data. In Section 4 we present the results Throughout this paper we use Vega magnitudes, and assume $(\Omega_M, \Omega_\Lambda) = (0.3, 0.7)$, with a Hubble constant of $H_0 = 70\ \mathrm{km\ s^{-1}\ Mpc^{-1}}$.

4.2 Spectroscopy

4.2.1 Sample selection and Observations

We selected galaxies in the Chandra Deep Field-South (CDFS) and the RDCS1252.9-2927 cluster field (CL1252 Rosati et al., 2004), which both have deep optical imaging from the Advanced Camera for Surveys (ACS) on the HST. GOODS[1] provides publicly available imaging in four filters (Giavalisco et al., 2004): F475W, F606W, F775W, and F850LP (hereafter b, v, i, and z). As these data were not yet available when we started this project, we used ground-based COMBO-17 photometry (Wolf et al., 2003) to select our sample for the first observing run. For subsequent runs version

[1]http://www.stsci.edu/science/goods/

0.5 of the ACS GOODS data were available, and for the last run we used the version 1.0 data release. Blakeslee et al. (2003) provide ACS imaging on the CL1252 field in the i and z bands.

In order to construct a sample of early-type galaxies at $z \sim 1$ in the CDFS, we selected objects with $i - z > 0.86$ and COMBO-17 photometric redshifts in the range $0.8 < z_{\rm phot} < 1.4$. (We use z when we mean 'redshift', and $z_{\rm mag}$ if we mean z-band magnitude, but when indicating a color we omit the $\rm mag$ subscript for clearity.) This color cut selects galaxies redder than a local Sbc galaxy at $z = 1$. Therefore, this study only includes galaxies that are on the red sequence at $z \sim 1$. We morphologically classified all galaxies satisfying these criteria and brighter than $z_{\rm mag} = 21.5$, distinguishing between early- and late-type galaxies using the ACS imaging. The classification was based on compactness, regularity and the presence of spiral arms. 26 out of the 52 galaxies satisfying our selection criteria we classified as early-type galaxies. We designed multi-slit masks for three different pointings, selected by the number of primary targets that could be included. Open spaces in the masks were filled with early-type galaxies satisfying the color and redshift criteria but fainter than $z_{\rm mag} = 21.5$, early-type galaxies with lower photometric redshifts and late-type galaxies with $i - z > 0.85$ and redshifts $0.8 < z_{\rm phot} < 1.4$. Switching from using ground-based $i - z$ colors from COMBO-17 to ACS $i - z$ colors from GOODS did not lead to large differences between the selected samples, although several objects changed priority.

The same selection criteria were used for the CL1252 field. However, the mask design for the CL1252 field was geometrically constrained because the primary targets were cluster galaxies at $z = 1.24$. The two brightest galaxies in the cluster are the two central galaxies, which had to be included in a single slit because of their small angular separation of $1\farcs5$. Therefore, not only the positions, but also the position angles of the designed masks were fixed. Unfortunately, only two galaxies brighter than $z_{\rm mag} = 21.5$, redder than $i - z = 0.85$ and early-type morphologies could be included, additionally to the cluster galaxies. Similarly to the CDFS masks, fillers were included.

We carried out the observations with FORS2 in MXU mode on ESO's Kueyen, one of the VLT unit telescopes. We used the 600z grism together with the OG590 order separation filter to obtain a sufficiently high spectral resolution ($\sigma \approx 80$ km s^{-1}) and to cover the wavelength range around the Balmer/4000Å break for galaxies at $z \sim 1$. The observations were carried out in series of four dithered exposures with spatial offsets of $1\farcs5$ or $2''$ and equal exposure times ranging from 14 to 30 minutes each.

In total, 51 hours of scientifically useful integration time was acquired, of which 38 hours had seeing better than $1''$. The cumulative integration time for the three pointings in the CDFS is 27 hours, with a median seeing of $0\farcs95$. The single pointing in the CL1252 field has an integration time of 24 hours, with a median seeing of $0\farcs65$. These observations were carried out during five different observing runs from September 2002 to November 2003.

The sample described in this paper consists of 38 galaxies with velocity dispersions, of which 20 are early-type galaxies at $z \sim 1$, and 18 are early-type galaxies at lower redshift, or late-type galaxies. 100% of our primary targets yielded velocity dispersions. The CL1252 observations also yielded four velocity dispersions of cluster galaxies. The FP of the 1252 cluster is discussed by Holden et al. (2005).

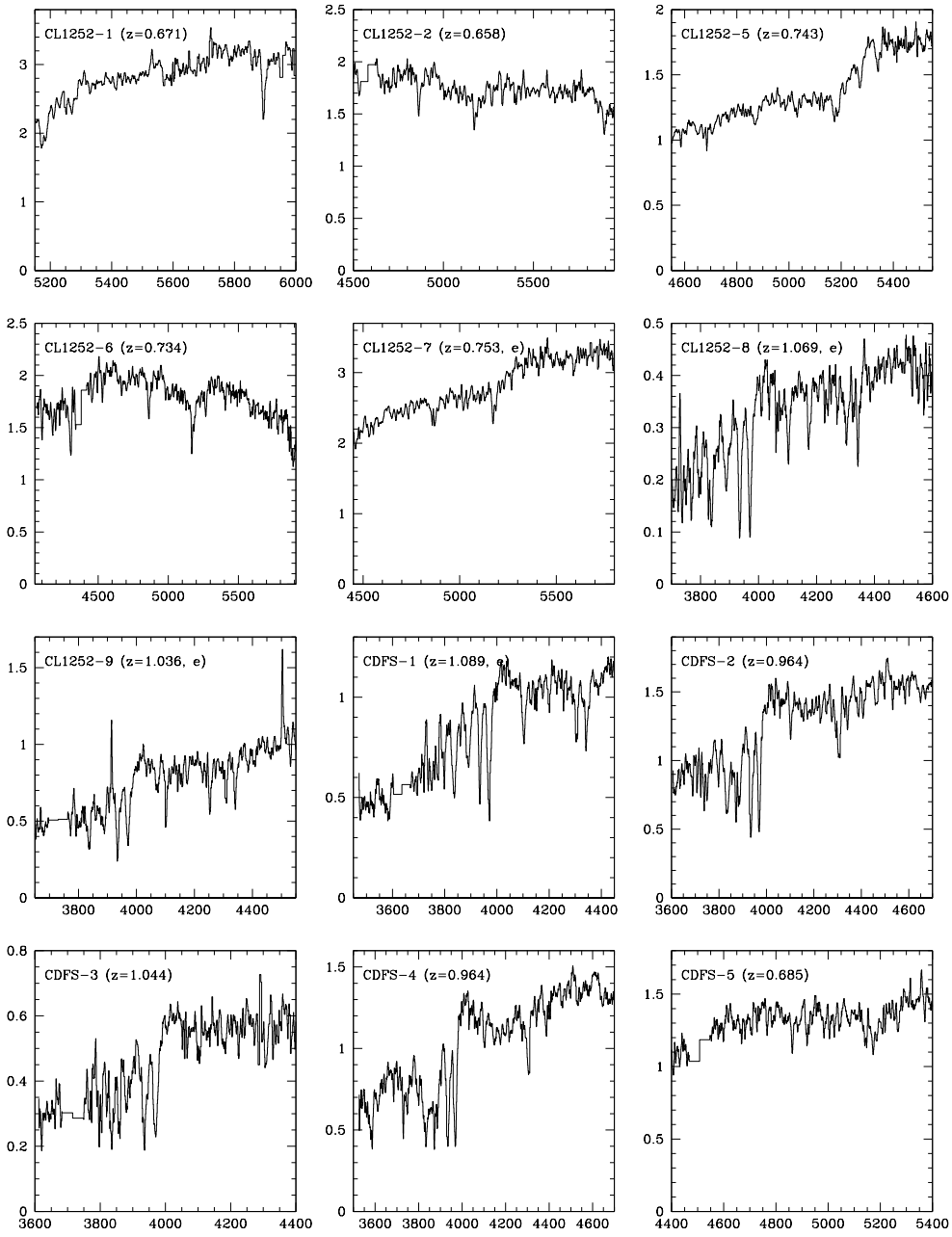

Figure 4.1: Rest-frame spectra in 8Å bins of the galaxies in our sample with early-type morphologies, used in the analysis in the subsequent sections. The area around 7600Å (observed wavelength) and the positions of bright skylines are excluded from the binning. The wavelength range differs from object to object due to differences in redshift and slit position. Every spectrum is labeled with the redshifts and an 'e' if the spectrum shows one or more emission lines.

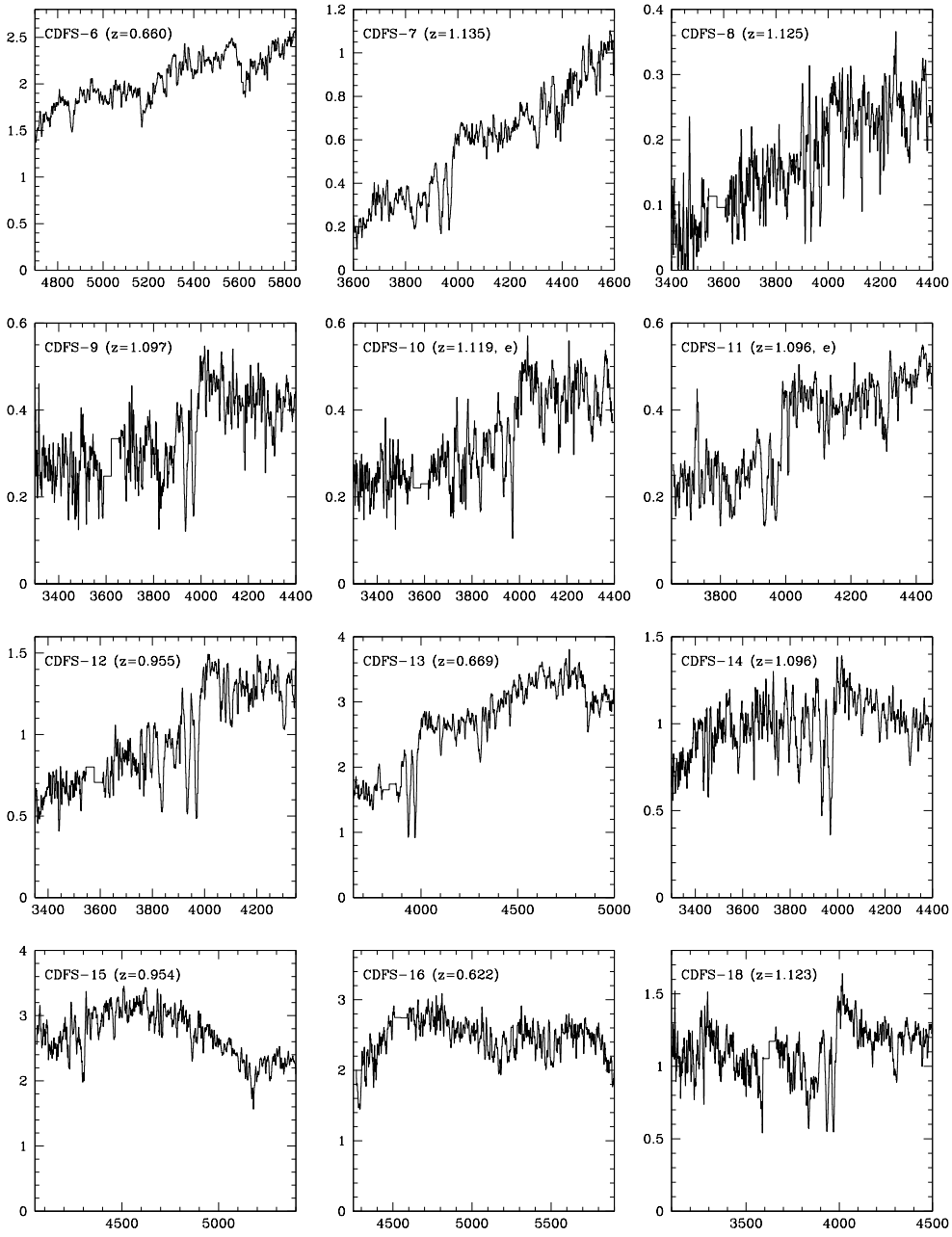

Figure 4.1: Continued

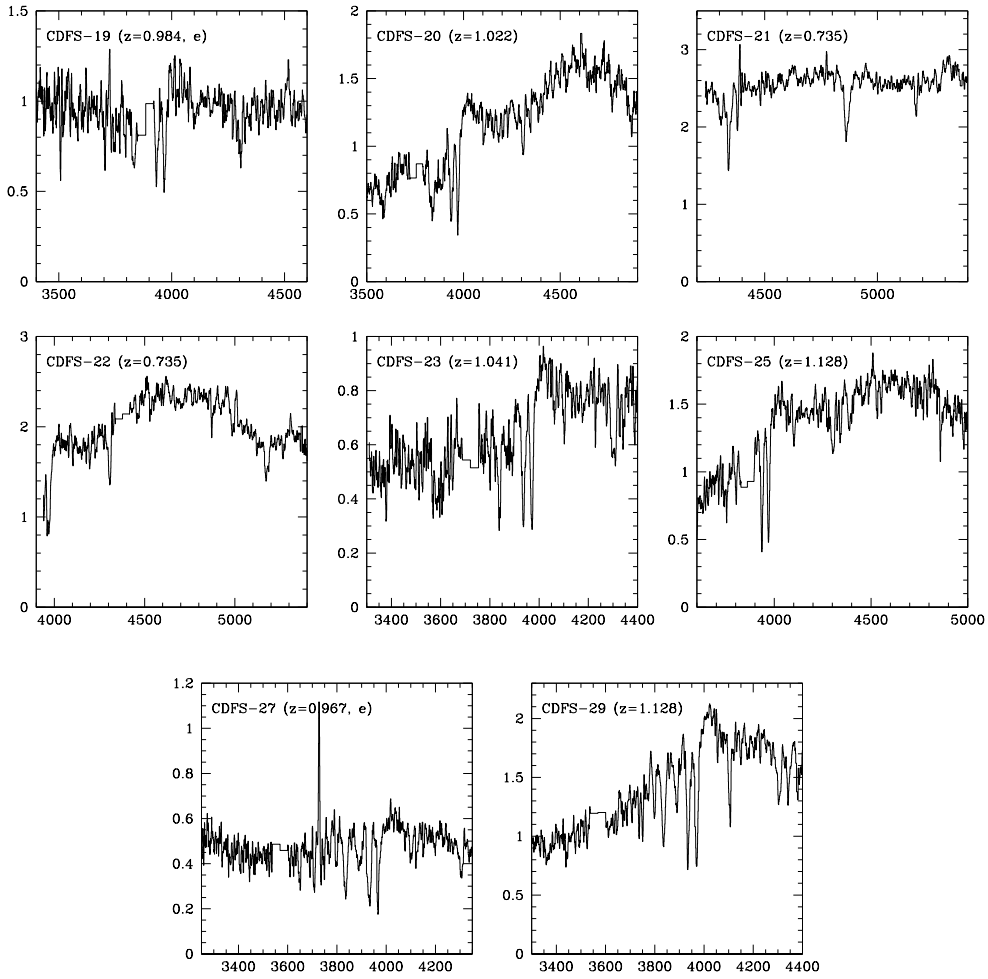

Figure 4.1: Continued

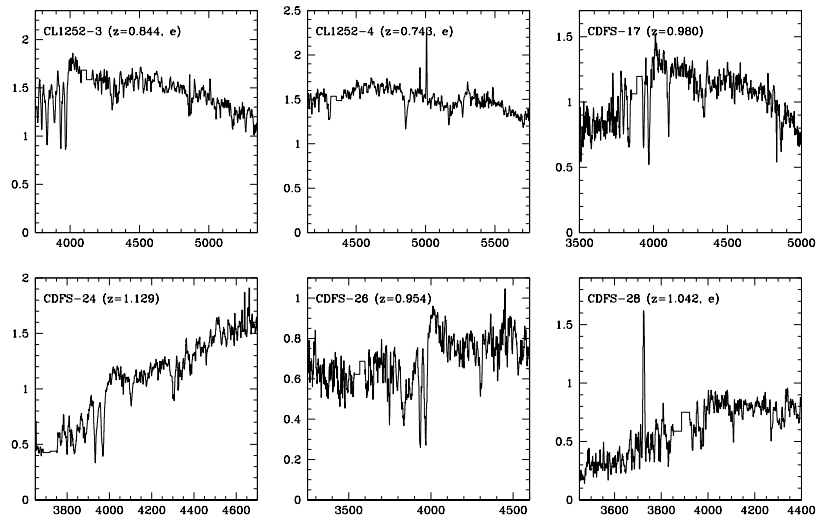

Figure 4.2: Rest-frame spectra in 8Å bins of the galaxies in our sample with late-type and irregular morphologies. These are not included in the analysis in the subsequent sections. For further explanation of the spectra, see Figure 4.1

4.2.2 Data Reduction

The spectroscopic data were reduced using standard IRAF tasks. Lamp flat fields were taken before or after each night, in sequences of five exposures. We used the sequence closest in time to the science observation. Cosmic rays were removed using the L.A.Cosmic task (van Dokkum, 2001). Afterward, all frames were checked manually. We subtracted a two-dimensional sky spectrum from each exposure, obtained by median averaging the four dithered exposures in a sequence, masking the target and secondary or serendipitous objects, if present. The atmospheric emission lines, which are bright and abundant in the observed wavelength range, were used to perform the wavelength calibration. We corrected for distortion in the spatial direction by tracing the target. All individual exposures were optimally weighted to obtain maximum S/N.

There are various atmospheric absorption features in the observed wavelength range. Because the strength and shape of these features change with airmass and atmospheric conditions we needed to correct each exposure separately. To this end we included a blue star in each of our masks, which was reduced along with the galaxy spectra. After the final combination, the regions in the galaxy spectra with atmospheric features were divided by the normalized spectrum of the blue star. Spectroscopic standard stars were used to do a relative flux calibration. One-dimensional spectra were extracted by adding those pixel rows with more than 25% of the flux of the brightest row, weighting optimally.

The smoothed one-dimensional spectra are shown in Figure 4.1. The coordinates of the objects for which we measured velocity dispersions (see Section 4.2.3) in Table 4.1. Redshifts, S/N and emission lines are given in Table 4.2.

Table 4.2: The galaxy sample

ID	e	X-ray	$z_{\rm spec}$	S/N	σ (km s^{-1})	Type	$r_{\rm eff}$ ($''$)	$\mu_{\rm eff,z}$	$z_{\rm mag}$	$i-z$	K	$J-K$
CL1252-1	-	A	0.671	48	219 ± 12	K2	0.46	21.69	20.72	0.53	17.27	1.95
CL1252-2	-	-	0.658	75	216 ± 6	G2	0.18	20.04	20.35	0.46	-	-
CL1252-3*	OIII	A	0.844	83	166 ± 7	F6	1.04	22.78	19.30	0.54	-	-
CL1252-4*	OIII	-	0.743	93	202 ± 8	F8	1.02	23.00	19.56	0.41	17.49	1.58
CL1252-5	-	A	0.743	61	251 ± 9	K1	0.36	21.07	19.91	0.53	16.98	1.81
CL1252-6	-	-	0.734	123	211 ± 5	G2	0.24	20.43	20.19	0.51	17.51	1.77
CL1252-7	OII	A	0.753	135	213 ± 5	G8	0.33	20.53	19.56	0.47	-	-
CL1252-8	OII	-	1.069	19	63 ± 13	F4	0.27	21.92	21.41	1.00	-	-
CL1252-9	-	-	1.036	18	102 ± 16	F8	0.22	21.71	21.59	0.88	-	-
CDFS-1	OII	A	1.089	27	231 ± 15	F4	0.44	21.97	20.36	1.12	17.70	1.83
CDFS-2	-	-	0.964	40	200 ± 9	G0	0.39	21.47	20.10	1.04	17.15	1.74
CDFS-3	-	-	1.044	17	300 ± 30	G4	0.15	20.39	21.14	1.07	18.29	1.75
CDFS-4	-	X	0.964	33	336 ± 18	G0	1.00	22.94	19.55	1.11	16.44	1.89
CDFS-5	-	-	0.685	32	194 ± 15	K1	0.37	21.64	20.42	0.66	18.27	1.81
CDFS-6	-	-	0.660	49	208 ± 9	G0	0.15	19.36	20.10	0.59	17.32	1.67
CDFS-7	-	-	1.135	17	232 ± 19	G4	0.74	23.32	20.58	1.14	17.26	1.97
CDFS-8	-	-	1.125	6	253 ± 70	G4	0.20	21.53	21.66	1.19	18.70	1.84
CDFS-9	-	-	1.097	8	215 ± 45	G0	0.21	21.20	21.21	1.22	18.09	1.86
CDFS-10	OII	-	1.119	9	275 ± 49	F6	0.091	19.68	21.50	1.10	18.72	1.70
CDFS-11	OII	-	1.096	10	208 ± 33	G2	0.23	21.87	21.67	1.23	17.93	1.9
CDFS-12	-	-	1.123	20	262 ± 20	G4	0.14	20.42	21.29	1.17	18.00	1.87
CDFS-13	-	-	0.980	46	247 ± 10	G4	0.20	20.93	20.17	1.05	17.22	1.83
CDFS-14	-	-	0.984	18	197 ± 21	G4	0.39	22.19	20.85	1.01	17.25	1.78
CDFS-15	-	-	0.622	55	317 ± 21	G8	0.31	20.94	20.09	0.62	17.41	1.73
CDFS-16	-	-	0.669	31	262 ± 36	G8	0.33	21.09	20.12	0.66	17.32	1.81
CDFS-17*	-	-	0.954	18	305 ± 31	F4	0.83	23.33	20.35	0.89	17.84	1.81
CDFS-18	-	-	1.096	14	324 ± 32	G0	0.51	22.21	20.3	1.20	16.98	1.92

ID	e	X-ray	$z_{\rm spec}$	S/N	σ (km s^{-1})	Type	$r_{\rm eff}$ ($''$)	$\mu_{\rm eff,z}$	$z_{\rm mag}$	$i-z$	K	$J-K$
CDFS-19	OII	-	0.955	15	229 ± 35	G4	0.34	20.35	19.30	0.49	17.53	1.56
CDFS-20	-	-	1.022	25	199 ± 15	G2	0.34	21.69	20.65	1.19	16.94	1.93
CDFS-21	-	-	0.735	56	149 ± 8	F4	0.073	18.52	20.81	0.56	18.05	1.59
CDFS-22	-	A,X	0.735	46	225 ± 11	K1	0.67	22.25	19.73	0.76	16.84	1.77
CDFS-23	-	-	1.041	13	70 ± 15	G4	0.39	22.59	21.23	1.09	18.51	1.77
CDFS-24*	-	A	1.042	25	210 ± 16	F8	1.87	24.35	19.60	0.96	17.10	2.00
CDFS-25	-	-	0.967	28	258 ± 18	F6	0.13	20.02	21.10	1.02	18.13	1.65
CDFS-26*	-	-	1.129	14	249 ± 25	G0	1.12	23.83	20.19	1.14	17.43	1.99
CDFS-27	OII	-	1.128	8	135 ± 30	F6	0.67	23.68	21.15	0.91	18.69	1.58
CDFS-28*	OII	A	0.954	12	445 ± 84	G4	0.80	23.54	20.64	0.80	18.52	1.78
CDFS-29	-	-	1.128	19	221 ± 17	F6	0.21	20.89	20.86	1.12	17.58	1.65

IDs labeled with an asterisk are late-type galaxies. An 'A' in the third column indicates an AGN, an 'X' indicates an extended X-ray source. The S/N in column 5 in per Å (1.6Å per pixel). σ is the aperture corrected central velocity dispersion measured with the best fitting stellar template. 'Type' indicates which spectral type fits best to the galaxy spectrum. The error on the effective radius may be taken from Table 4.3, which lists the physical sizes of the galaxies. $\mu_{\rm eff,z}$ is the surface brightness in the z-band at the effective radius. The errors may be taken from the errors on the surface brightness in the rest-frame B-band, given in Table 4.3.

Table 4.3: Physical parameters of the galaxy sample

ID	$z_{\rm spec}$	$\log(R_{\rm eff})$ kpc	$\mu_{\rm eff,B}$ mag/arcsec^2	$\log(M)$ $M_\odot$	$\log(M/L_B)$ $M_\odot/L_\odot$	$\Delta\ln(M/L_B)$	$U-B$	$B-I$
CL1252-1	0.671	0.58 ± 0.02	23.64 ± 0.07	11.34 ± 0.04	0.57	-0.86 ± 0.07	0.68	2.04
CL1252-2	0.658	0.18 ± 0.02	21.92 ± 0.10	10.92 ± 0.02	0.29	-1.32 ± 0.04	0.61	-
CL1252-3*	0.844	0.88 ± 0.02	24.35 ± 0.05	11.39 ± 0.04	0.15	-1.82 ± 0.06	0.42	-
CL1252-4*	0.743	0.86 ± 0.01	24.61 ± 0.06	11.54 ± 0.03	0.54	-1.01 ± 0.06	0.52	1.67
CL1252-5	0.743	0.44 ± 0.02	22.80 ± 0.10	11.31 ± 0.03	0.43	-1.20 ± 0.05	0.68	1.91
CL1252-6	0.734	0.24 ± 0.02	22.17 ± 0.06	10.95 ± 0.02	0.23	-1.45 ± 0.03	0.62	1.87
CL1252-7	0.753	0.38 ± 0.01	22.17 ± 0.04	11.11 ± 0.02	0.08	-1.88 ± 0.03	0.47	-
CL1252-8	1.069	0.33 ± 0.05	23.39 ± 0.18	10.00 ± 0.17	-0.73	-3.05 ± 0.28	0.21	-
CL1252-9	1.036	0.25 ± 0.04	23.21 ± 0.16	10.34 ± 0.13	-0.28	-2.23 ± 0.21	0.14	-
CDFS-1	1.089	0.56 ± 0.05	23.41 ± 0.17	11.35 ± 0.05	0.17	-1.81 ± 0.09	0.22	1.62
CDFS-2	0.964	0.50 ± 0.03	23.10 ± 0.09	11.17 ± 0.04	0.08	-1.89 ± 0.07	0.29	1.72
CDFS-3	1.044	0.08 ± 0.05	21.89 ± 0.22	11.10 ± 0.08	0.30	-1.42 ± 0.15	0.19	1.63
CDFS-4	0.964	0.90 ± 0.02	24.58 ± 0.09	12.02 ± 0.04	0.72	-0.89 ± 0.07	0.35	1.93
CDFS-5	0.685	0.42 ± 0.04	23.59 ± 0.13	11.06 ± 0.06	0.60	-0.65 ± 0.13	0.28	1.93
CDFS-6	0.660	0.02 ± 0.02	21.26 ± 0.10	10.73 ± 0.04	0.15	-1.53 ± 0.07	0.23	1.76
CDFS-7	1.135	0.79 ± 0.04	24.69 ± 0.13	11.59 ± 0.07	0.41	-1.35 ± 0.13	0.22	1.79
CDFS-8	1.125	0.21 ± 0.09	22.93 ± 0.36	11.08 ± 0.21	0.37	-1.23 ± 0.37	0.26	1.62
CDFS-9	1.097	0.23 ± 0.05	22.62 ± 0.21	10.97 ± 0.16	0.10	-1.76 ± 0.26	0.33	1.77
CDFS-10	1.119	-0.13 ± 0.11	21.09 ± 0.43	10.82 ± 0.14	0.05	-1.86 ± 0.23	0.17	1.52
CDFS-11	1.096	0.27 ± 0.07	23.29 ± 0.29	10.98 ± 0.13	0.30	-1.30 ± 0.23	0.35	1.81
CDFS-12	1.123	0.06 ± 0.05	21.82 ± 0.22	10.97 ± 0.06	0.10	-1.79 ± 0.11	0.24	1.64
CDFS-13	0.980	0.38 ± 0.04	22.54 ± 0.15	11.23 ± 0.03	0.15	-1.81 ± 0.05	0.27	1.72
CDFS-14	0.984	0.49 ± 0.04	23.78 ± 0.22	11.15 ± 0.09	0.33	-1.32 ± 0.14	0.22	1.62
CDFS-15	0.622	0.32 ± 0.03	22.96 ± 0.13	11.40 ± 0.06	0.93	-0.11 ± 0.09	0.36	1.96
CDFS-16	0.669	0.36 ± 0.04	23.07 ± 0.16	11.27 ± 0.11	0.72	-0.51 ± 0.13	0.29	1.95
CDFS-17*	0.954	0.82 ± 0.05	24.93 ± 0.15	11.85 ± 0.08	0.87	-0.46 ± 0.14	0.15	1.64
CDFS-18	1.096	0.62 ± 0.03	23.63 ± 0.09	11.71 ± 0.08	0.48	-1.29 ± 0.14	0.32	1.83

ID	$z_{\rm spec}$	$\log(R_{\rm eff})$ kpc	$\mu_{\rm eff,B}$ mag/arcsec^2	$\log(M)$ $M_\odot$	$\log(M/L_B)$ $M_\odot/L_\odot$	$\Delta\ln(M/L_B)$	$U-B$	$B-I$
CDFS-19	0.955	0.43 ± 0.03	21.84 ± 0.14	11.22 ± 0.12	-0.23	-2.66 ± 0.20	-0.32	1.30
CDFS-20	1.022	0.43 ± 0.05	23.24 ± 0.20	11.10 ± 0.06	0.15	-1.71 ± 0.11	0.36	1.73
CDFS-21	0.735	-0.28 ± 0.04	20.27 ± 0.14	10.14 ± 0.05	-0.32	-2.28 ± 0.10	0.23	1.57
CDFS-22	0.735	0.69 ± 0.03	24.21 ± 0.10	11.46 ± 0.04	0.65	-0.74 ± 0.07	0.30	2.09
CDFS-23	1.041	0.50 ± 0.05	24.10 ± 0.17	10.27 ± 0.17	-0.50	-2.65 ± 0.22	0.26	1.68
CDFS-24*	1.042	1.18 ± 0.05	25.86 ± 0.13	11.90 ± 0.06	0.48	-1.33 ± 0.11	0.08	1.47
CDFS-25	0.967	0.00 ± 0.08	21.63 ± 0.36	10.90 ± 0.06	0.21	-1.52 ± 0.10	0.25	1.60
CDFS-26*	1.129	0.96 ± 0.04	25.24 ± 0.11	11.83 ± 0.08	0.52	-1.22 ± 0.14	0.17	1.59
CDFS-27	1.128	0.74 ± 0.06	25.10 ± 0.17	11.07 ± 0.18	0.16	-1.62 ± 0.26	-0.06	1.34
CDFS-28*	0.954	0.80 ± 0.06	25.12 ± 0.18	12.17 ± 0.15	1.29	0.30 ± 0.27	-0.03	1.50
CDFS-29	1.128	0.24 ± 0.06	22.30 ± 0.20	11.00 ± 0.07	-0.04	-2.10 ± 0.10	0.16	1.42

IDs labeled with an asterisk are late-type galaxies. The rest-frame B-band surface brightness at the effective radius is corrected for cosmological surface brightness dimming. The error on M/L in solar units is the same as the error on M. $U-B$ and $B-I$ are rest-frame colors.

4.2.3 Velocity Dispersions

Velocity dispersions are obtained by fitting template spectra to the observed galaxy spectra. The fitting method is extensively described by van Dokkum & Franx (1996). The continua of both the observed and the template spectra are filtered out in Fourier space and the template spectrum is convolved with a Gaussian to match the width of the absorption lines in the galaxy spectrum. The part of the galaxy spectrum used in the fit is as large as possible. Therefore, our measurements do not rely on a few high S/N absorption features.

As templates we use Coudé spectra of 132 stars with the appropriate wavelength range from the sample constructed by Valdes et al. (2004), with a spectral range from F0 to M6, including both very low and high metallicity stars, and different luminosity classes. These spectra have a FWHM resolution of about 1Å. Each stellar spectrum needs to be smoothed to each galaxy spectrum separately before being re-binned. A second order function is fitted to the width of atmospheric emission lines as a function of wavelength to obtain the spectral resolution to which the template spectra are smoothed.

When fitting the galaxy spectra, we weight with the inverse of the sky brightness, and we mask the region around the atmospheric A band at 7600Å. The spectrum above 9300Å is omitted because of the strong atmospheric absorption, the ever increasing brightness of the sky emission lines and the decreasing system throughput.

After performing the fit for a small number of templates, masking and weighting as described, we check the residuals from the fit. Regions with emission lines, large sky line residuals and remaining data artifacts such as cosmic ray remnants are masked if present. We then apply fit the galaxy spectrum with all template spectra. We check whether the obtained parameters change strongly if one or two strong features are masked out, but we conclude that this generally is not the case: excluding the strongest features from the fit increases the χ^2-value but does not change the results significantly in most cases. For some spectra, however, including Balmer lines in the fit leads to different results, probably because unseen emission line contributions contaminate these features. For low quality spectra ($S/N \leq 10$ per 1.6Å pixel in the extracted, one-dimensional spectra) the contributions of Balmer lines or other strong features can hardly be checked because excluding these strong features leaves insufficient signal to obtain a proper fit. Therefore, we exclude objects with $S/N < 12$ spectra from our analysis, but we mention the effect of including these.

For all spectra with $S/N \geq 12$ the random errors are below 3% for $\sigma > 200\mathrm{km\ s^{-1}}$, and below 5% for $\sigma < 200\mathrm{km\ s^{-1}}$. Adding a systematic uncertainty (including template mismatch and the error on the resolution of the galaxy spectra) of about 10% for $S/N = 10$ spectra and 2% for the highest S/N spectra the total errors range from 3% to 17% with a median of 7.5% for our sample of early-type galaxies with $S/N \geq 12$. Some galaxies have measured velocity dispersions that are not much larger than the resolution of the spectra. Although these are included in the analysis, they play no important role in the derivation of our results.

The best fitting stellar spectral type and the measured velocity dispersion are listed in Table 4.2. These velocity dispersions are aperture corrected to a $3''4$ diameter circular aperture at the distance of Coma as described by Jorgensen, Franx & Kjærgaard (1995). This correction ranges from 5% to 7%.

4.3 Photometry

4.3.1 Profile Fitting and Morphologies

The ACS provides us with an unprecedented combination of deep and high resolution imaging. The spatial resolution (FWHM) at $z = 1$ is $0.8\mathrm{kpc}$, allowing us to accurately measure the effective radii of early-type galaxies at this redshift, which typically are a few kpc. We use the single, unstacked, flat-fielded frames publicly available through the HST MAST archive. For the CDFS the number of frames for different positions ranges from 8 to 24 (with $530\mathrm{s}$ exposure time each). For the CL1252 field the number of frames ranges from 10 to 40 (with $1200\mathrm{s}$ exposure time each), but is mostly 10 as only the center of the cluster has 40 overlapping images.

For each galaxy each individual z band image is fitted by $r^{1/n}$-models (with $n = 1, 2, 3, 4$) convolved by a position dependent PSF created with TinyTim (Krist, 1995), measuring r_{eff} (the effective radius), μ_{eff} (the surface brightness at r_{eff}), the position angle and the ellipticity. Each individually derived set of model parameters is distortion corrected by calculating the pixel scales in the x- and y-directions, using the polynomial distortion coefficients available through the WWW[2]. We then average the results and compute the measurement error from the scatter. The error is generally about 6% in r_{eff}, but the combination of the uncertainty in r_{eff} and μ_{eff} is such that it is directed almost parallel to the local FP. The error relevant to the offset from the FP is typically 2%. Thus, uncertainties in the offset from the local FP are dominated by the uncertainty in σ, of which the error is pointed almost perpendicular to the FP. The effective radii and surface brightnesses are given in Table 4.2. For consistency with earlier studies, these are the values obtained from fitting a de Vaucouleur profile in our analysis.

To transform the observed z band surface brightnesses to the rest-frame B band, we use the technique described by van Dokkum & Franx (1996), using the templates from Coleman, Wu & Weedman (1980) and observed colors (see Section 4.3.2) to interpolate between the pass-bands. The calculated rest-frame B band surface brightnesses only depend very weakly on the spectral type of the template used. The typical difference found for using the Sbc template instead of the E template is less than $0.02\ \mathrm{mag}$. The transformations are a function of redshift. As an example we give the transformation (based on the E template) for a galaxy at $z = 1$:

$$B_{\mathrm{z}} = z + 0.165(i - z) + 1.398 \tag{1}$$

Physical sizes and rest-frame B-band surface brightnesses are given in Table 4.3.

Figures 4.3 and 4.4 show the combined residuals of the $r^{1/4}$-fits along with the color images of the 38 galaxies with velocity dispersions. Figure 4.3 shows the early-type galaxies, Figure 4.4 the late-type galaxies. Two numbers are used to characterize the magnitude of the residuals. At the upper right of each residual image the absolute value of the flux in the asymmetric part of the residual is given as a percentage of the total flux of the galaxy, obtained by subtracting the residual rotated by 180 degrees from the residual itself. In the upper left the absolute value of the flux in the symmetric part of the residual is given as a percentage of the total flux of the galaxy. We

[2]http://www.stsci.edu/hst/acs/analysis/PAMS

find that the asymmetric residual is a good indicator of morphology. Our final morphological qualification is a combination of the magnitude of the asymmetric residual and visual inspection of the cause of the asymmetry. Some of the early-type galaxies (Figure 4.3) have significant asymmetric residuals, but these are caused by features on a very small scale, in the centers of the galaxies, i.e. not by features attributed to spiral arms or other large scale irregularities. The late-type galaxies (Figure 4.4) have large asymmetric residuals, caused by large scale structures like spiral arms. We note that the Sercic number does not distinguish well between late- and early-type galaxies. For example, the most massive galaxy in our sample has n=2 and some galaxies that we classify as late-type galaxies have n=4.

4.3.2 Colors

We supplement the ACS imaging with ground-based optical and near-IR imaging from FORS2 and ISAAC on the VLT and SOFI on the NTT (Vandame et al., In preparation). GOODS ACS imaging of the CDFS provides photometry in the b, v, i, and z bands (data release version 1.0), and ESO's imaging survey[3] provides SOFI and ISAAC imaging in the J and K bands. Since the CDFS is not entirely covered by ISAAC we use the SOFI data for the objects outside the ISAAC pointings. All images were smoothed to match the resolution of the K band data with the worst seeing, which is $0\farcs8$ for the ISAAC imaging and $1''$ for the SOFI imaging. The photometric differences between the ISAAC and SOFI datasets are small (< 0.01 mag), since the zero-points of the ISAAC data are based on SOFI photometry. For the CL1252 field we use optical imaging from ACS (i and z) and FORS2 (B, V, and R) and near-IR imaging from ISAAC (J and K, Lidman et al., 2004)). Again, all images were smoothed to match the ground-based data with the worst seeing, which is $0\farcs6$ in the B band.

We measure the flux in each band for each of our spectroscopic targets within several apertures with different radii ($1/2/3r_{\rm eff}$ and $0\farcs8$). Contaminating objects within the aperture are masked. We choose to use the fluxes measured within a radius of $2r_{\rm eff}$, with a minimum of $0\farcs8$, trading off between the measurement accuracy and the amount of contamination. The $i-z$ and $J-K$ colors are given in Table 4.2, as well as total *AUTO* z band and K band magnitudes, as obtained with SExtractor (Bertin & Arnouts, 1996).

The availability of near-IR photometry not only allows us to compute rest-frame $U-B$ colors, but also rest-frame $B-I$ colors. To transform the observed colors to rest-frame $U-B$ and $B-I$ we use the same method as used to calculate rest-frame B band surface brightnesses (see Section 4.3.2). For $z=1$, using the E template, the transformation is:

$$(U-B)_{\rm z} = 0.836(i-z) + 0.276(v-i) - 1.111 \quad (2)$$

$$(B-I)_{\rm z} = z - K + 0.165(i-z) - 0.513(J-K) - 0.282 \quad (3)$$

Rest-frame colors are given in Table 4.3.

[3] http://www.eso.org/science/eis/

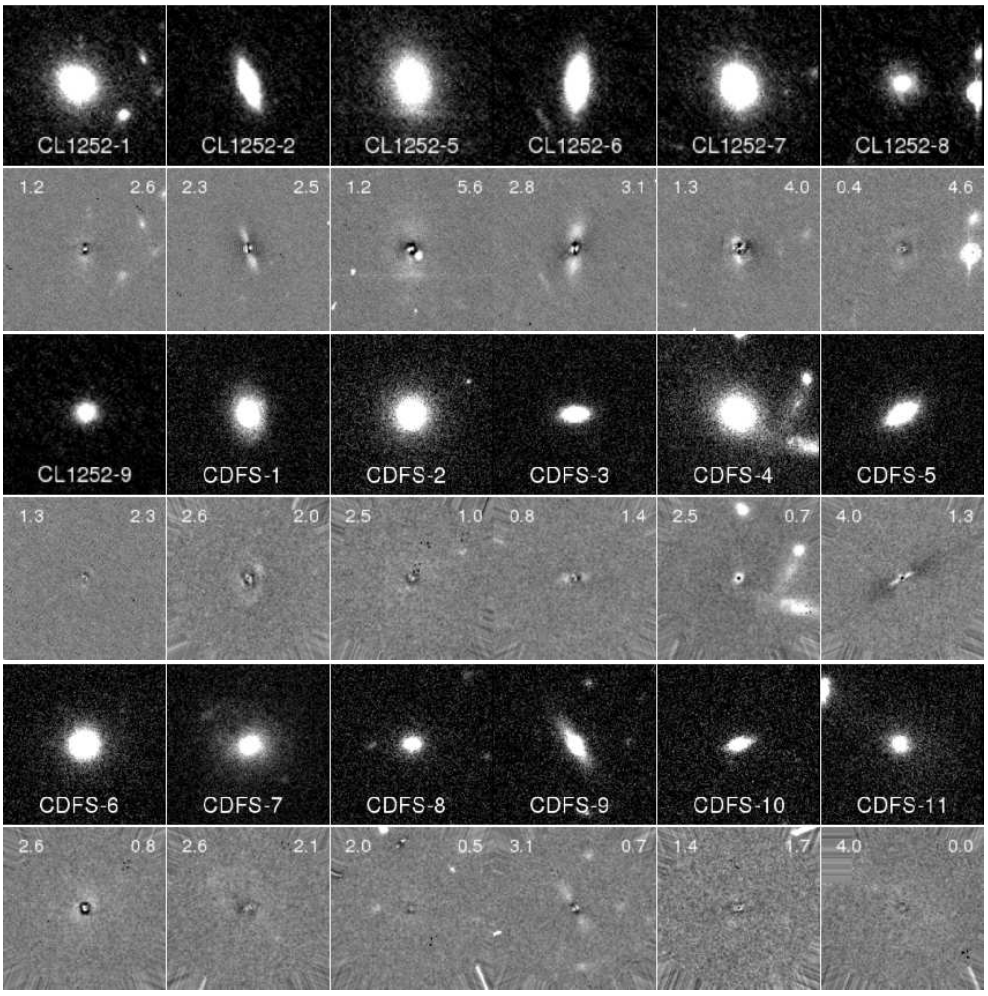

Figure 4.3: Color images and $r^{1/4}$-profile fit residuals of the early-type galaxies used in the analysis in the subsequent sections. The color images of the objects in the CL1252 field consist of i and z band images, the color images of the objects in the CDFS consist of v, i and z band images. The residuals are shown in the z band for all objects. The boxes are $5''.4$ on a side. The residual images are not distortion corrected, which causes the small dissimilarities between the color and residual images. The numbers at the upper left and right of the residual images are, respectively, the symmetric and asymmetric fluxes in the absolute residuals within two effective radii, expressed as percentages of the total fluxes of the galaxies within the same radius.

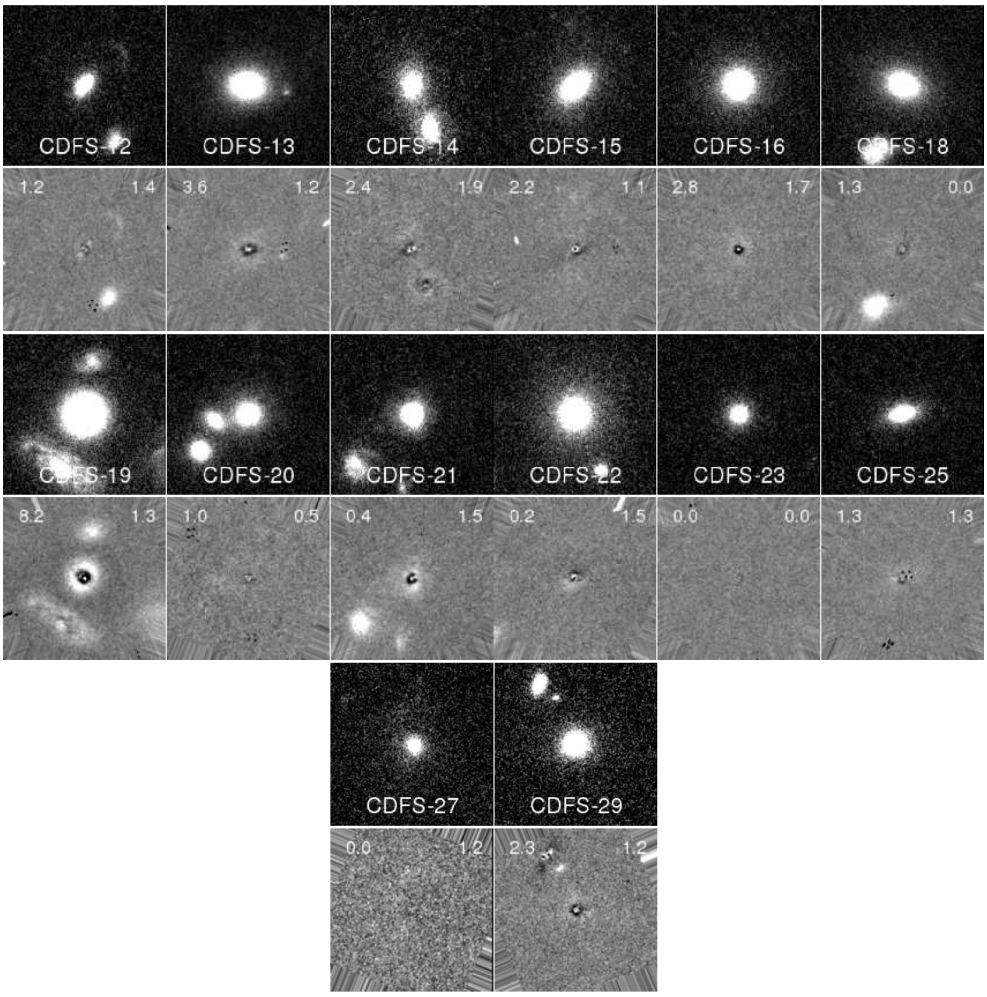

Figure 4.3: Continued

4.3.3 X-ray Data

For both the CDFS and the CL1252 field deep X-ray data from Chandra are available, such that we can check for the presence of AGN in our galaxy sample. Giacconi et al. (2002) and Alexander et al. (2003) provide catalogs of the CDFS data. The Chandra data of the CL1252 field is described by Rosati et al. (2004), who also constructed a point source catalog. Eight galaxies in our sample of 38 are identified as AGN, based on their large X-ray luminosities (typically $> 10^{42}$erg s^{-1}). Five of these are early- type galaxies, of which two have emission lines in their spectra. Besides the eight AGN, two galaxies in our sample are identified as extended X-ray sources. This X-ray radiation is accounted for by diffuse halo gas. The X-ray luminosities of CDFS-4 and CDFS-22 are 7.15×10^{41} erg s^{-1} and 3.42×10^{42} erg s^{-1}, respectively. It is not surprising that CDFS-4 and CDFS-22 turn out to be two of the most massive galaxies in our sample. Also, CDFS-22 is one of the galaxies with an AGN. The X-ray properties of our sample of galaxies are given in Table 4.2.

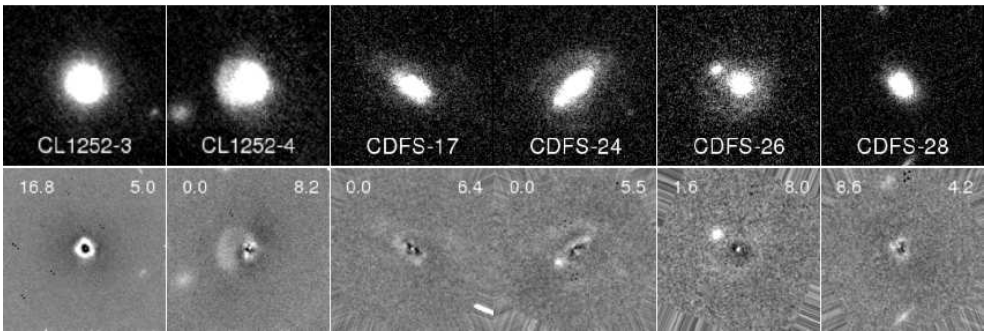

Figure 4.4: Color images and $r^{1/4}$-profile fit residuals of the galaxies with late-type or irregular morphologies. These galaxies have measured velocity dispersions but are not included in the analysis in the subsequent sections. For an explanation of the images and the numbers, see Figure 4.3

4.4 Masses, Mass-to-Light Ratios and Stellar Populations of Early-Type Galaxies at $z = 1$

4.4.1 The Fundamental Plane

Jørgensen, Franx & Kjærgaard (1996) have shown that the FP for cluster galaxies in the local universe can be described by

$$\log R_{\rm eff} = 1.2 \log \sigma - 0.83 \log I_{\rm eff,B} + \gamma, \tag{4}$$

where $R_{\rm eff}$ is the effective radius in $\rm kpc$, σ the central velocity dispersion in $\rm km\ s^{-1}$, $I_{\rm eff,B}$ the surface brightness in the B band ($\log I_{\rm eff,B} = -0.4 \mu_{B_z}$), and γ the intercept. The values of the coefficients are derived from the early-type galaxies in ten nearby clusters, and imply that mass and M/L scale as $M/L_B \propto M^{0.28}$. From the sample of Faber et al. (1989) we derived that the intercept of the FP lies lower by 0.04 in the projection given above. The offsets of the high-z galaxies are computed using a local FP with coefficients from Jørgensen et al. (1996) but with the intercept derived from the Faber et al. (1989) sample.

Besides the form of the local FP, we need a large sample of local field early-type galaxies, for example to address issues such as selection effects. We construct our local field sample as in Bernardi et al. (2003): we take early-type galaxies from the Sloan Digital Sky Survey and include those with less than 10 neighbors brighter than $M_i = -20.55$ and closer than $1.4\ \rm Mpc$. We convert the rest-frame g and r band surface brightnesses to a B band surface brightness using the conversion given by Jørgensen et al. (1996). As we need the surface brightness in the g and r bands at the same radius, and Bernardi et al. derive effective radii separately for each band, we compute the surface brightness in the r band at the effective radius as measured in the g band. We note that the FP coefficients as derived by Bernardi et al. are different from those from Jørgensen et al. (1996), but this does not lead to different results. The reason we use the FP coefficients as derived from the Faber et al. data, and not the Bernardi et al. data, is that Faber et al. use B-band photometric data.

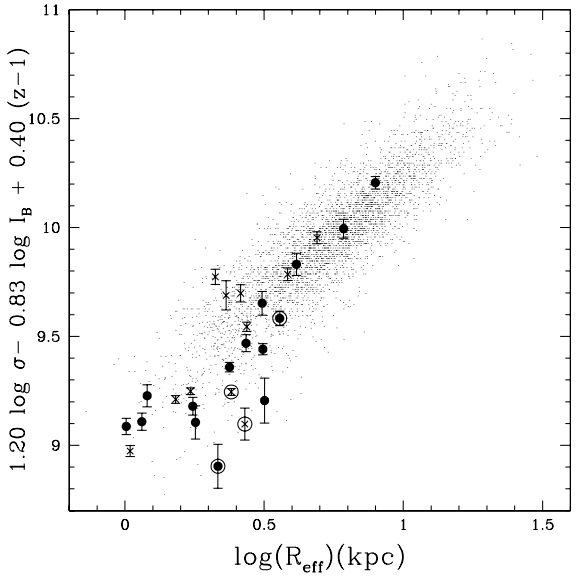

Figure 4.5: The Fundamental Plane of our sample of early-type galaxies compared to the field early-type galaxy sample from SDSS (small dots, Bernardi et al. 2003). The primary sample, early-type galaxies at $z \sim 1$ that satisfy all of our selection criteria, are indicated by the filled symbols. The crosses are fillers, mainly galaxies at redshifts $z \sim 0.7$. Encircled objects have one or more emission lines in their spectra. The surface brightness, I_B, of every galaxy in this figure is corrected for evolution to a value it would have at $z = 1$, assuming $\Delta \ln(M/L_B) = -1.12z$, which is the evolution of massive cluster galaxies. The FP already existed at $z = 1$ for a large range in size.

In Figure 4.5 we show the FP of the SDSS galaxies and our sample, where the surface brightnesses of all galaxies are transformed to the value they would have at $z = 1$, assuming luminosity evolution found for massive cluster galaxies, $\Delta \ln (M/L_B) = -1.12z$. This value for the M/L evolution of massive cluster galaxies is derived from compiling all existing data in the literature for galaxies more massive than $M = 2 \times 10^{11} M_{\odot}$ (van Dokkum & Franx, 1996; Kelson et al., 2000; van Dokkum & Stanford, 2003; Wuyts et al., 2004; Holden et al., 2005). Our field sample shown in Figure 4.5 includes all early-type galaxies with spectra with $S/N \geq 12$. This is also the sample used in the analysis throughout the rest of the paper, and in the subsequent figures. As can be seen, the FP already existed at $z = 1$ for a large range in size. At low masses outliers occur, but the interpretation is not straightforward, as selection effects play a major role in this regime (see Section 4.3).

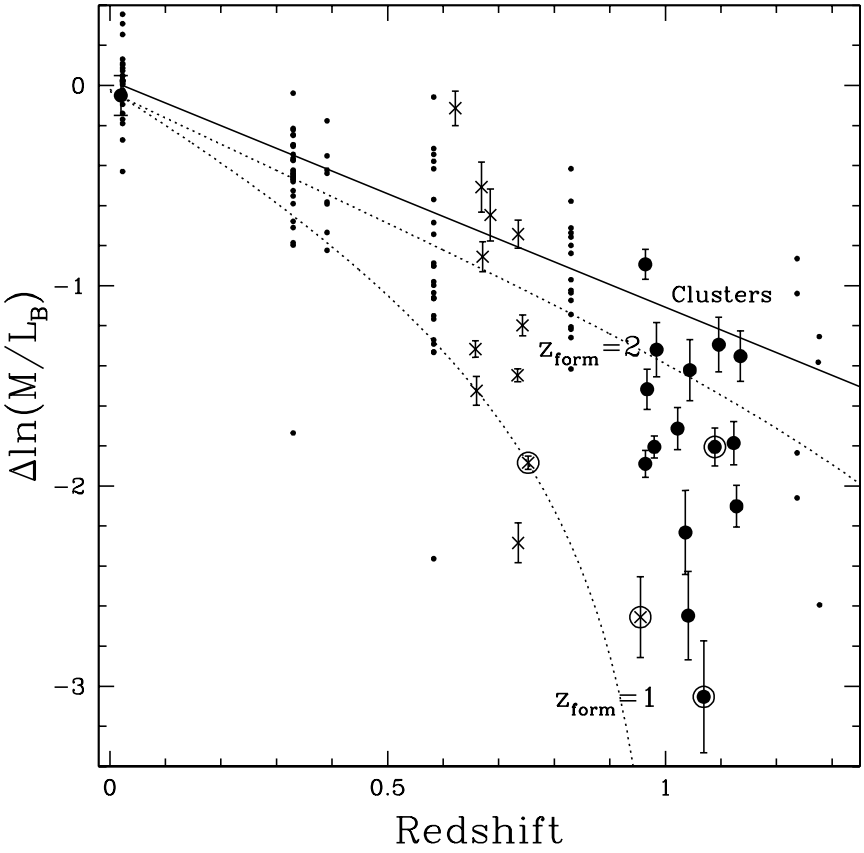

Figure 4.6: The offset from the local FP in the rest-frame B band for individual cluster galaxies taken from the literature (small dots) and the early-type galaxies with high S/N spectra in our sample. We distinguish, as in Figure 4.5, between the primary sample (filled symbols) and the fillers (crosses). The red symbols are galaxies with masses $M > 2\times10^{11}M_{\odot}$. The blue symbols are less massive galaxies. The cluster samples are taken from Jørgensen et al. (1996), Kelson et al. (2000), van Dokkum & Franx (1996), Wuyts et al. (2004), Holden et al. (2004), and van Dokkum & Stanford (2003). The solid line is $\Delta\ln(M/L_B) = 1.12z$, which is the best fitting straight line for the evolution of cluster galaxies with masses $M > 2\times10^{11}M_{\odot}$. The dotted lines are model tracks for a single stellar population with formation redshifts 1 (lower line) and 2 (upper line) (see text for a more detailed explanation). These model tracks are forced to go through the black point at $z = 0.02$ which represents the field galaxies in the sample of Faber et al. (1989). The range in offsets from the local field FP is large, but there is a strong correlation with mass. Massive field galaxies evolve as fast as equally massive cluster galaxies, while less massive galaxies evolve faster.

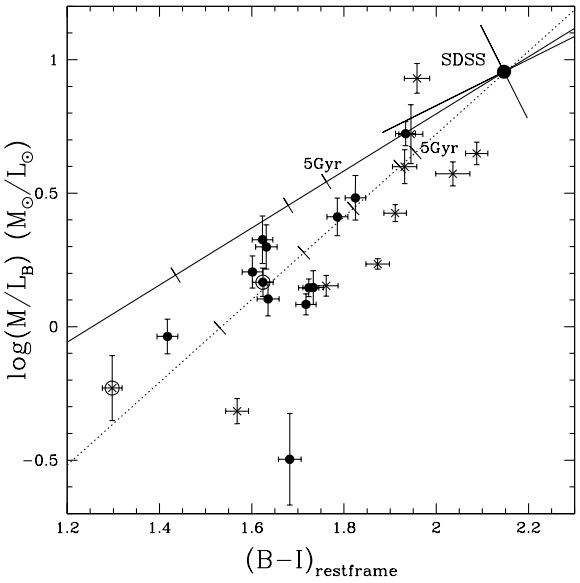

Figure 4.7: Rest-frame $B-I$ color versus M/L_B for our early-type galaxy sample. For an explanation of the symbols, see Figure 4.6. The large symbol at the upper right indicates the median $B-I$ and M/L_B of the massive galaxies ($M > 2 \times 10^{11} M_\odot$) in the SDSS field early-type galaxy sample. The orientation of the distribution around the median values and the amount of scatter are indicated by the tilted error bars. The dotted line is a solar metallicity Bruzual-Charlot model for a single stellar population. The solid line is a model with exponentially declining star formation ($\tau = 1$ Gyr). Both model tracks are shifted vertically to match the SDSS data point. Model ages are indicated by ticks at intervals of 1 Gyr. The correlation between M/L and color implies that the observed scatter in M/L is real, and can be ascribed to age differences between the stellar populations of the galaxies. Our $i-z \geq 0.86$ color selection limit roughly corresponds to $B-I \geq 1.1$ according to the Bruzual-Charlot models. This shows that our selection criterion only excludes galaxies with ages less than 1 Gyr, and does not affect our conclusions regarding the massive, red galaxies.

4.4.2 Evolution of M/L with redshift

The offset of high redshift galaxies from the local FP is interpreted as a difference in M/L as compared to equally massive local galaxies (e.g., van Dokkum & Franx, 1996). Figure 4.6 shows the offsets of our field galaxy sample in $\Delta \ln(M/L_B)$ as a function of redshift. The values are listed in Table 4.3. Cluster samples from the literature are also shown. The galaxies in our sample seem to evolve faster than the galaxies in the cluster samples, and the scatter in $\Delta \ln(M/L_B)$ is large. Before we interpret the scatter and the apparent difference between field and cluster galaxies, we need to investigate the origin of the scatter. In Figure 4.7 we show M/L_B as a function of the rest-frame $B-I$ color. Galaxies with low M/L are bluer than galaxies with high M/L, as expected from the stellar population models shown in the figure. In Figure 4.8 we show a similar relation between rest-frame $U-B$ and M/L_B, but

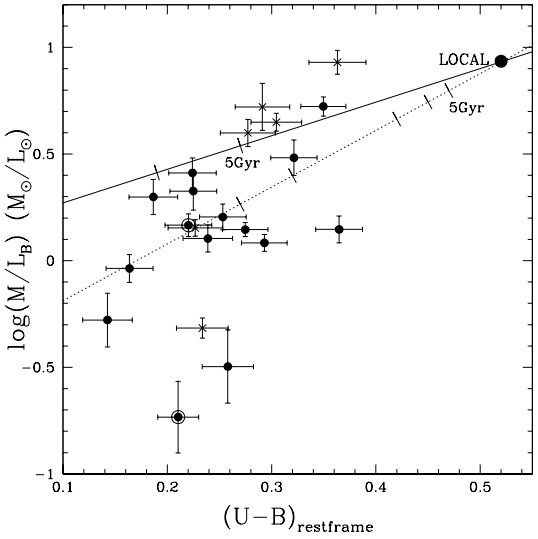

Figure 4.8: Rest-frame $U-B$ color versus M/L_B for the early-type galaxy sample. For an explanation of the symbols, see Figure 4.6. The 'Local' data point is taken from Gebhardt et al. (2003). There is a similar relation as in Figure 4.7, but it is less clear because the range of colors in much smaller in $U-B$ than in $B-I$. Our $i-z \geq 0.86$ color criterion corresponds to $U-B \geq 0.07$ at $z=1$, which demonstrates that this criterion would only exclude the most extremely blue galaxies (with ages well below 1 Gyr).

in this case the correlation is less clear, due to the fact that the range of $U-B$ colors is much smaller than the range of $B-I$ colors, and probably also because $U-B$ is more sensitive to small variations in the star formation history. Considering the correlation between color and M/L and the fact that M/L evolves with redshift, one expects that color evolves with redshift as well. In Figure 4.9 we show $B-I$ as a function of redshift; note the strong similarities between Figures 4.6 and 4.9. The strong correlation between color and M/L, and the similarity in M/L evolution and color evolution confirm that the observed evolution and scatter of M/L are intrinsic, and not due to measurement errors.

We calculate the evolution of M/L of our field sample by performing a linear fit and minimizing the mean deviation, weighting by the inverse of the error, and forcing the fit to go through the $z=0.02$ data point derived from the Faber et al. (1989) sample. We separately consider the evolution of the primary sample, which contains the galaxies satisfying all of our selection criteria. We find that the average evolution of our entire early-type galaxy sample is $\Delta \ln(M/L_B) = (-1.75 \pm 0.16)z$ ($(-1.72 \pm 0.15)z$ for the primary sample alone), which is significantly faster than the evolution found for cluster galaxies, which is $\Delta \ln(M/L_B) = (-1.28 \pm 0.08)z$ (van Dokkum & Franx, 1996; Kelson et al., 2000; van Dokkum & Stanford, 2003; Wuyts et al., 2004; Holden et al., 2005). The scatter in $\Delta \ln(M/L_B)$ is 0.58 for our field galaxy sample (0.54 for the primary sample), and 0.28 for the MS1054 cluster sample (Wuyts et al., 2004).

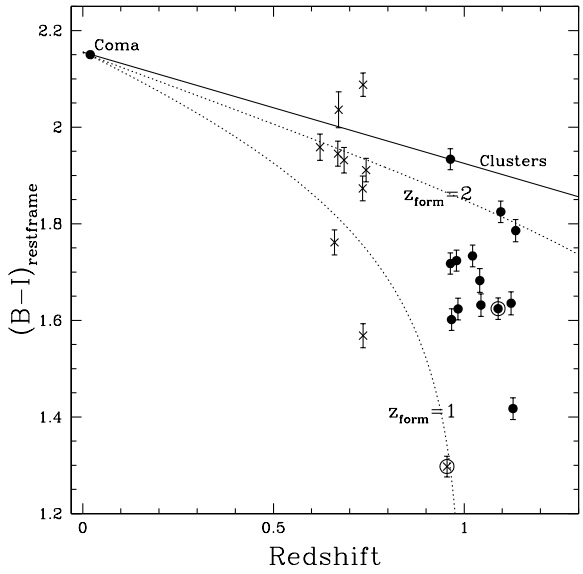

Figure 4.9: The evolution of the rest-frame $B-I$ color with redshift. For an explanation of the symbols, see Figure 4.6. As already suggested by the tight relation between $B-I$ and M/L in Figure 4.7, the evolution of color with redshift is very similar to the evolution of M/L with redshift. Massive galaxies are the reddest in the local universe, and their color evolves slower than the color of low mass galaxies. Also, the color of the most massive field galaxies is very similar to the color of massive cluster galaxies.

Figure 4.5 suggests that the M/L evolution may depend on galaxy mass, as galaxies with small $r_{\rm eff}$ and low σ tend to lie lower with respect to the local FP as compared to galaxies with large $r_{\rm eff}$ and high σ. This was also found for cluster galaxies by Wuyts et al. (2004). We estimate M and M/L in solar units as described by van Dokkum & Stanford (2003). The values are listed in Table 4.3. We explore the mass dependence by color coding the galaxies in Figure 4.6 according to their masses. Red points are galaxies with masses larger than $M = 2\times10^{11}M_{\odot}$; blue points are galaxies that have masses lower than $M = 2\times10^{11}M_{\odot}$. There is a striking difference between low and high mass galaxies. For galaxies with masses $M > 2\times10^{11}M_{\odot}$ we measure $\Delta\ln(M/L_B) = (-1.20\pm0.18)z$ for our field sample and $(-1.12\pm0.06)z$ for the cluster samples. For the massive galaxies in the primary sample alone we find $\Delta\ln(M/L_B) = (-1.26\pm0.18)z$. The observed scatter is decreased to 0.34 for the field sample (0.32 for the primary sample), and to 0.28 for the cluster samples. When changing this mass cut to $3\times10^{11}M_{\odot}$, as is done by Wuyts et al. (2004), but thereby limiting the number of galaxies in our sample to four, we find $(-1.12\pm0.13)z$ and $(-0.99\pm0.10)z$ for our sample and the cluster samples, respectively. We conclude that for high-mass galaxies, there is no difference between the cluster samples and our field sample. The galaxies with masses $M < 2\times10^{11}M_{\odot}$ in our sample evolve much faster: $\Delta\ln(M/L_B) = (-1.97\pm0.16)z$ ($(-1.90\pm0.17)z$ for the primary sam-

ple alone). We verify that these results do not change if galaxies with spectra with $S/N < 12$ are included as well. Therefore, the accuracy of our results is not limited by the quality of the velocity dispersions.

In Figures 4.6 and 4.9 we show evolutionary tracks for a single stellar population for formation redshifts $z = 1$ and 2. This very simple model assumes that luminosity evolves with time as $L \propto (t - t_{\rm form})^{\kappa}$, where κ is derived from stellar population models (see van Dokkum et al., 1998, for more details). These tracks indicate a large spread in formation redshifts. We note, however, that κ is sensitive to the IMF. Here we use a single stellar population from Bruzual & Charlot (2003) with a Salpeter IMF and solar metallicity, which yields $\kappa = 0.97$ in the B band and 0.43 in the I band. According to this model the massive galaxies have high luminosity weighted formation redshifts ($z \geq 2$), whereas less massive galaxies in our sample have lower formation redshifts ($1 < z < 2$).

4.4.3 The relation between M and M/L and the role of selection effects

Figure 4.10 illustrates the tight relation between mass and M/L_B. We also show the SDSS field sample described in Section 4.1. M and M/L_B are calculated as described by van Dokkum & Stanford (2003): $\log M = 2\log\sigma + \log r_{\rm eff} + 6.07$; $\log M/L_B = 2\log\sigma + 0.4(\mu_{\rm eff,B} - 27) - \log r_{\rm eff} - 1.29$. The M/L of all galaxies have been corrected for evolution as derived from massive cluster galaxies, $\Delta \ln (M/L_B) = -1.12z$.

At $z = 1$, the relation between M/L and M seems much steeper than in the local universe. However, we have to take selection effects into account. Since we selected our sample in the z band, we can transform our magnitude limit into a luminosity limit in the rest-frame B band, which is close to the observed z band at $z \sim 1$ (the median redshift of our sample of 16 $z \sim 1$ galaxies is $z = 1.04$). Because this luminosity limit only applies to our primary sample, this discussion does not involve the fillers (mainly galaxies at $z \sim 0.7$). Afterward, we will comment on these galaxies.

We first test whether the observed distribution can be fully explained by selection effects, assuming that the slope and the scatter of the FP do not evolve. The probability that the observed distribution is drawn from a population with the same distribution as the SDSS galaxies is 0.14%, if the M/L evolution is the same for all galaxies. Therefore, the slope evolves, the scatter evolves, or both. If there is an age difference between high and low mass galaxies, the scatter will most probably also evolve differently for high and low mass galaxies. We cannot exclude with high confidence that the observed distribution of M/L is due to a larger scatter at high redshift: if the scatter in M/L at $z = 1$ is twice as large as in the local universe, the probability of a non-evolving slope is 8.0%. However, we see no evidence for an increase in the scatter at the high mass end, where selection effects do not play a role. Hence, if the scatter evolves, this is only true for galaxies with masses $M \sim 10^{11} M_{\odot}$. Since the increased scatter is most likely caused by young ages, low mass galaxies would have lower M/L, and hence the slope of the relation would also be changed. We consider these findings as strong evidence for mass-dependent evolution of early-type galaxies. To confirm that we observed a change in the slope of the FP, deeper and larger surveys are needed.

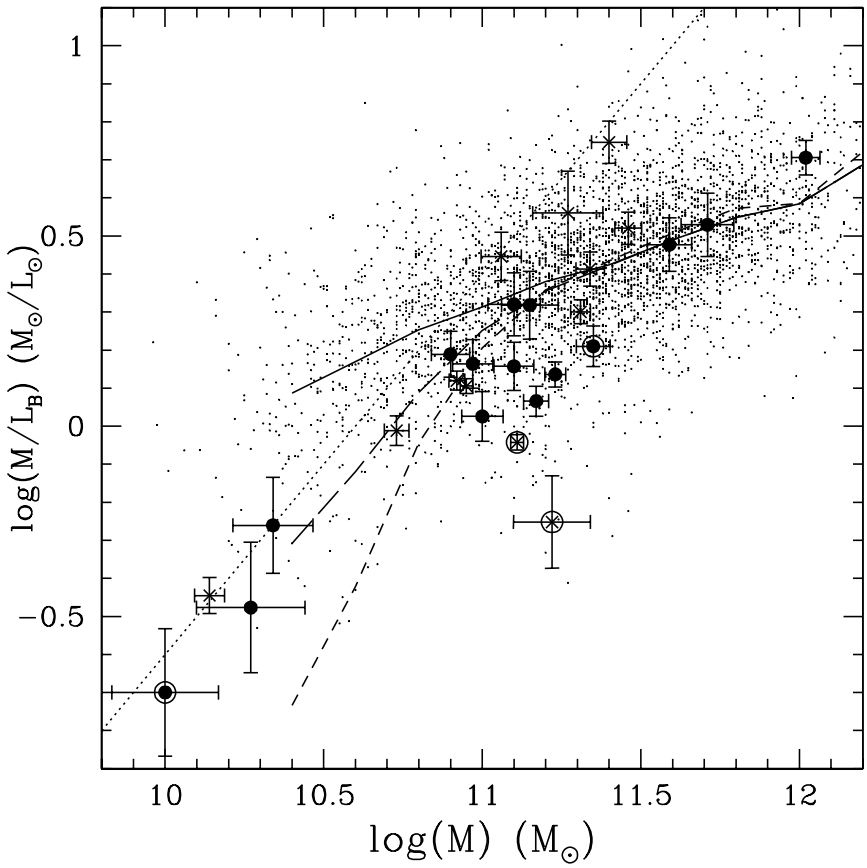

Figure 4.10: M versus M/L_B as derived from the FP for the early-type galaxies in our sample and for the nearby sample from the SDSS. For an explanation of the symbols, see Figure 4.6. All data points have been corrected for M/L evolution as found for massive cluster galaxies, $\Delta \ln(M/L_B) = -1.12z$, normalizing at $z = 1$. The dotted line indicates our magnitude limit, translated into a luminosity limit at $z = 1$. Therefore, this limit only applies to the filled circles. The full drawn line indicates the median M/L_B of the SDSS early-type galaxies population. The long-dashed line indicates the median M/L_B of galaxies that are brighter than our luminosity limit at $z = 1$. Assuming that the scatter in M/L at $z = 1$ is a factor 2 larger than in the local universe, the median of the M/L of galaxies brighter than the luminosity limit follows the short-dashed line. It is clear that for the three galaxies in the primary sample with the lowest masses selection effects play such a dominant role that we cannot include these objects in our efforts to correct for this bias. Between $6 \times 10^{10} M_\odot$ and $2 \times 10^{11} M_\odot$ selection effects are relevant, but not dominant. For higher masses, selection effects do not affect our sample. The difference between galaxies with masses of $\approx 10^{11} M_\odot$ and masses $\approx 10^{12} M_\odot$ cannot be explained without an increase in the scatter with redshift, or assuming mass-dependent ages.

The location of the luminosity limit at $z = 1$ in Figure 4.10 shows that our $z \sim 1$ sample is dominated by selection effects for masses $M < 6 \times 10^{10} M_{\odot}$. The objects which such low masses are only included in the sample because of their probably extreme M/L. We cannot correct the M/L of that subsample for the bias introduced by our luminosity limit.

On the other hand, for the sample of galaxies with higher masses, we can correct for selection effects, because they are relevant, but not dominant, as can be seen in Figure 4.10. The average evolution of the galaxies in the primary sample with masses $M > 6 \times 10^{10} M_{\odot}$ is $\Delta \ln (M/L_B) = (-1.55 \pm 0.16)z$. The median mass of this subsample of 12 galaxies is $M = 1.9 \times 10^{11} M_{\odot}$. We estimate the maximum bias by assuming that the slope is the same at $z = 1$ and in the local universe, but that the scatter is a factor two larger at $z = 1$ than at $z = 0$. In that case the observed distribution is expected to follow the short-dashed line in Figure 4.10. At a given mass, the difference between the solid line and the short-dashed line is the bias introduced by the selection effects in luminosity. We increase the observed M/L of each galaxy in our primary sample by the difference between the solid line and the short-dashed line at the mass of that galaxy. For galaxies more massive than $M = 2 \times 10^{11} M_{\odot}$ this correction is negligible, but for the galaxies with masses $M \approx 6 \times 10^{10} M_{\odot}$ this correction is about 30%. Using this method, we find a bias corrected evolution of the galaxies with masses $M > 6 \times 10^{10} M_{\odot}$ of $\Delta \ln (M/L_B) = (-1.43 \pm 0.16)z$. Given the uncertainty in the intrinsic scatter, deeper observations are necessary to confirm this value.

Besides a bias due to the luminosity limit, errors in the velocity dispersion produce correlated errors in M and M/L, hence underestimating the measured evolution. Taking the errors in σ into account, we find that this introduces a bias at the level of only 2-3%, which is several times smaller than our measurement accuracy.

The above analysis only involves $z \sim 1$ galaxies satisfying all our selection criteria, but we note that the relation between M/L and M exists for the $z \sim 0.7$ galaxies as well. However, this subsample is selected in an inhomogeneous way, therefore it is impossible to correct the observed evolution. Since all the galaxies roughly lie along lines of constant luminosity, the bias toward low M/L galaxies likely explains the observed relation between M and M/L for this sub-sample.

Besides by luminosity and morphology, the galaxies in our sample are also selected by color. This potentially introduces an important bias in the measured evolution, because of the exclusion of galaxies with blue colors, i.e., low M/L. Our color criterion, however, is quite generous. Even the very blue, low mass galaxies satisfy this criterion. For typical Bruzual-Charlot models, our color limit ($i - z = 0.86$) corresponds to $U - V \sim 0.67$ at $z = 1$, which is 0.2 mag bluer than the limit applied by Bell et al. (2004) to select galaxies on the red sequence at $z \sim 1$. Our color cut is 0.45 mag bluer than the color-magnitude relation found by the same authors. From Bruzual-Charlot models we estimate that we only miss galaxies that are younger than ~ 1 Gyr (see Figures 4.7 and 4.8). Furthermore, Bell et al. (2004) did not find blue, massive galaxies in the entire COMBO-17 dataset. Hence it is very unlikely that we miss any blue galaxy at the bright end of our sample because of our color selection criterion.

4.4.4 Independent evidence for mass-dependent evolution of early-type galaxies

It is particularly interesting to compare our results to the results from studies involving lensing galaxies, since those samples are mass selected. Rusin et al. (2003) and van de Ven et al. (2003) find $\Delta \ln (M/L_B) = (-1.29 \pm 0.09)z$ and $(-1.43 \pm 0.30)z$, respectively, using the same dataset. This seems somewhat low compared to the evolution of our sample and results found in the literature, but the lensing galaxies typically have high masses (see Table 4.4). The data for individual galaxies published by van de Ven et al. (2003) show that the median mass of the lens sample is $M = 2 \times 10^{11} M_{\odot}$, whereas the median mass of our early-type galaxy sample is $M = 1.3 \times 10^{11} M_{\odot}$. The galaxies in the lens sample that are more massive than $M = 2 \times 10^{11} M_{\odot}$ evolve as $\Delta \ln (M/L_B) = (-1.13 \pm 0.31)z$. The galaxies less massive than this evolve much faster: $(-1.71 \pm 0.29)z$. The similarity between the results from the lensing sample and our sample is striking, especially because the lensing sample is mass selected. Hence, it is very hard to see how a bias toward low M/L galaxies can be responsible for the observed mass dependence in the lensing sample. It is possible that not all the low mass lenses are genuine early-types. If we omit the most irregular lenses (FBQ0951+2635, SBS1520+530, and B1608+656), we still find rapid evolution, $(-1.64 \pm 0.24)z$, for low mass lensing galaxies. Hence, these results provide strong evidence that the observed dependence of M/L evolution on mass in our sample is real. One possible complicating factor is that the lensing cross-section of galaxies in groups is larger than that of galaxies in the lowest density environments. This may lead to a difference between the populations of the lensing sample are our sample.

4.4.5 Ongoing star formation and morphological deviations

It is interesting to see that galaxies with emission lines have relatively low M/L, as can be seen from both Figure 4.6 and 4.10. Treu et al. (2001) have already shown that a substantial fraction of the massive early-type galaxy population at high redshift shows evidence for ongoing star formation by the presence of emission lines. Galaxies with emission lines in our sample, however, tend to have low masses. Figure 4.10 suggests that several of the galaxies with masses $\sim 3 \times 10^{10} M_{\odot}$ are included in the magnitude limited sample only because they are forming stars. When excluding galaxies with emission lines, the evolution of the sample (without applying a mass cut), is $\Delta \ln (M/L_B) = (-1.61 \pm 0.18)z$. The galaxies with emission lines evolve faster: $\Delta \ln (M/L_B) = (-2.41 \pm 0.45)z$. On average, the mass of the galaxies without emission lines is 1.5 times larger than the mass of the galaxies with emission lines.

Mergers or interactions, accompanied with star formation, can lead to both deviations from smooth $r^{1/n}$-profiles and low M/L values. van Dokkum & Ellis (2003) have shown tentative examples of this phenomenon. Figure 4.11 shows the magnitude of the asymmetric residual, (described in Section 4.3.1), versus the offset from the FP, corrected for luminosity evolution. There is no correlation between deviations from smooth surface profiles and M/L, and we find no evidence for a connection between star formation activity and interactions or mergers.

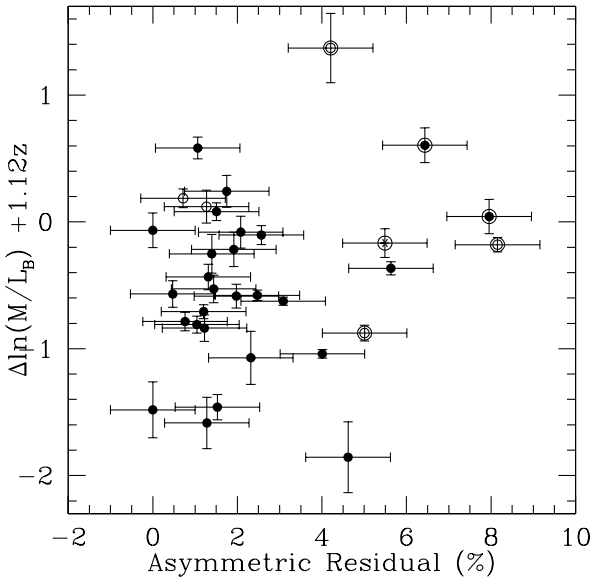

Figure 4.11: Asymmetric residuals of the $r^{1/4}$-profile fits (see Figures 4.3 and 4.4) versus the offset from the local FP of the early-type galaxies in our sample, corrected for evolution. Filled circles are galaxies best fit with $r^{1/4}$-profiles, asterisks with $r^{1/3}$, and open circles with $r^{1/2}$. Encircled objects are galaxies with late-type morphologies. A 2% or more residual indicates a significant deviation from symmetry in the light profile. There is no clear relation between M/L and deviations from smooth surface brightness profiles.

4.4.6 AGN

Four out of 11 early-type galaxies at $z < 0.8$ have AGN, and one out of 16 for the $z > 0.9$ sample, as determined from X-ray imaging (see section 3.3). Of the five early-type galaxies with AGN, three are more massive than $M = 2 \times 10^{11} M_{\odot}$ and two have emission lines in their spectra. The M/L evolution of galaxies in our sample with AGN is $\Delta \ln (M/L_B) = (-1.64 \pm 0.31)z$, which is not very different from the value for galaxies without AGN: $(-1.76 \pm 0.20)z$. However, the galaxies with AGN are twice as massive than the galaxies without AGN. Considering high mass galaxies only ($M > 2 \times 10^{11} M_{\odot}$), we find $(-1.46 \pm 0.24)z$ for galaxies with AGN and $(-1.02 \pm 0.41)z$ for galaxies without AGN. Now, the trend is reversed, but only one out of the five galaxies with an AGN has a particularly blue $B - I$ color for its M/L. Therefore, a larger sample is needed to confirm that the epochs of star formation and AGN activity are related. Woo et al. (2004) find that up to $z \sim 0.5$ the evolution of the FP for galaxies selected to have AGN is indistinguishable from otherwise selected galaxies. Our results provide tentative evidence that a difference may set in at higher redshift.

4.5 Comparison with previous results

Various other authors have measured the M/L evolution of field early-type galaxies. In this section we compare these previous results with our findings, and we comment on the apparent inconsistencies that exist in the literature. In Table 4.4 we give the M/L evolution as reported by other papers, as well as the values we derive using the tabulated datasets given in those papers.

Treu et al. (2001) find $\Delta \ln (M/L_B) = (-1.66 \pm 0.31)z$. This number is corrected for selection effects, while the value in Table 4.4 is uncorrected, to make a fair comparison with other results. The median mass of the sample presented by Treu et al. (2001) is $2.5 \times 10^{11} M_{\odot}$ for a sample extending to $z \sim 0.6$. Tabulated data are only available for the lower redshift galaxies presented in Treu et al. (2002). Only the galaxies with very low redshifts ($z \sim 0.1$) have low masses, therefore the comparison between high and low mass galaxies cannot be made. We note that the evolution of the entire Treu et al. sample is consistent with the evolution of our entire sample, $(-1.75 \pm 0.16)z$, and that the evolution of the massive galaxies in our sample is only mildly inconsistent with the evolution of the Treu et al. sample. Several of the high mass galaxies in the Treu et al. sample have emission lines in their spectra, which contrasts with our sample.

van Dokkum et al. (2001) find $(-1.35 \pm 0.35)z$ for an average redshift $z = 0.42$. The galaxy masses range from $3 \times 10^{10} M_{\odot}$ to $10^{12} M_{\odot}$ and are evenly distributed in $\log (M)$. Remarkably, when taking the tabulated data of the individual galaxies, and applying our fitting method, we find a larger value: $(-1.67 \pm 0.23)z$ (see Table 4.4). van Dokkum et al. (2001) create redshift bins in which they calculate the bi-weight center of the M/L offset. This method is sensitive to the bin choice, which leads to the difference between the reported value and the value calculated with our fitting method. We note that, when using our fitting method, the result of van Dokkum et al. (2001) is very similar to the result presented in this paper. Splitting the van Dokkum et al. sample into low and high mass galaxies (at $M = 2 \times 10^{11} M_{\odot}$), we find $(-1.29 \pm 0.39)z$ for the high mass galaxies, and $(-1.94 \pm 0.34)z$ for the low mass galaxies. We verified that this 2.5σ difference can be explained entirely by the fact that the galaxies are luminosity selected, not mass selected. Contrary to this study and the work of Treu et al., van Dokkum et al. did not select the galaxies by color, but by morphology and magnitude only.

van Dokkum & Ellis (2003) find $(-1.25 \pm 0.25)z$. The difference in fitting method, mentioned above, applies to this study as well. Additionally, their transformation from I-band surface brightness to rest-frame B-band surface brightness, using $V - I$ colors, is uncertain. Namely, using $V - I$ is an extrapolation for galaxies at $z > 0.8$. This leads to a different value for the M/L evolution if we use our method to fit to the individual galaxy data of the samples of van Dokkum et al. (2001) and van Dokkum & Ellis (2003): $(-1.68 \pm 0.13)z$, a value very similar to the result yielded by our sample. Using the bi-weight center to measure the evolution effectively gives very low weighting factors to outliers. If the two galaxies with the lowest M/L in the high-z sample of van Dokkum et al. are omitted, we find $(-1.53 \pm 0.13)z$. The measurement accuracy, together with the uncertain transformation to rest-frame properties can explain the remaining difference. The new sample described by van Dokkum & Ellis (2003) is too small to verify whether there is a trend with galaxy mass. There is one galaxy

more massive than $M = 2 \times 10^{11} M_{\odot}$ with $\Delta \ln (M/L_B) = (-1.57 \pm 0.14)z$. As is the case for the sample of van Dokkum et al. (2001), the sample of van Dokkum & Ellis (2003) is not selected by color. This did not lead to faster evolution due to including blue early-type galaxies, which indicates that the color cuts in the other studies are adequately generous to avoid this bias.

Gebhardt et al. (2003) (hereafter G03) report a brightening in the rest-frame B band of early-type galaxies by 2.4 magnitudes at $z = 1$, which is derived from fitting a cubic spline to the offsets of the galaxies from the local FP. With our fitting method, we find $(-1.94 \pm 0.20)z$, using the data of the individual galaxies in that sample. This is consistent with the result presented in this paper. The difference between the value reported by G03 and our result using their data is caused by the three galaxies at redshifts $z > 0.9$. Our linear fit to their data and their fit agree well up to $z = 0.8$ (1.6 magnitudes brightening). If we split the G03 sample into high and low mass galaxies, we find an evolution of $(-1.59 \pm 0.50)z$ for galaxies more massive than $M = 2 \times 10^{11} M_{\odot}$, and $(-2.05 \pm 0.17)z$ for less massive galaxies. For low mass galaxies our result, $(-1.97 \pm 0.16)z$, and that of G03 agree well. The fast evolution for massive galaxies in their sample remains unexplained, but given the large uncertainty and the small number of objects the inconsistency is only mild. We note, however, that contrary to the early-type galaxies in our sample, the early-type galaxies in the G03 sample do not show a correlation between M/L and rest-frame $U - B$ color. One of the galaxies in the G03 sample serves as an example of the uncertainty. HST14176+5226 has been observed spectroscopically before by both Ohyama et al. (2002) and Treu & Koopmans (2004), and happens to be in the sample of lensing galaxies of Rusin et al. (2003) and van de Ven et al. (2003). The three independent spectroscopic velocity dispersions are $\sigma_* = 222 \pm 8$ km s^{-1} (G03), 245 ± 15 km s^{-1} (Ohyama et al., 2002), and 224 ± 15 km s^{-1} (Treu & Koopmans, 2004), all corrected to the same aperture. van de Ven et al. report a value of $\sigma = 292 \pm 29$ km s^{-1} as derived from the lensing model. This might be an indication that using dispersions derived from lensing models leads to slower evolution than using spectroscopic dispersions. Also, the consistency among the different spectroscopic dispersions show that it remains unclear why G03 find somewhat faster evolution than the other authors. Repeated observation of the galaxies in the G03 sample may be illuminating.

We conclude that all the results found in the literature are mutually consistent, once differences in calculating and presenting the results have been taken into account.

Table 4.4: Comparison with previous results

Ref.	$\Delta \ln (M/L_B)/z$ reported	$\Delta \ln (M/L_B)/z$ fitted	$\Delta \ln (M/L_B)/z$ fitted, high-mass	$\Delta \ln (M/L_B)/z$ fitted, low-mass	$< (M/M_\odot) >$	$< z >$	N
Treu et al. (2001)	-1.64 ± 0.12	-1.64 ± 0.34	-1.55 ± 0.27	-1.47 ± 1.89	2.3×10^{11}	0.29	19
van Dokkum et al. (2001)	-1.35 ± 0.35	-1.67 ± 0.23	-1.29 ± 0.39	-1.94 ± 0.33	1.5×10^{11}	0.42	18
Treu et al. (2002)	-1.84	-	-	-	2.5×10^{11}	0.38	29
van Dokkum & Ellis (2003)	-1.25 ± 0.25	-1.68 ± 0.13	-1.41 ± 0.29	-1.77 ± 0.24	1.3×10^{11}	0.56	27
Gebhardt et al. (2003)	-2.21	-1.94 ± 0.20	-1.59 ± 0.49	-2.05 ± 0.17	8.5×10^{10}	0.64	21
This paper	-1.75 ± 0.16	-1.75 ± 0.16	-1.20 ± 0.18	-1.97 ± 0.16	1.6×10^{11}	0.90	27
Rusin et al. (2003)	-1.24 ± 0.21	-	-	-	-	0.54	21
van de Ven et al. (2003)	-1.43 ± 0.30	-1.36 ± 0.18	-1.13 ± 0.31	-1.71 ± 0.30	2.3×10^{11}	0.54	21

Column 2 lists the values of $\Delta \ln (M/L_B)$ as reported in the cited papers. Column 3 lists the values we derive using our fitting technique on the tabulated data of the individual galaxies in the cited papers. Column 4 lists the evolution of galaxies more massive than $M = 2 \times 10^{11} M_\odot$, using our fitting technique, and column 5 lists the evolution of less massive galaxies. Average masses, redshifts, and sample sizes (N) of the samples are also listed. When two references are given, the results presented in the newest paper are based on data of both papers. Treu et al. (2002) only list redshifts and velocity dispersions of the galaxies. The reported values are all uncorrected for selection effects. Treu et al. (2002) only give an error for the uncorrected value, and Gebhardt et al. (2003) do not give an error. Besides the magnitude limited samples, the two studies of the same sample of lensing galaxies are also listed. We only fitted the tabulated data from van de Ven et al. (2003), but the data presented by Rusin et al. (2003) yield the same results.

4.6 Conclusions

We obtained ultra-deep spectroscopy for 27 field early-type galaxies with redshifts $0.6 < z < 1.15$. The offset of these high redshift galaxies from the local FP is used as a measure of the evolution of M/L and as an age estimator.

The average evolution of the early type galaxies in our sample is $\Delta \ln (M/L_B) = (-1.75 \pm 0.16)z$. The value we find for galaxies in the primary sample, those galaxies satisfying all our selection criteria, is the same. The scatter in $\Delta \ln (M/L_B)$ is large: 0.58. This shows that some galaxies must have high luminosity weighted formation redshifts ($z > 2$), while others have formed a large fraction of their stars at redshifts $1 < z < 2$. Emission lines in the spectra indicate that some galaxies show signs of ongoing star formation at the epoch of observation. This is in agreement with the presence of massive early-type galaxies with emission lines at $z \sim 0.5$ (Treu et al., 2001), although the galaxies with emission lines in our sample tend to have low masses.

We find a tight correlation between M/L and rest-frame color, which shows that the variation in M/L among the galaxies in the sample is intrinsic, and due to differences in the stellar populations. The galaxies in our sample span a large range of masses. We find that low mass galaxies have larger offsets from the local FP than high mass galaxies. Because luminosity selected samples are biased toward galaxies with low M/L this is a trend that is expected. We carefully analyze whether the observed correlation between mass and M/L can entirely be explained by this selection effect or not. We find that galaxies with masses $M < 6 \times 10^{10} M_{\odot}$ are only included in our sample because they have low M/L. For galaxies at $z \sim 1$ with masses larger than $M = 6 \times 10^{10} M_{\odot}$, our sample is biased, but to a limited amount. Taking into account the selection effect, we exclude with high confidence that the distribution of mass and M/L of our $z \sim 1$ galaxy sample with masses $M > 6 \times 10^{10} M_{\odot}$ has the same distribution as the low redshift field early-type galaxy sample taken from Bernardi et al. (2003), corrected for evolution. We do not claim that we have observed a change of the slope of the FP, because we cannot exclude the possibility that our sample is drawn from a distribution that has the same slope as the Bernardi et al. (2003) sample, but with a scatter that is twice as large at $z = 1$. However, the outliers do not occur at the high mass end ($M \sim 10^{12} M_{\odot}$) of our galaxy sample, but at lower masses, namely $M \sim 10^{11} M_{\odot}$. Therefore, our results show that the evolution of early-type galaxies is mass-dependent, whether by an increase in the scatter at lower masses, or by systematic faster evolution of lower mass galaxies as compared to higher mass galaxies, or, which is the most natural explanation, by a combination of these effects. Assuming the scatter has decreased from $z = 1$ to the present day by a factor of 2, we find that the for bias corrected M/L evolution of $z \sim 1$ early-type galaxies with masses $M > 6 \times 10^{10} M_{\odot}$ is $\Delta \ln (M/L_B) = (-1.43 \pm 0.16)z$.

Previous studies (Treu et al., 2001, 2002; van Dokkum et al., 2001; van Dokkum & Ellis, 2003; Gebhardt et al., 2003), that claimed to have derived mutually exclusive results, are in fact consistent with our results, if the same fitting method is applied to the different datasets. Particularly interesting is the consistency of our results with the results from a sample of lensing galaxies (Rusin et al., 2003; van de Ven et al., 2003), which also shows the mass-dependence, even though this sample is not biased toward galaxies with low M/L: because of the selection technique, the lens sample contains

galaxies with typical M/L at a given mass. Our luminosity limited sample is sensitive to outliers, which are present indeed. The combination of these independent results strengthens the evidence for mass-dependent evolution and the combined increase in both slope and scatter with redshift.

Bell et al. (2004) claim that the mass density of red sequence galaxies increases by at least a factor of 2 from $z \sim 1$ to the present. This is partly based on the observation that the luminosity density is constant out to $z = 1$. The M/L evolution of our galaxy sample implies an increase by a factor of 4 in the mass density. In the local universe, most of the mass density in early-type galaxies is accounted for by galaxies with a velocity dispersion of ≈ 225 km s^{-1} (Kochanek, 1994) or a mass of $\approx 3 \times 10^{11} M_{\odot}$. If those galaxies, which evolve somewhat slower, dominate the evolution of the mass density, the increase is slightly less $(3 - 3.5)$.

The correlation between mass and M/L has been observed in clusters as well (Wuyts et al., 2004), but this can entirely be explained by selection effects. Both our field sample and the cluster samples found in the literature are not strongly biased for galaxy masses $M > 2 \times 10^{11} M_{\odot}$. When applying this mass cut, the evolution for cluster galaxies is $\Delta \ln (M/L_B) = (-1.12 \pm 0.06)z$, and the evolution for field galaxies is $\Delta \ln (M/L_B) = (-1.07 \pm 0.17)z$ ($-1.04z$ for galaxies in the primary sample). Galaxies with masses comparable to the mass of L^* galaxies in the local universe ($\approx 3 \times 10^{11} M_{\odot}$) have luminosity weighted ages that imply formation redshifts $z \geq 2$, independent of environment. If progenitor bias is important, the luminosity weighted age of typical early-type galaxies in the local universe can be considerably lower.

In hierarchical formation models, the predicted difference between the M/L of field and cluster galaxies is $\Delta \ln (M/L_B) = 0.55$, independent of redshift (van Dokkum et al., 2001). This large difference is related to the difficulty of constructing isolated galaxies without active star formation, i.e. to the lack of a mechanism that truncates star formation from within the galaxy. Our results rule out this prediction at the 99.6% confidence level, up to $z = 1.1$.

Our findings are consistent with down-sizing (Cowie et al., 1996; Kodama et al., 2004). This idea is independently corroborated by other observations, such as the decrease of the mass of 'E+A' galaxies with time (Tran et al., 2003), the lack of star formation in massive galaxies at redshifts $z \leq 1$ (De Lucia et al., 2004), the fossil record of star formation in local early-type galaxies (Thomas et al., 2005), and the claim of mass-dependent evolution of spiral galaxies (Ziegler et al., 2002; Böhm et al., 2004). The lack of age differences between field and cluster galaxies, and the suggested mass-dependent evolution of early-type galaxies show that individual properties of a galaxy, and not environment, play an important role in its formation.

We have shown that rest-frame optical colors can be used to measure galaxy masses at high redshift. This can be regarded as a step toward accurately calibrating SED fitting as a mass estimator. Certainly including Spitzer photometry in the rest-frame near-infrared will provide tight correlations between dynamically derived M/L and M/L derived from SED fitting. Line-strengths of absorption features in our high S/N spectra will connect low redshift fossil record studies to evolutionary studies such as these, and constrain the metallicity range of early-type galaxies at $z \sim 1$, lifting the age-metallicity degeneracy. Using the mass calibration for high-redshift galaxies, the evolution of the mass density and the mass function can be determined from volume limited samples. This will provide strong constraints on formation the-

ories and the importance of progenitor bias.

We thank the referee for many useful comments, enhancing the quality and the readability of the work. We thank the ESO staff for their professional and effective assistance during the observations. The Lorentz center is thanked for its hospitality during various workshops and the Leidsch Kerkhoven-Bosscha Fonds for its financial support.

References

Alexander, D. M. et al. 2003, *AJ* **126**, 539

Böhm, A. et al. 2004, *A&A* **420**, 97

Bell, E. F., McIntosh, D. H., Katz, N., & Weinberg, M. D. 2003, *ApJS* **149**, 289

Bell, E. F. et al. 2004, *ApJ* **608**, 752

Bernardi, M. et al. 2003, *AJ* **125**, 1866

Bertin, E. & Arnouts, S. 1996, *A&AS* **117**, 393

Blakeslee, J. P. et al. 2003, *ApJ* **596**, L143

Bruzual, G. & Charlot, S. 2003, *MNRAS* **344**, 1000

Cole, S., Lacey, C. G., Baugh, C. M., & Frenk, C. S. 2000, *MNRAS* **319**, 168

Coleman, G. D., Wu, C.-C., & Weedman, D. W. 1980, *ApJS* **43**, 393

Cowie, L. L., Songaila, A., Hu, E. M., & Cohen, J. G. 1996, *AJ* **112**, 839

De Lucia, G. et al. 2004, *ApJ* **610**, L77

Diaferio, A., Kauffmann, G., Balogh, M. L., White, S. D. M., Schade, D., & Ellingson, E. 2001, *MNRAS* **323**, 999

Djorgovski, S. & Davis, M. 1987, *ApJ* **313**, 59

Dressler, A., Lynden-Bell, D., Burstein, D., Davies, R. L., Faber, S. M., Terlevich, R., & Wegner, G. 1987, *ApJ* **313**, 42

Faber, S. M., Wegner, G., Burstein, D., Davies, R. L., Dressler, A., Lynden-Bell, D., & Terlevich, R. J. 1989, *ApJS* **69**, 763

Franx, M. 1993, *PASP* **105**, 1058

Gebhardt, K. et al. 2003, *ApJ* **597**, 239 (G03)

Giacconi, R. et al. 2002, *ApJS* **139**, 369

Giavalisco, M. et al. 2004, *ApJ* **600**, L93

Holden, B. P. et al. 2005, *ApJ* **620**, L83 (Chapter 2)

Jørgensen, I., Franx, M., & Kjærgaard, P. 1996, *MNRAS* **280**, 167

Jorgensen, I., Franx, M., & Kjærgaard, P. 1995, *MNRAS* **276**, 1341

Kauffmann, G. & Charlot, S. 1998, *MNRAS* **297**, L23

Kelson, D. D., Illingworth, G. D., van Dokkum, P. G., & Franx, M. 2000, *ApJ* **531**, 184

Kochanek, C. S. 1994, *ApJ* **436**, 56

Kochanek, C. S. et al. 2000, *ApJ* **543**, 131

Kodama, T. et al. 2004, *MNRAS* **350**, 1005

Krist, J. 1995, in *ASP Conf. Ser. 77: Astronomical Data Analysis Software and Systems IV*, p.349

Lidman, C., Rosati, P., Demarco, R., Nonino, M., Mainieri, V., Stanford, S. A., & Toft, S. 2004, *A&A* **416**, 829

Ohyama, Y. et al. 2002, *AJ* **123**, 2903

Rosati, P. et al. 2004, *AJ* **127**, 230

Rusin, D. et al. 2003, *ApJ* **587**, 143

Thomas, D., Maraston, C., Bender, R., & de Oliveira, C., M. 2004, *ApJ* **621**, 673

Tran, K. H., Franx, M., Illingworth, G., Kelson, D. D., & van Dokkum, P. 2003, *ApJ* **599**, 865

Treu, T. & Koopmans, L. V. E. 2004, *ApJ* **611**, 739

Treu, T., Stiavelli, M., Bertin, G., Casertano, S., & Møller, P. 2001, *MNRAS* **326**, 237

Treu, T., Stiavelli, M., Casertano, S., Møller, P., & Bertin, G. 2002, *ApJ* **564**, L13

Valdes, F., Gupta, R., Rose, J. A., Singh, H. P., & Bell, D. J. 2004, *ApJS* **152**, 251

van de Ven, G., van Dokkum, P. G., & Franx, M. 2003, *MNRAS* **344**, 924

van der Wel, A., Franx, M., van Dokkum, P. G., & Rix, H.-W. 2004, *ApJ* **601**, L5 (Chapter 3)

van Dokkum, P. G. 2001, *PASP* **113**, 1420

van Dokkum, P. G. & Ellis, R. S. 2003, *ApJ* **592**, L53

van Dokkum, P. G. & Franx, M. 1996, *MNRAS* **281**, 985

van Dokkum, P. G., Franx, M., Kelson, D. D., & Illingworth, G. D. 1998, *ApJ* **504**, L17

van Dokkum, P. G., Franx, M., Kelson, D. D., & Illingworth, G. D. 2001, *ApJ* **553**, L39

van Dokkum, P. G. & Stanford, S. A. 2003, *ApJ* **585**, 78

Wolf, C., Meisenheimer, K., Rix, H.-W., Borch, A., Dye, S., & Kleinheinrich, M. 2003, *A&A* **401**, 73

Woo, J., Urry, C. M., Lira, P., van der Marel, R. P., & Maza, J. 2004, *ApJ* **617**, 903

Wuyts, S., van Dokkum, P. G., Kelson, D. D., Franx, M., & Illingworth, G. D. 2004, *ApJ* **605**, 677

Ziegler, B. L. et al. 2002, *ApJ* **564**, L69

Chapter 5

Evolution of the Color-Magnitude Relation of Field Early-Type Galaxies; Implications for the Tilt of the Fundamental Plane at $z = 1$

Abstract

We determine the color-magnitude relation (CMR) of field early-type galaxies at $z \sim 1$. A sample of 270 galaxies with spectroscopic redshifts in the range $0.55 < z < 1.15$ is constructed, with quantitative morphological classifications from high-resolution HST imaging. This allows us to compare the zero-point, slope, and scatter of the high-z and local CMR. We find no evolution of the slope, a mild increase of the scatter and a significantly bluer zero-point at $z = 1$ ($B-I = 1.73$ for $M_I = -23$). Because of the empirical relation between dynamically determined M/L and color of early-type galaxies at $z \sim 1$, the absent or slow evolution of the slope of the CMR suggests that the tilt of the FP does not evolve significantly, or that the relation between M/L and color breaks down for low-mass galaxies. In the first case, the observed steep relation between M and M/L at $z \sim 1$, found by previous FP studies, is due to selection effects, and not intrinsic. Furthermore, the M/L-evolution of field early-type galaxies is $\Delta \ln M/L_B = -1.41z$ if we take selection effects into account. To verify the applicability of the relation between M/L and color, dynamical mass measurements of low-luminosity early-type galaxies are required.

van der Wel, A., Franx, M., van Dokkum, P.G., Rix, H.-W. & Illingworth, G.D.

5.1 Introduction

The color-magnitude relation (CMR, Sandage, 1972; Bower, Lucey & Ellis, 1992) and the fundamental plane (FP, Djorgovski & Davis, 1987; Dressler et al., 1987) are tight relations that can be used to constrain the evolution of early-type galaxies. van Dokkum et al. (2000) and Blakeslee et al. (2003) have measured the evolution of the zero-point, slope, and scatter of the CMR of cluster galaxies at $z = 0.83$ and $z = 1.24$, respectively. FP studies of cluster galaxies out to similar redshifts (van Dokkum & Stanford, 2003; Holden et al., 2005) have measured the evolution of M/L. These studies show that at least part of the massive galaxy population must have formed their stars at very high redshifts ($z > 3$).

FP studies of field early-type galaxies out to $z \sim 1$ (van der Wel et al., 2004; Treu et al., 2005a; van der Wel et al., 2005; Treu et al., 2005b; di Serego Alighieri et al., 2005) yielded similar star formation epochs for massive field galaxies, but these authors also found a strong correlation between the rate of evolution and galaxy mass, with low-mass galaxies evolving faster, implying lower formation redshifts. In other words, the tilt of the FP apparently steepens toward higher redshifts.

van der Wel et al. (2005) (hereafter, vdW05) argue that the apparent tilt evolution is mostly caused by selection effects, and that the intrinsic tilt evolution is only mild. Treu et al. (2005b) and di Serego Alighieri et al. (2005), on the other hand, claim that the tilt evolution is intrinsically strong. If that were the case, the relation between color and M/L as found by Treu et al. (2005a) and vdW05 implies that color-evolution is also mass-dependent, such that measuring the evolution of the CMR may provide an additional constraint on the relevance of selection effects in the high-z FP studies.

For cluster galaxies it has been shown that the slope and scatter of the CMR are non- or slowly evolving out to $z \sim 1.3$ (van Dokkum et al., 2000; Blakeslee et al., 2003). Bell et al. (2004b) have shown that the CMR exists for field galaxies out to $z \sim 1$ based on photometric redshifts. By determining morphologies, Bell et al. (2004a) extend their analysis, and show that the galaxies that populate the CMR are mainly early-type galaxies. They determine the slope of the CMR for a color-selected sample. Therefore it is not clear how the CMR of the field early-type galaxy population evolves. Koo et al. (2005) have studied bulges of field galaxies (including ellipticals) out to $z \sim 1$. They find no significant evolution of the slope. However, the errors on the photometry are quite large because of the bulge-disk separation. As a result, only an upper-limit of the intrinsic scatter was determined.

We combine our spectroscopic sample (vdW05) with the K20 spectroscopic survey (Cimatti et al., 2002; Mignoli et al., 2005) and the GOODS spectroscopic survey (Vanzella et al., 2005). This provides a sample of 90 early-type galaxies at redshifts $0.55 < z < 1.15$. In Section 5.2 we describe the quantitative morphological classification of the compiled sample, using high-resolution HST imaging. This allows us to measure the zero-point, slope, and scatter of the CMR of a morphologically selected sample of field early-type galaxies out to $z = 1$ (Section 5.3). Subsequently, in Section 5.4, the derived high-z CMR together with the known relation between M/L and color is used to derive the expected tilt of the $z = 1$ FP. This then is compared to the results from the dynamical FP studies.

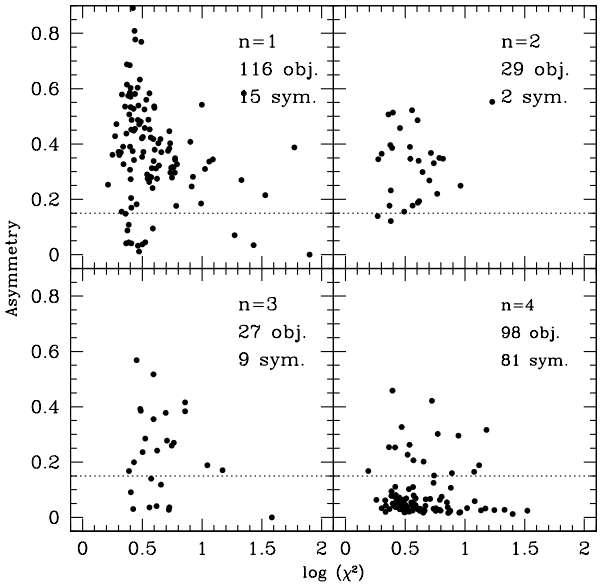

Figure 5.1: Morphological indicators of 270 galaxies in the CDFS with redshifts $0.55 < z < 1.15$. The sample is divided into sub-samples according to the best-fitting Sércic n parameter as measured from ACS i-band images. χ^2 indicates the quality of the fit, and the asymmetry parameter A indicates which fraction of the total flux of the object is contained in the asymmetric part of the light distribution. As expected, objects with $n = 4$ are mostly (83%) symmetric, whereas objects with $n = 1$ are mostly (87%) asymmetric. The division line between symmetric and asymmetric objects at 0.15 is chosen based upon visual inspection of the ACS images. We include the 90 galaxies with $n \leq 3$ and $A < 0.15$ in the early-type galaxy sample.

5.2 Constructing the Early-Type Galaxy Sample

vdW05 provide redshifts of 29 galaxies in the CDFS, most of which were visually classified as early-type galaxies, in the range $0.60 < z < 1.15$ with a median $z = 0.94$. A color-criterion of $i_{775} - z_{850} = 0.86$ was applied. All of these galaxies are imaged by the Advanced Camera for Surveys (ACS) on HST (GOODS, Giavalisco et al., 2004) and by ISAAC on the VLT (GOODS/EIS, Vandame et al., In Preparation).

The K20 survey (Cimatti et al., 2002) provides spectroscopy for a nearly complete sample of K-band selected objects (Mignoli et al., 2005). This sample includes 169 galaxies in the redshift range $0.55 < z < 1.15$ (with a median $z = 0.74$) within the GOODS-ACS field.

The ESO spectroscopic survey conducted as part of GOODS (Vanzella et al., 2005) provides 134 redshifts of galaxies within the GOODS-ACS mosaic in the redshift range $0.55 < z < 1.15$ (with a median $z = 1.00$). This sample is primarily selected by color ($i_{775} - z_{850} > 0.6$) in order to include early-type galaxies at $z \gtrsim 0.7$ and bluer, star-forming galaxies at $z \gtrsim 1.2$.

If we exclude the overlap between the three spectroscopic samples and a small

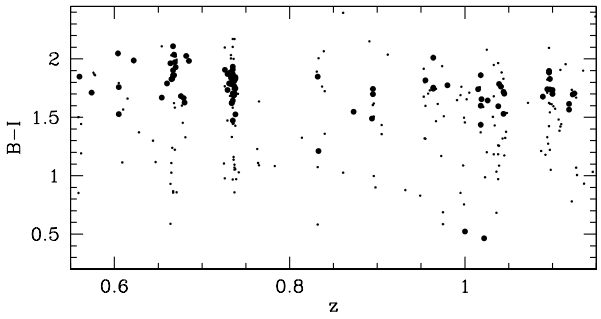

Figure 5.2: Redshift vs. rest-frame $B-I$ color. Large symbols are early-type galaxies; small symbols are late-type galaxies. Our quantitative morphological classification (see Figure 5.1), which is entirely independent of color, succeeded in distinguishing the red sequence: only 3 out of 90 early-type galaxies have particularly blue colors. Red galaxies that have not been assigned early-type morphologies can easily be recognized *a posteriori* as dusty, star-forming galaxies or mergers upon visible inspection of the ACS images. Note the clear signatures of large scale structure are visible at $z \sim 0.67$, $z \sim 0.73$, and ~ 1.10.

number of galaxies outside the K-band mosaic, we have a final sample of 270 galaxies in the redshift range $0.55 < z < 1.15$ with a median redshift $z = 0.86$.

Photometry is performed on the registered and PSF-matched ACS (b_{435}-, v_{606}-, i_{775}-, and z_{850}-band) and ISAAC (J- and K-band) mosaic images. Colors are measured within a $2''0$ diameter aperture. We derive rest-frame $B-I$ colors by using the method described by van Dokkum & Franx (1996).

We fit Sércic-models (convolved with the PSF) to the ACS i_{775}-band images of all 270 galaxies, measuring χ^2-values for $n = 1, 2, 3, 4$. By rotating the images by 180 degrees and subtracting the rotated images from the original images, we also measure the fractional flux A in the asymmetric parts of the images. The best-fitting Sércic-n parameter together with A provides a quantitative morphological classification. In Figure 5.1 we show that this method efficiently distinguishes between early- and late-type galaxies. We use our criteria $n \geq 3$ and $A < 0.15$ to divide our sample into 90 early-type galaxies (median redshift $z = 0.74$) and 180 late-type galaxies (median redshift $z = 0.91$). The effective radii and surface brightnesses obtained for $n = 4$ are used to calculate the total model magnitudes of the galaxies. Together with the color information these are used to determine rest-frame absolute magnitudes.

In Figure 5.2 we show the redshift-color distribution, distinguishing between late- and early-type galaxies. 87 out of 90 morphologically early-type galaxies are among the reddest half of the color-distribution. It is clear that our classification has succeeded in distinguishing the red sequence by using color-independent morphological indicators (see also, Bell et al., 2004a). Visual inspection of the ACS images of the red objects that are classified as late-type galaxies confirms that these are indeed irregular and apparently dusty galaxies, and not misclassified early-type galaxies. The three blue early-type galaxies are not misclassified either: these truly have smooth and compact morphologies. There are clear signatures of large-scale structure at $z \sim 0.66$, $z \sim 0.74$, and $z \sim 1.10$, previously noticed by Vanzella et al. (2005).

5.3 The High-Redshift Color-Magnitude Relation

We divide the sample into two redshift bins: $0.55 < z < 0.85$ (55 early-types; 80 late-types) and $0.85 < z < 1.15$ (35 early-types; 100 late-types). Within these bins we correct the rest-frame luminosities and colors for evolution to the values they would have at $z = 0.70$ and $z = 1.00$, respectively. The adopted luminosity and color evolution are taken from vdW05. We apply such a correction to all galaxies, but in principle it is only applicable to early-type galaxies. The corrections, however, are only small ($\lesssim 0.03$ mag) because of the narrow redshift distributions within the two sub-samples. Our results do not change significantly if the correction is omitted.

We show the color-magnitude diagram in Figure 5.3, distinguishing between late- and early-type galaxies. As was already demonstrated by Bell et al. (2004a), early-type galaxies not only populate the reddest part of the color-magnitude distribution at high redshift, but also constitute the brightest part of the galaxy population. We measure the slope of the CMR in both redshift bins by performing a linear least-squares fit, iterating to reject galaxies that deviate by more than 3σ. This results in the rejection of the 3 blue galaxies that clearly stand out in Figure 5.2. At $z = 0.7$ we find $B - I = (-0.034 \pm 0.021)(M_I + 23) + 1.843 \pm 0.026$, with a scatter in $B - I$ of 0.131 ± 0.013. At $z = 1.0$ we find $B - I = (-0.043 \pm 0.022)(M_I + 23) + 1.728 \pm 0.0221$, with a scatter in $B - I$ of 0.119 ± 0.015. Given the photometric errors of typically 0.04 mag in $B-I$, the values of the intrinsic scatter are 0.125 ± 0.013 and 0.112 ± 0.015 for $z = 0.7$ and $z = 1.0$, respectively. All errors are derived by the bootstrap method. The linear fits are shown by solid lines in Figure 5.3.

Two of the three samples used in this study are selected by both optical color and optical magnitude. This might bias the derived slope of the CMR. The K20 sample is K-band selected, without a color-criterion, and is therefore suitable to test for selection effects. If we only use the K20 sample, we find no significantly different CMR compared to the relations given above. We evaluate the possible color bias in the K-band selected sample in the following way. We calculate the $B - I$ colors for the four different spectral templates from Coleman, Wu & Weedmane (1980), and the rest-frame I-band luminosities for $K = 20$ at $z = 0.7$ and $z = 1.0$. These luminosities and colors are shown by crosses connected by solid lines in Figure 5.3. Because the selection limit is almost perpendicular to the CMR, we do not miss large numbers of blue or red galaxies. We conclude that the CMR as derived above is not biased due to magnitude- and/or color-limits of the sub-samples.

Bernardi et al. (2003b) derive the local CMR from a sample of ~ 9000 early-type galaxies extracted from the SDSS database. We transform their CMR for $g - r$ vs. M_r into $B - I$ vs. M_I, using the E template of Coleman et al. (1980). We find $B - I = -0.049(M_I + 23) + 2.166$ with an intrinsic scatter of 0.101 for $z = 0$. Hence, the zero-point changes significantly by -0.44 between $z = 1$ and $z = 0$ (-0.39 if we correct for luminosity evolution), but we find little evolution of the slope of the CMR. Furthermore, we find tentative evidence (at the 90% confidence level) for a higher scatter at high redshift (0.112 ± 0.015 at $z = 1$ and 0.125 ± 0.013 at $z = 0.7$ vs. 0.101 at $z = 0$).

We conclude that the slope of the CMR for cluster and field galaxies are the same at low redshift, and both do not significantly evolve out to $z \sim 1$. (See van Dokkum et al. (2000) and Blakeslee et al. (2003) for studies of the high-redshift cluster CMR.)

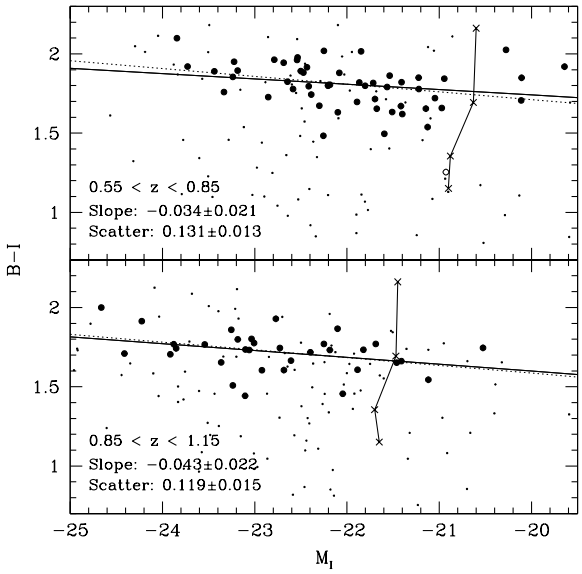

Figure 5.3: Rest-frame $B-I$ vs. rest-frame M_I of the sample of 270 galaxies divided into two redshift bins. The large symbols are early-type galaxies; the small symbols are late-type galaxies. Every data-point is corrected for evolution from its redshift to $z = 0.7$ (upper panel) or $z = 1.0$ (lower panel). The crosses connected by the solid lines represent the K20 magnitude limit at $z = 0.7$ and $z = 1.0$ transformed into rest-frame absolute magnitude limits for galaxies with different colors. We fit the CMR using the linear least-squares method, rejecting those galaxies that lie off the best-fit solid lines by more than 3σ. The early-type galaxies that are rejected from the fit are indicated by open circles. The errors in the slope and the scatter are obtained by the bootstrap method. Those errors dominate over the photometric errors on the individual galaxies, which are typically 0.05 mag in $B-I$. The dotted lines are the best fits if the slope is fixed at the slope of CMR in the local universe (-0.049). The small difference between the slope at low and high redshift is insignificant.

For the sample of early-types in a cluster at $z = 0.83$ of van Dokkum et al. (2000), we derive an intrinsic scatter in $B-I$ of 0.065 ± 0.011. This scatter is significantly smaller than for field galaxies (0.125 ± 0.013 at z=0.07 and 0.112 ± 0.015 at $z = 1.0$), similar to the situation at lower redshifts (Bernardi et al., 2003b).

5.4 Implications for the Evolution of the FP

In the top panel of Figure 5.4 we show M and M/L_B as inferred dynamically by vdW05 for 15 early-type galaxies at $z \sim 1$. The luminosity limit of this sample is indicated by the solid line. The observed relation between is $M/L_B \propto M^{\alpha}$ with $\alpha = 0.64 \pm 0.07$ (the error is obtained by the bootstrap method). This is much steeper than the local relation ($\alpha = 0.25$) as implied by the tilt of the FP (e.g., Jørgensen, Franx & Kjærgaard, 1996). At $z = 1$ Treu et al. (2005b) find $\alpha = 0.69^{+0.14}_{-0.05}$, taking

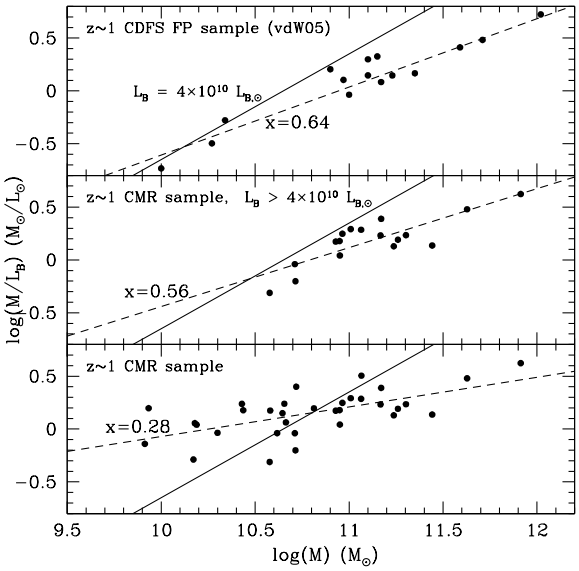

Figure 5.4: The upper panel shows the dynamical M and M/L_B of the galaxies in the $z \sim 1$ sample of vdW05. The solid line represents the z_{850}-magnitude limit of that survey transformed into a B-band luminosity limit at $z = 1$. The dashed line shows the linear fit to the data-points. The middle panel shows that part of the $z \sim 1$ sample shown in Figure 5.3 which is brighter than the luminosity limit of the FP sample. M and M/L_B are derived from the relation between M/L_B and $B - I$ found by vdW05. Again, the dashed line shows the linear fit. The bottom panel shows the $z \sim 1$ sample without a luminosity limit. It is clear that the luminosity limit affects the observed tilt of the FP at $z = 1$. The lack of evolution of the slope of the CMR implies that the evolution of the tilt of the FP is consistent with zero and is at most modest.

into account selection effects. This implies that selection effects do not strongly affect the observed relation between M and M/L_B.

It has been shown by vdW05 that there is a strong relation between $B - I$ and $\log(M/L_B)$. From the early-type galaxy samples of vdW05 and Holden et al. (2005) (31 objects at $0.6 < z < 1.3$ with accurate dynamical M/L) we derive that $\log(M/L_B) = 1.678(B-I) - 2.648$. This linear relation is forced to match the average $B-I$ color and $\log(M/L_B)$ of local galaxies with similar velocity dispersions as the galaxies in the high-z sample (~ 230 km s^{-1}). We use this relation to estimate M and M/L_B for the 33 early-type galaxies at $z \sim 1$ shown in Figure 5.3 from their $B - I$ colors.

The middle panel shows the thus obtained M and M/L_B for the 20 out of 33 galaxies that are brighter than the luminosity limit that applies to the FP sample. The relation between M and M/L_B has a similar slope as for the FP sample: $\alpha = 0.56 \pm 0.11$. This error also includes the uncertainty in the relation between $B-I$ and $\log(M/L)$. In the bottom panel of Figure 5.4 we show all 33 galaxies. Without the luminosity cut, we find $\alpha = 0.28 \pm 0.06$, which is not significantly different from the local relation ($\alpha = 0.25$).

Apart from the observed tilt of the FP, the luminosity limit of the FP sample also affects the observed M/L-evolution between $z = 0$ and $z = 1$. vdW05 measure $\Delta \ln M/L_B = -1.72z$ for the 15 galaxies shown in the top panel of Figure 5.4. By taking selection effects into account, they correct the measured evolution for galaxies more massive than $M = 6 \times 10^{10} M_{\odot}$ to $\Delta \ln M/L_B = -1.43z$. The average M/L evolution of the 33 galaxies shown in the bottom panel, as inferred from their $B - I$ colors, is $\Delta \ln M/L_B = -1.41z$ for galaxies down to $M = 10^{10} M_{\odot}$.

The limitation to this analysis is the applicability of the observed relation between $B - I$ and $\log(M/L_B)$. There may be several problems with the current use of this relation. First, it is unknown whether it can be applied to low-mass galaxies, since these have not been observed kinematically. Second, there may be systematic uncertainties in the relation. There are hints that the residual from the relation correlates with mass. This residual is also visible in the middle panel of Figure 5.4, where the tilt is slightly shallower than in the upper panel. After a first-order correction for this mass-dependent residual we obtain a tilt of $\alpha = 0.4$ (instead of $\alpha = 0.28$). This is an indication of the systematic effects in our approximation.

5.5 Conclusions

We find that the slope of the CMR of field galaxies does not significantly evolve from $z = 1$ to the present. These results corroborate the findings by Bell et al. (2004a) and Koo et al. (2005) who also find no evidence for evolution of the slope. We do find, for the first time, evidence at the 90% confidence level for a mild increase in the scatter.

One should bear in mind that roughly half of the early-type galaxy population had not yet assembled at $z = 1$ (Bell et al., 2004b). Our CMR analysis does not take this 'progenitor bias' (van Dokkum & Franx, 2001) into account. Some part of the progenitors of the local early-type galaxy population are not included in our high-z sample because they do not yet have early-type morphologies, or they are to faint and grow to their present masses through merging. Gas-poor merging only has a small effect on the CMR, as the color barely changes in the process. On the contrary, the transition of blue, late-type galaxies into red, early-type galaxies between $z = 1$ and the present causes the color evolution of the progenitors of the entire local early-type galaxy population to be stronger than that of morphologically selected early-type galaxy samples. Because red, early-types are the brightest and most massive galaxies at any redshift $z \lesssim 1$ (Bell et al., 2004b), most morphological transformations take place at low masses. Hence, the slope of the CMR for all progenitors will be steeper than the slope derived from our morphologically selected sample. Likewise, the scatter at low luminosities will be larger than at high luminosities.

We use the empirical relation between color and M/L to calculate the expected slope of the FP. Assuming that the relation between M/L and color does not break down at low masses, we find no evidence for strong evolution of the tilt of the FP out to $z = 1$. We conclude that the apparent evolution of the tilt of the FP (van der Wel et al., 2005; Treu et al., 2005b; di Serego Alighieri et al., 2005) is probably caused by a combination of selecting by luminosity rather than mass, and an increase in the scatter of the FP and the CMR.

We note that the sample of Treu et al. (2005b) is in the HDF-N. It will interesting

to compare the CMR of the early-type galaxies in the HDF-N such that the selection effects in that sample can be directly studied. Due to the uncertainty in the relations between M, M/L and color over a large range of galaxy masses, it is currently not possible to constrain the evolution of the tilt of the FP more quantitatively. To measure this, extending dynamical measurements of early-type galaxies at $z \sim 1$ further down the mass-function is essential.

References

Bell, E. F. et al. 2004a, *ApJ* **600**, L11

Bell, E. F. et al. 2004b, *ApJ* **608**, 752

Bernardi, M. et al. 2003b, *AJ* **125**, 1882

Blakeslee, J. P. et al. 2003, *ApJ* **596**, L143

Bower, R. G., Lucey, J. R., & Ellis, R. S. 1992, *MNRAS* **254**, 601

Cimatti, A. et al. 2002, *A&A* **392**, 395

Coleman, G. D., Wu, C.-C., & Weedman, D. W. 1980, *ApJS* **43**, 393

di Serego Alighieri, S. et al. 2005, *A&A* in press, astro-ph/0506655

Djorgovski, S. & Davis, M. 1987, *ApJ* **313**, 59

Dressler, A., Lynden-Bell, D., Burstein, D., Davies, R. L., Faber, S. M., Terlevich, R., & Wegner, G. 1987, *ApJ* **313**, 42

Giavalisco, M. et al. 2004, *ApJ* **600**, L93

Holden, B. P. et al. 2005, *ApJ* **620**, L83 (Chapter 2)

Jørgensen, I., Franx, M., & Kjærgaard, P. 1996, *MNRAS* **280**, 167

Koo, D. C. et al. 2005, *ApJS* **157**, 175

Mignoli, M. et al. 2005, *A&A* accepted, astro-ph/0504248

Sandage, A. 1972, *ApJ* **176**, 21

Treu, T., Ellis, R. S., Liao, T. X., & van Dokkum, P. G. 2005a, *ApJ* **622**, L5

Treu, T. et al. 2005b, *ApJ* in press, astro-ph/0502028

van der Wel, A., Franx, M., van Dokkum, P. G., & Rix, H.-W. 2004, *ApJ* **601**, L5 (Chapter 3)

van der Wel, A., Franx, M., van Dokkum, P. G., Rix, H.-W., Illingworth, G., & Rosati, P. 2005, *ApJ* in press, astro-ph/0502228 (vdW05, Chapter 4)

van Dokkum, P. G. & Franx, M. 1996, *MNRAS* **281**, 985

van Dokkum, P. G. & Franx, M. 2001, *ApJ* **553**, 90

van Dokkum, P. G., Franx, M., Fabricant, D., Illingworth, G. D., & Kelson, D. D. 2000, *ApJ* **541**, 95

van Dokkum, P. G. & Stanford, S. A. 2003, *ApJ* **585**, 78

Vanzella, E. et al. 2005, *A&A* **434**, 53

Chapter 6

The Evolution of Rest-Frame K-band Properties of Early-Type Galaxies from $z = 1$ to the Present

Abstract

We measure the evolution of the rest-frame K-band Fundamental Plane from $z = 1$ to the present by using IRAC imaging of a sample of early-type galaxies in the Chandra Deep Field-South at $z \sim 1$ with accurately measured dynamical masses. We find that M/L_K evolves as $\Delta \ln (M/L_K) = (-1.18 \pm 0.10)z$, which is slower than in the B-band ($\Delta \ln (M/L_B) = (-1.46 \pm 0.09)z$). In the B-band the evolution has been demonstrated to be strongly mass dependent. In the K-band we find a weaker trend: galaxies more massive than $M = 2 \times 10^{11} M_\odot$ evolve as $\Delta \ln (M/L_K) = (-1.01 \pm 0.16)z$; less massive galaxies evolve as $\Delta \ln (M/L_K) = (-1.27 \pm 0.11)z$. Qualitatively our results agree with stellar population models: the evolution in M/L_K is slower than the evolution in M/L_B. Various models, however, differ significantly in their prediction of $\Delta \ln (M/L_K)$ versus $B - K$. Contrary to the Maraston model, the Bruzual-Charlot model does not fit well to our results unless the IMF is assumed to be flat ($x = 0.35$ instead of 1.35). These results show that the interpretation of rest-frame near-IR photometry is severely hampered by model uncertainties and therefore that the determination of galaxy masses from rest-frame near-IR photometry may be harder than was thought before.

van der Wel, A., Franx, M., van Dokkum, P.G., Huang, J., Rix, H.-W. & Illingworth, G.D.
The Astrphysical Journal, submitted

6.1 Introduction

The formation and evolution of early-type galaxies has been a major subject of research during the past decades. Both theoretical and empirical studies indicate that the stellar mass density of the early-type galaxy population has increased by at least a factor of two between $z = 1$ and the present day (Kauffmann & Charlot, 1998; Bell et al., 2004) At the same time, studies at $z \sim 1$ show that massive early-type galaxies were already several Gyr old at that epoch (van Dokkum & Stanford, 2003; Holden et al., 2005; Treu et al., 2005; van der Wel et al., 2005). It is an intriguing puzzle to explain these seemingly contradictory results in one picture describing early-type galaxy formation.

These results hinge on determining galaxy masses, This remains very hard to do at high redshift. Typically, mass estimates for high-z galaxies are obtained by comparing their photometric properties with stellar population models in order to infer a mass-to-light ratio (M/L) (see, e.g., Bell et al., 2003; Bundy, Ellis & Conselice, 2005; Shapley et al., 2005). Such SED-fitting methods are intrinsically uncertain, and dynamical mass calibrations are needed to overcome the large uncertainty in the low mass end of the initial mass function (IMF), dark matter content, and, most importantly, to verify the validity of stellar population models. A more quantitative approach is to use the Fundamental Plane (FP, Djorgovski & Davis, 1987; Dressler et al., 1987) of early-type galaxies to directly measure the evolution of M/L at rest-frame optical wavelengths out to $z = 1.3$ (van Dokkum & Franx, 1996; van Dokkum et al., 1998; Kelson et al., 2000; Treu et al., 2001; van Dokkum et al., 2001; Treu et al., 2002; van Dokkum & Stanford, 2003; van Dokkum & Ellis, 2003; Gebhardt et al., 2003; van der Wel et al., 2004; Wuyts et al., 2004; Holden et al., 2005; Treu et al., 2005; van der Wel et al., 2005). This led to the conclusion that most of the stars in massive early-types at $z \sim 1$ have formed at high redshifts ($z > 2$).

Although the measurement of the evolution of M/L itself is model independent, the inferred age and formation redshift are sensitive to the choice of the parameters (e.g., IMF and metallicity) of the stellar population model, and even the choice of the model. By measuring the evolution of M/L at other wavelengths than the rest-frame B-band, the formation redshift can be established independently, and the range of possible model parameters constrained. Furthermore, the validity of different models can be verified. More specifically, different models predict a different evolution of the M/L in the near infra-red (NIR) relative to the evolution of the optical M/L. An advantage of measuring the evolution of the NIR M/L is that the NIR luminosity is less affected by the presence of a low mass young stellar population. Since measuring the evolution of M/L provides a luminosity-weighted age estimate, the evolution of the NIR M/L provides a less biased age estimate. With the arrival of the near Infra-Red Array Camera (IRAC, Fazio et al., 2004) on the Spitzer Space Telescope, studying the rest-frame NIR properties of the high-z early-type galaxy population has become feasible.

In this *Letter* we combine IRAC imaging with our high-z FP study (van der Wel et al., 2004, 2005), such that the evolution of M/L in the rest-frame K-band is measured for the first time. A calibration of galaxy masses derived from NIR luminosities is thus provided.

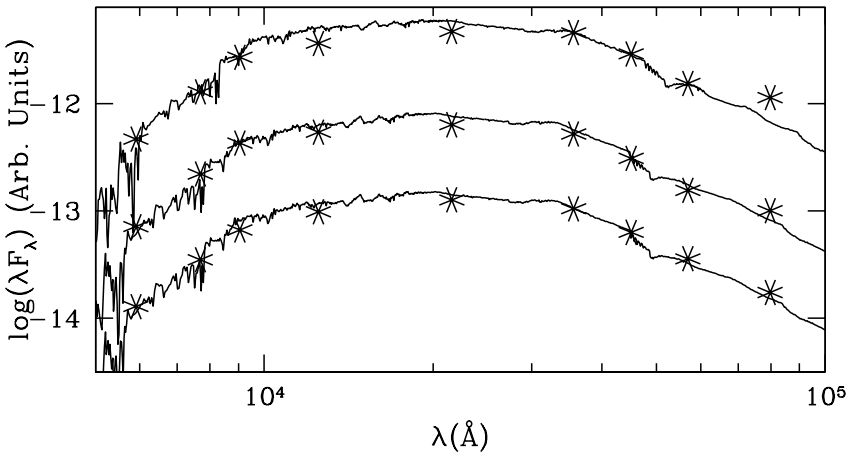

Figure 6.1: SEDs of three $z \sim 1$ early-type galaxies. The asterisks are observed fluxes in respectively the ACS (v, i, z), ISAAC (J, K), and IRAC (3.6, 4.5, 5.8, 8.0) bands. The lines are model spectra from Bruzual-Charlot (a 2 Gyr-old, dust-free SSP with solar metallicity and a Salpeter IMF) The photometric SEDs, including the IRAC data points, have plausible shapes of stellar populations of several Gyr old.

6.2 IRAC photometry of early-type galaxies at $z \sim 1$

van der Wel et al. (2005) provide a spectroscopic sample of 29 distant galaxies in the CDFS with accurate velocity dispersions. Spitzer GTO data are available, providing IRAC imaging in four channels (3.6μ, 4.5μ, 5.8μ, and 8.0μ) of a field containing the Chandra Deep Field-South (CDFS). Using the IRAC data we derive the rest-frame NIR photometry of those 20 galaxies in the spectroscopic sample with early-type morphologies and sufficiently high S/N spectra ($S/N \geq 12$ per Å). The average redshift of this sample is $z = 0.94$ and the average mass is $10^{11} M_{\odot}$. 12 galaxies in this sample are regarded as the 'primary sample': these objects are all at $0.95 < z < 1.15$ and satisfy all selection criteria applied by van der Wel et al. (2005). The other objects, mostly galaxies at $z \sim 0.7$ are referred to as the 'secondary sample' (see for more details van der Wel et al., 2005). The IRAC data are shallow (500s), but sufficiently deep to obtain high S/N photometry of all galaxies in the sample, certainly in the two shortest wavelength channels.

The IRAC fluxes were measured by matching the point spread functions of all available optical/NIR/IRAC images to the 8.0μ IRAC image (which has the lowest spatial resolution, $\mathrm{FWHM} = 2''3$). $5''0$ diameter aperture fluxes were measured using SExtractor (Bertin & Arnouts, 1996) to derive colors. The median formal errors in the IRAC fluxes of the galaxies in the sample are 0.01, 0.01, 0.10 and 0.13 mag for the four channels, respectively. Additionally, the systematic uncertainty in the IRAC zero-points is 0.03 mag. We transformed the observed colors to rest-frame $B - K$ colors using a procedure similar to what is described by van Dokkum & Franx (1996). The typical error in the rest-frame $B - K$ color is 0.06 mag, excluding the systematic error of 0.03 mag.

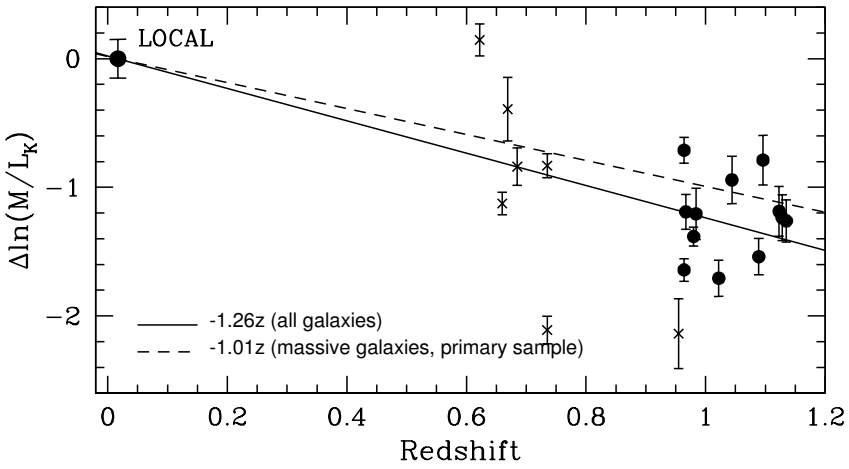

Figure 6.2: M/L_K evolution with redshift of early-type galaxies in the CDFS. The solid dots are objects in the primary sample, the crosses are the secondary sample (see text for an explanation). The data point labeled with 'Local' is derived from local cluster galaxies (Pahre et al. 1998), but a small difference between field and cluster galaxies is taken into account. The solid line indicates the evolution of the entire sample, the dashed line indicates the evolution of massive galaxies in the primary sample. The evolution of M/L_K of massive galaxies is $\sim 30\%$ slower than the evolution of M/L_B of the same sub-sample.

From the higher resolution K-band image we checked whether the IRAC photometry of our sample suffers from confusion. Three of the objects in our sample have close neighbors with such magnitudes that our photometry might be erroneous. However, we do not see a difference between these contaminated objects and the rest of the sample in either color, M/L, or any other parameter. In Figure 6.1 we show the SEDs of three high-redshift early-type galaxies. As an illustration we overplot a Bruzual & Charlot (2003) model spectrum for a 2 Gyr-old stellar population, demonstrating that the observed SEDs have reasonable shapes.

Besides measuring the colors of the galaxies in our spectroscopic sample, we also measured the colors of a sample of 41 early-type galaxies in the CDFS at lower redshifts ($0.6 < z < 0.8$). These were morphologically selected by eye from the available ACS imaging, and the redshifts are taken from COMBO-17 (Wolf et al., 2003). We use the average $B - K$ color of this sample to complement the $B - K$ evolution of the galaxies in the FP sample.

6.3 Evolution of M/L_K

If galaxies evolve passively, the offset of high-z galaxies from the local FP is a measure of the difference between the M/L of the distant galaxy and the M/L of comparably massive local galaxies (see van Dokkum & Franx, 1996). The rate of evolution is, in turn, a measure of the relative age difference between the distant galaxy and the local population.

To obtain the M/L evolution in the K-band, we compare the NIR properties of the distant galaxies with the local FP in the K-band (Pahre, Djorgovski & de Carvalho, 1998), i.e., we need effective radii ($r_{\rm eff}$) and surface brightnesses ($\mu_{\rm eff}$) of the distant galaxies in the rest-frame K-band. However, the spatial resolution of IRAC is obviously too low to measure galaxy sizes at $z \sim 1$. Instead we assume that $r_{\rm eff,K} = r_{\rm eff,B}$ and determine the surface brightness at this radius. Although this causes some error in the FP, previous work has shown that the combination of $r_{\rm eff}$ and $\mu_{\rm eff}$ which enters the FP is very stable against such errors (van Dokkum & Franx, 1996). The NIR surface brightness within the optical effective radius is provided by Pahre et al. (1998) for a local sample of cluster galaxies. For the distant sample we compute $\mu_{\rm eff,K}$ from $\mu_{\rm eff,B}$ and $(B-K)_{\rm eff}$, where $(B-K)_{\rm eff}$ is the color inside the effective radius. It is calculated from the total $B-K$ color by correcting for the negative color gradient measured by Peletier, Valentijn & Jameson (1990). The difference between $B-K$ and $(B-K)_{\rm eff}$ is -0.07 mag.

The local K-band FP is based on cluster galaxies, but our sample consists of field galaxies. Faber et al. (1989) have shown that field galaxies have $\sim 5\%$ lower M/L_B than cluster galaxies. Assuming that this difference is caused by either a difference in age or metallicity, this translates into a 2% difference in M/L_K, which follows from stellar population models from Bruzual & Charlot (2003). We take this difference into account when comparing the FP at high and low redshifts.

We show the evolution of M/L_K with redshift in Figure 6.2. It is readily apparent that M/L_K evolves significantly from $z \sim 1$ to the present. The evolution of the entire (primary plus secondary) sample is $\Delta \ln (M/L_K) = (-1.26 \pm 0.15)z$, obtained from a least squares linear fit. The primary sample alone evolves at a similar rate: $\Delta \ln (M/L_K) = (-1.18 \pm 0.10)z$. Comparing these numbers to the evolution of M/L_B ($\Delta \ln (M/L_K) = (-1.52 \pm 0.16)z$ and $(-1.46 \pm 0.09)z$, respectively), we see that the evolution in M/L_K is somewhat slower than the evolution in M/L_B. The scatter in $\Delta \ln (M/L_K)/z$ is 0.32, which is not much smaller than the scatter in the B-band (0.37). This is much larger than can be accounted for by measurement errors, and is most likely caused by an age spread of the stellar populations of the galaxies, as has been demonstrated before (van der Wel et al., 2005). In the B-band the measured evolution is strongly mass-dependent (van der Wel et al., 2004; Treu et al., 2005; van der Wel et al., 2005), mostly due to selection effects, but partially due to intrinsic differences between high- and low-mass galaxies (van der Wel et al., 2005). In the K-band the difference is much less pronounced, and only marginally significant. The galaxies in the primary sample with masses higher than $M = 2 \times 10^{11} M_{\odot}$ evolve as $\Delta \ln (M/L_K) = (-1.01 \pm 0.16)z$; galaxies less massive than that as $\Delta \ln (M/L_K) = (-1.27 \pm 0.11)z$. In the B-band these numbers are, respectively, $(-1.20 \pm 0.14)z$ and $(-1.60 \pm 0.09)z$. These numbers are consistent with the model prediction that M/L_K is less sensitive than M/L_B to the age of a stellar population and recent star formation activity.

Concluding, we find that the evolution of M/L_K from $z = 1$ to the present is $\sim 30\%$ slower than the evolution of M/L_B. We note that this direct measurement deviates from previous determinations of the evolution of M/L_K that were based on extrapolating observed SEDs (including the K-band as the longest wavelength data) to the rest-frame K-band at $z \sim 1$ using stellar population models. Such studies found that M/L_K evolves at least twice as slow as M/L_B (see, e.g., Drory et al.,

2004). This demonstrates that extrapolating observed K-band photometry of high-z galaxies to rest-frame K-band M/L is a hazardous procedure, which is strongly model dependent.

6.4 Discussion

Our results allow us to compare the evolution of M/L_B and M/L_K directly with predictions from stellar population models. We compare our results with the predictions of three models: Bruzual & Charlot (2003), Vazdekis et al. (1996), and Maraston (2004) (hereafter, BC03, V96, and M04, respectively). A critical aspect of the models is the method that is used to implement late stellar evolutionary phases. BC03 and V96 compute isochrones up to the early AGB phase, and subsequently include an ad hoc prescription for the thermally pulsating- (TP-) and post-AGB phases. On the contrary, M04 adopt the 'fuel consumption' approach, which allows implementation of short-duration but very luminous evolutionary stages, such as the TP- and post-AGB phases, in an analytical and numerically stable way.

In Figure 6.3 we compare the evolution from $z = 1$ to the present of M/L_B and M/L_K, and the related change in the rest-frame $B - K$ color. The BC03 model with solar metallicity and a Salpeter IMF does not fit the data: the predicted evolution of M/L_K against M/L_B is significantly slower than observed. Before investigating different models and model parameters, we consider several possible explanations for an apparently fast evolution of M/L_K with respect to M/L_B that are unrelated to stellar populations. First, a difference in dust content between local early-types and $z \sim 1$ early-types could lead to redder colors at $z = 1$ than expected from dust-free models. However, the BC03 model needs to be extincted by more than $A_V = 1$, to account for the $B - K$ colors of half of the galaxies in the primary sample. That amount of dust in unlikely, given the nature of these galaxies. Alternatively, the red colors might be produced by AGN in the $z \sim 1$ sample that are obscured in the optical, but not entirely in the NIR. This would lead to an upturn in the SEDs at 8μ, which is, however, not observed.

Now, we test whether changing parameters within the BC03 model can improve the consistency between the model and the data. Increasing the metallicity does not change the predictions by much. Changing the star formation history (SFH) does not lead to improved fits to the evolution of M/L_B and M/L_K either. Replacing the SSP model by models with exponentially declining SFHs or double bursts both shift the model curves toward the upper left in Figure 6.3, away from the data points. Flattening the slope of the IMF (from 1.35 to 0.35) does shift the model curve toward our data points, leading to an acceptable fit. There are indications that the IMF of the stellar populations of early-type galaxies are indeed top-heavy, because their star formation time scales are supposedly short. (see, e.g., Baugh et al., 2005), and because observed iron and α-elements abundances are reproduced by models assuming a top-heavy IMF (Nagashima et al., 2005).

Besides looking for a set of parameters within the BC03 model, it is worthwhile to compare our results to other models. As can be seen in Figure 6.3, the V96 and M04 models with a Salpeter IMF and solar metallicity provide better fits than BC03. Note that the differences between the models with identical parameters are very large;

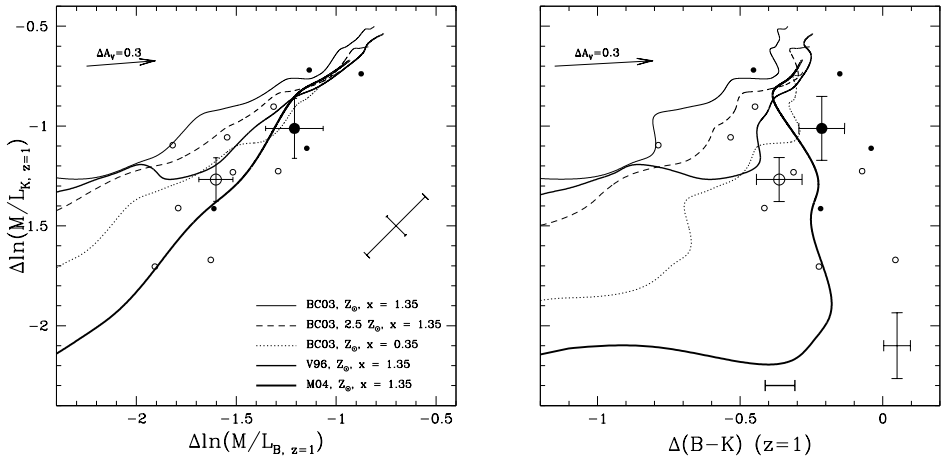

Figure 6.3: In this figure we compare the M/L evolution in the rest-frame B- and K-bands and the $B-K$ colors of our $z\sim1$ early-type galaxy sample. (Left): the evolution of M/L_B versus the evolution of M/L_K, normalized at $z=1$. The large filled symbol with error bars is the average of the four galaxies in the primary sample with masses larger than $M=2\times10^{11}M_\odot$. The large open symbol with error bars represents the eight less massive galaxies in the primary sample. The smaller symbols are the individual galaxies in the primary sample. The diagonal error bar at the right shows the typical (correlated) error in $\Delta\ln M/L_B$ and $\Delta\ln M/L_K$ for the individual data points. The shorter side of the error bar represents the uncertainty in $B-K$. We also show the effect of adding dust to the models. (Right): the evolution of $B-K$ versus the evolution of M/L_K, normalized at $z=1$. The thick horizontal error bar at the bottom indicates the average $B-K$ evolution extrapolated to $z=1$ of a sample of 41 early-type galaxies at $0.6<z<0.8$. The model tracks indicate the expected evolution between $z=1$ and the present, varying the formation redshift along the tracks. The Bruzual-Charlot models with a Salpeter IMF are excluded. A model with a flat IMF provides a better fit. Remarkably, the Maraston and Vazdekis models with a Salpeter IMF also provide better fits.

e.g., BC03 predict a correlation between color and $\Delta\ln(M/L)$, whereas M04 does not. We note that the spread of the data points representing the individual galaxies is large, but that there is no clear correlation between $\Delta\ln(M/L_K)$ and $\Delta(B-K)$. Even assuming a flat IMF, the BC03 model cannot reproduce the data points at the bottom right part of Figure 6.3b. The M04 model does fit to those data points. On the other hand, data points at the upper left of Figure 6.3b are not fit well by the M04 model, but, as described above, changing the SFH shifts model curves toward the upper left, enabling the M04 model to fit all data presented in Figure 6.3.

We can use the simple single burst models to estimate the average, luminosity-weighted formation redshift of the stellar populations of the galaxies. The formation redshift as estimated from the evolution of M/L_B is $1.6\leq z_{\rm form}\leq1.9$ and $1.5\leq z_{\rm form}\leq1.9$, using the models from BC03 and M04, respectively, with a Salpeter IMF and solar metallicity. According to the same models, the evolution of M/L_K suggests that $1.2\leq z_{\rm form}\leq1.5$ and $1.6\leq z_{\rm form}\leq2.0$, respectively. The BC03 model with a flat IMF provides a better fit to our results than the BC03 model with a Salpeter

IMF and produces $1.7 \leq z_{\rm form} \leq 2.7$, both from the evolution in the M/L_B and the evolution in M/L_K. As can be seen, the constraints on $z_{\rm form}$ are not improved by measuring the evolution of M/L_K. This is entirely due to the rather large model uncertainty in the rest-frame K-band evolution. Obviously, it is of the greatest relevance to improve our knowledge of AGB and post-AGB phases to improve upon this situation. We note that early-type galaxies are thought to be relatively simple systems, with simple SFHs. It is likely that the uncertainties are even higher for galaxies with a more complex SFH. The results presented here therefore suggest that even the rest-frame K-band photometry of such galaxies may be very difficult to interpret, and does require better models. Observations such as presented in this work provide a critical test for these models. In the next paper, we will explore full SED fitting, the uncertainties in determining stellar masses, and distinguish between the applicability of different stellar population models.

We thank Stijn Wuyts and Ivo Labbé for discussing photometry on IRAC data.

References

Baugh, C. M. et al. 2005, *MNRAS* **356**, 1191

Bell, E. F., McIntosh, D. H., Katz, N., & Weinberg, M. D. 2003, *ApJS* **149**, 289

Bell, E. F. et al. 2004, *ApJ* **608**, 752

Bertin, E. & Arnouts, S. 1996, *A&AS* **117**, 393

Bruzual, G. & Charlot, S. 2003, *MNRAS* **344**, 1000

Bundy, K., Ellis, R. S., & Conselice, C. J. 2005, *ApJ* in press, astro-ph/0502204

Djorgovski, S. & Davis, M. 1987, *ApJ* **313**, 59

Dressler, A., Lynden-Bell, D., Burstein, D., Davies, R. L., Faber, S. M., Terlevich, R., & Wegner, G. 1987, *ApJ* **313**, 42

Drory, N., Bender, R., Feulner, G., Hopp, U., Maraston, C., Snigula, J., & Hill, G. J. 2004, *ApJ* **608**, 742

Faber, S. M., Wegner, G., Burstein, D., Davies, R. L., Dressler, A., Lynden-Bell, D., & Terlevich, R. J. 1989, *ApJS* **69**, 763

Fazio, G. G. et al. 2004, *ApJS* **154**, 10

Gebhardt, K. et al. 2003, *ApJ* **597**, 239

Holden, B. P. et al. 2005, *ApJ* **620**, L83 (Chapter 2)

Kauffmann, G. & Charlot, S. 1998, *MNRAS* **297**, L23

Kelson, D. D., Illingworth, G. D., van Dokkum, P. G., & Franx, M. 2000, *ApJ* **531**, 184

Maraston, C. 2004, *MNRAS* submitted, astro-ph/0410207

Nagashima, M., Lacey, C. G., Okamoto, T., Baugh, C. M., Frenk, C. S., & Cole, S. 2005, *MNRAS* submitted, astro-ph/0504618

Pahre, M. A., Djorgovski, S. G., & de Carvalho, R. R. 1998, *AJ* **116**, 1591

Peletier, R. F., Valentijn, E. A., & Jameson, R. F. 1990, *A&A* **233**, 62

Shapley, A. E. et al. 2005, *ApJ* accepted, astro-ph/0503485

Treu, T. et al. 2005, *ApJ* in press, astro-ph/0502028

Treu, T., Stiavelli, M., Bertin, G., Casertano, S., & Møller, P. 2001, *MNRAS* **326**, 237

Treu, T., Stiavelli, M., Casertano, S., Møller, P., & Bertin, G. 2002, *ApJ* **564**, L13

van der Wel, A., Franx, M., van Dokkum, P. G., & Rix, H.-W. 2004, *ApJ* **601**, L5 (Chapter 3)

van der Wel, A., Franx, M., van Dokkum, P. G., Rix, H.-W., Illingworth, G., & Rosati, P. 2005, *ApJ* in press, astro-ph/0502228 (Chapter 4)

van Dokkum, P. G. & Ellis, R. S. 2003, *ApJ* **592**, L53

van Dokkum, P. G. & Franx, M. 1996, *MNRAS* **281**, 985

van Dokkum, P. G., Franx, M., Kelson, D. D., & Illingworth, G. D. 1998, *ApJ* **504**, L17

van Dokkum, P. G., Franx, M., Kelson, D. D., & Illingworth, G. D. 2001, *ApJ* **553**, L39

van Dokkum, P. G. & Stanford, S. A. 2003, *ApJ* **585**, 78

Vazdekis, A., Casuso, E., Peletier, R. F., & Beckman, J. E. 1996, *ApJS* **106**, 307

Wolf, C., Meisenheimer, K., Rix, H.-W., Borch, A., Dye, S., & Kleinheinrich, M. 2003, *A&A* **401**, 73

Wuyts, S., van Dokkum, P. G., Kelson, D. D., Franx, M., & Illingworth, G. D. 2004, *ApJ* **605**, 677

Chapter 7

Random and Systematic Uncertainties in Photometric Mass Determinations of $z \sim 1$ Galaxies: A Comparison with Dynamical Masses

Abstract

We compare dynamical masses of samples of distant ($z \sim 1$) and local early-type galaxies with stellar masses inferred from their broadband spectral energy distributions (SEDs), ranging from the rest-frame UV to the rest-frame near-infrared. We find that the relation between dynamical mass and inferred stellar mass has significant scatter and a zeropoint which is highly model-dependent. Furthermore, if we include the rest-frame infrared in the SED fits, the zeropoint of the relation is generally different for galaxies at different redshifts. In particular, "standard" Bruzual & Charlot (2003) models imply larger stellar masses for the distant galaxies relative to the stellar masses of the local galaxies. The discrepancy is as large as a factor of $\sim 2-3$ for models with Solar metallicity and a Salpeter IMF. If we use the Maraston (2004) stellar population model with the same parameters, we find no such discrepancy. If the rest-frame near-infrared is excluded from the fits, the systematic difference between the zeropoints of high- and low-redshift galaxy masses is close to zero for all models. This implies that the bias and systematic uncertainties originate in the near-infrared. We also show that if we include the rest-frame UV and allow the star-formation history and dust content to vary as free parameters do not change the photometric mass estimates significantly. Our results have far-reaching implications: determinations of the evolution of the stellar mass-density based on the Bruzual-Charlot model and rest-frame near-infrared photometry ($\lambda > 1\mu$) will underestimate the real evolution, and the systematic uncertainty is of the same order (a factor of $\gtrsim 2$) as the evolution of the mass-density from $z = 1$ to the present.

van der Wel, A., Franx, M., van Dokkum, P.G., Rix, H.-W. & Illingworth, G.D.

7.1 Introduction

Galaxy masses are an essential link between theories for galaxy formation and observations of the galaxy population and the evolution thereof. In the local universe masses can be measured accurately by modeling the luminosity distribution and the dynamical structure of galaxies (see, e.g., Cappellari et al., 2005). Scaling relations such as the fundamental plane for early-type galaxies (Djorgovski & Davis, 1987; Dressler et al., 1987) and the Tully-Fisher relation for spiral galaxies (Tully & Fisher, 1977) can be used to measure the evolution of the mass-to-light ratio (M/L) from high redshift to the present (Franx, 1993). This technique has been applied successfully and has provided constraints on the formation epoch of massive early-type galaxies out to $z \sim 1.3$ (e.g., van Dokkum & Stanford, 2003).

The number of galaxies with dynamically measured masses at intermediate redshifts ($z \sim 1$) is small, because obtaining those is observationally expensive. Furthermore, those samples are severely hampered by selection effects (see van der Wel et al., 2005b). Therefore, it is not yet possible to obtain directly the galaxy mass density at high redshift. Also, even though the redshift at which dynamical masses can be measured is steadily increasing, the most active era of galaxy formation, $z \geq 2$, is not accessible in that respect with the current generation of instruments. For all of these reasons, one has to rely on less accurate mass estimates to construct a picture of the high-z galaxy population (Shapley et al., 2003; Papovich et al., 2003; Förster Schreiber et al., 2004; Labbé et al., 2005; Shapley et al., 2005) and the evolution of the mass density with redshift (Bell et al., 2004; Drory et al., 2004). In these studies, broadband photometry is compared to predictions from stellar population models (most commonly, Bruzual & Charlot, 2003) in order to constrain the physical properties of high z-galaxies, and thereby their stellar masses.

The uncertainties, however, are large. It is well-known that parameters such as age, dust content and metallicity are degenerate, leaving M/L uncertain. The lack of knowledge of the IMF also leads to a (probably large) systematic uncertainty. If one observes at rest-frame near-infrared wavelengths may give a better idea of the stellar masses of dusty, star-forming galaxies, but the stellar M/L has been shown to be better constrained by optical colors than near-infrared colors (Bell & de Jong, 2001). Furthermore, there are large differences among the near-infrared properties of different stellar population models (Maraston, 2004; van der Wel et al., 2005a). Interpreting the rest-frame near-infrared luminosities of high-redshift galaxies obtained, for example, through IRAC (Fazio et al., 2004), is therefore not straightforward, and the conversion to stellar mass systematically uncertain. In this paper we constrain the severeness of such systematic problems. By comparing the masses obtained through SED fitting of high- and low-redshift early-type galaxies with known dynamical masses, we analyse the ability of different stellar population models to reproduce color- and M/L-evolution simultaneously. This yields a quantitative measurement of the accuracy of SED mass estimates, which depends on the wavelength range and the choice of model and its parameters.

Table 7.1: Photometry

ID	b_{435}	v_{606}	i_{775}	z_{850}	J	K	3.6μ	4.5μ	5.8μ	8.0μ
CDFS-1	24.49 ± 0.12	23.79 ± 0.11	22.10	20.95	19.95	18.12	16.68	16.46	16.44 ± 0.08	15.73 ± 0.08
CDFS-2	24.95 ± 0.18	23.33 ± 0.07	21.51	20.45	19.52	17.79	16.54	16.40	16.43 ± 0.08	15.87 ± 0.09
CDFS-3	25.70 ± 0.33	23.69 ± 0.10	22.47	21.44	20.53	18.84	17.47	17.05	17.50 ± 0.21	17.03 ± 0.24
CDFS-4	24.02 ± 0.08	22.70 ± 0.04	21.01	19.98	18.88	17.04	15.79	15.62	15.53 ± 0.04	15.27 ± 0.05
CDFS-5	> 26.4	23.90 ± 0.12	21.91	21.24	20.24	18.52	17.53	17.60	17.45 ± 0.20	17.98 ± 0.50
CDFS-6	25.23 ± 0.23	22.66 ± 0.04	20.98	20.39	19.57	17.94	17.18	17.08	16.96 ± 0.13	16.87 ± 0.21
CDFS-7	25.32 ± 0.25	23.48 ± 0.08	22.01	20.92	19.78	17.86	16.39	16.14	15.83 ± 0.05	15.95 ± 0.09
CDFS-12	24.41 ± 0.11	23.75 ± 0.10	22.24	21.28	20.31	18.50	17.15	16.93	17.04 ± 0.14	16.45 ± 0.15
CDFS-13	25.49 ± 0.28	23.14 ± 0.06	21.40	20.42	19.41	17.62	16.50	16.36	16.39 ± 0.08	16.26 ± 0.12
CDFS-14	24.97 ± 0.18	23.28 ± 0.07	21.56	20.55	19.56	17.79	16.37	16.33	16.15 ± 0.06	15.97 ± 0.10
CDFS-15	24.89 ± 0.17	22.67 ± 0.04	20.99	20.37	19.51	17.85	16.99	17.08	16.45 ± 0.08	16.83 ± 0.20
CDFS-16	25.07 ± 0.20	22.67 ± 0.04	21.02	20.34	19.50	17.73	16.81	16.87	16.87 ± 0.12	16.87 ± 0.21
CDFS-18	24.60 ± 0.13	23.03 ± 0.05	21.48	20.46	19.36	17.52	16.19	16.03	15.95 ± 0.05	15.66 ± 0.07
CDFS-19	23.52 ± 0.05	22.17 ± 0.02	20.86	20.17	19.32	17.62	16.43	16.23	16.01 ± 0.06	15.84 ± 0.08
CDFS-20	26.20 ± 0.49	23.34 ± 0.07	21.62	20.46	19.42	17.50	16.14	15.96	16.07 ± 0.06	15.60 ± 0.07
CDFS-21	24.30 ± 0.10	22.86 ± 0.05	21.18	20.58	19.78	18.19	17.05	17.02	16.67 ± 0.10	16.36 ± 0.13
CDFS-22	25.23 ± 0.23	22.68 ± 0.04	20.81	20.08	19.12	17.38	16.33	16.41	16.22 ± 0.07	16.10 ± 0.11
CDFS-23	26.12 ± 0.46	25.43 ± 0.41	23.12	21.91	20.84	19.16	17.64	17.46	17.54 ± 0.22	16.67 ± 0.18
CDFS-25	> 26.4	24.49 ± 0.19	22.58	21.42	20.34	18.76	17.37	17.28	16.89 ± 0.13	16.66 ± 0.17
CDFS-29	–	22.43 ± 0.03	21.40	20.46	19.65	18.10	16.79	16.53	16.75 ± 0.11	15.86 ± 0.09

Photometry of the high-redshift field galaxy sample. IDs are the same as in van der Wel et al. (2005b). All magnitudes within a $5''$-diameter aperture of PSF-matched images. The two lower-limits that occur in the table are 3σ-limits. Object CDFS-29 falls outside the b_{435} ACS mosaic. The photometry in the columns without listed errors have errors on all individual objects of 0.05 mag or less. The typical errors on the i_{775}, z_{850}, J, K, 3.6μ, and 4.5μ data points are 0.02, 0.01, 0.01, 0.01, 0.01, and 0.01 mag, respectively.

We describe the dynamical masses of the galaxy samples in Section 7.2. The photometry, the stellar population models, and our fitting method to obtain stellar masses are described in Section 7.3. In Section 7.4 we present our results, and we discuss the consistency of the models with our empirical results, and the dependence on the fitted wavelength range. In Section 7.5 we discuss the biases that are revealed by this work, and how this affects estimates of high-z galaxy masses and the evolution of the mass density. Throughout we use the Vega magnitude system, and the concordance cosmology, $(\Omega_M, \Omega_\Lambda, h) = (0.3, 0.7, 0.7)$.

7.2 Dynamical Masses of Early-Type Galaxies

Dynamical masses are computed as $M_{\rm dyn} = C r_{\rm eff} \sigma_{\rm c}^2 / G$, where C is a constant, $\sigma_{\rm c}$ is the central velocity dispersion, $r_{\rm eff}$ is the effective radius, and G is the gravitational constant. Kochanek (1994), assuming spherical symmetry, no rotation and fixed anisotropy, has shown that the velocity dispersion of the dark matter in elliptical galaxies equals the central line-of-sight velocity dispersion, as measured within a $2'' \times 4''$ sized aperture. This implies $C = 4$ if $M_{\rm dyn}$ is assumed to be twice the mass within the effective radius. In terms of the dispersions we use (corrected to an $3''4$-diameter aperture at the distance of the Coma cluster), we would have to use $C = 4.11$, taking the differences in aperture and distance between the samples into account. In the literature, $C = 5$ is used more often (e.g., Jørgensen, Franx & Kjærgaard, 1996). Therefore, we choose to use $C = 5$ in order for the masses remain consistent with previous studies. This number is based on an isotropic density model, which projects onto an $r^{1/4}$-law (see, e.g., Cappellari et al., 2005). In units of solar masses, the dynamical mass becomes $M/M_\odot = 1.17 \times 10^6 \; r_{\rm eff} \sigma_{\rm c}^2$, with $r_{\rm eff}$ in $\rm kpc$ and $\sigma_{\rm c}$ in $\rm km \; s^{-1}$. We note, however, that the precise value of C does not affect our analysis as long as it does not evolve with redshift (see Section 7.5).

van der Wel et al. (2005b) provide velocity dispersions and structural parameters for 20 early-type galaxies in the CDFS with a median redshift of $z = 0.98$. The median mass of this sample is $1.5 \times 10^{11} M_\odot$. As a low-redshift comparison sample we use 23 early-type galaxies in the nearby ($z = 0.024$) Coma cluster with measured $\sigma_{\rm c}$ and $r_{\rm eff}$ (Dressler et al., 1987; Faber et al., 1989). The median mass of this sample,$M = 1.8 \times 10^{11} M_\odot$, is comparable to that of the $z \sim 1$ sample.

7.3 Derivation of Stellar Masses from Photometry

7.3.1 Photometric Data

A large range of photometric data is available for the CDFS. GOODS provides ACS imaging in 4 filters (F435W, F606W, F775W, F850LP, hereafter b_{435}, v_{606}, i_{775}, z_{850}), ESO provides J- and K-band imaging, and IRAC GTO observations from the *Spitzer Space Telescope* are available (channels 1-4; 3.6μ, 4.5μ, 5.8μ, and 8.0μ, respectively). The photometry is described by van der Wel et al. (2005a) and is presented here in Table 7.1. The magnitudes are measured within a fixed aperture with a diameter of $5''$, used on registered and PSF-matched images.

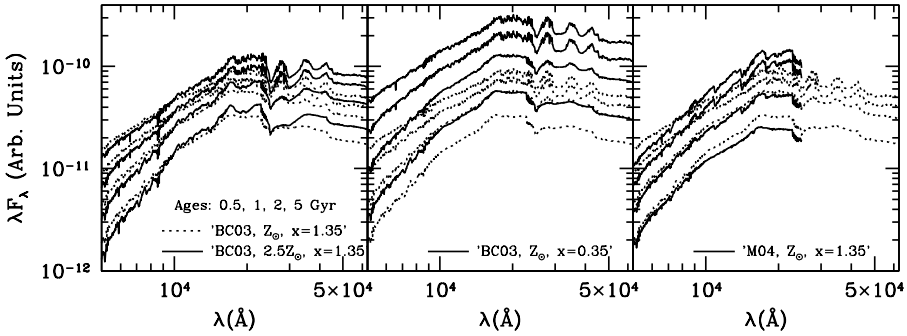

Figure 7.1: Various model spectra for a range of ages and parameters. The labels 'BC03' identify Bruzual & Charlot (2003) models; the label 'M04' identifies the Maraston (2004) model. Metallicity and IMF slope are also indicated ($x = 1.35$ corresponds to the Salpeter IMF). The indicated ages run from top to bottom. M04 does not provide realistic spectra for $\lambda > 2.5\mu$. Note the different color evolution predicted by the "standard" BC03 models and the M04 model (right panel).

For the local sample of Coma galaxies we need photometry that samples a similar rest-frame wavelength range as we have for the $z \sim 1$ sample. Faber et al. (1989) and Scodeggio, Giovanelli & Haynes (1998) provide the optical surface photometry, and Pahre, Djorgovski & de Carvalho (1998) provide the K-band surface photometry. We use the effective surface brightnesses and effective radii in the B-, V-, I-, and K-bands to compute the colors within apertures of 67", used by Faber et al., which typically corresponds to $4r_{\rm eff}$ at the distance of the Coma cluster. The average colors are $B - V = 0.96$, $V - I = 1.18$, and $I - K = 1.96$.

7.3.2 Stellar Population Models

For our purpose we need stellar population models that provide synthetic spectra over a large wavelength range $(0.3 - 4\mu)$. In recent years, Bruzual & Charlot (2003) (hereafter, BC03) and Maraston (2004) (hereafter, M04), have provided such spectra. M04 provide realistic spectra only up to 2.5μ, which limits our SED fitting range to the 4.5μ-channel. This is not a severe limitation as the photometric errors in the two longest-wavelength channels are much larger than in the other two channels (see Table 7.1), and observed 4.5μ at $z \sim 1$ corresponds to the reddest filter (K) available for the nearby sample.

The BC03 and M04 models are similar in their predictions of the optical properties of stellar populations for all ages of interest for this study. However, in the rest-frame near-infrared the predictions deviate significantly from each other. This difference stems from the different methods used to incorporate very late stellar evolutionary stages. While BC03 follow the isochrone synthesis approach, which characterizes the properties of the stellar population per mass bin, M04 adopt the fuel consumption approach, which calculates luminosity contributions from different stellar types by the amount of fuel used during a certain evolutionary stage. These two approaches

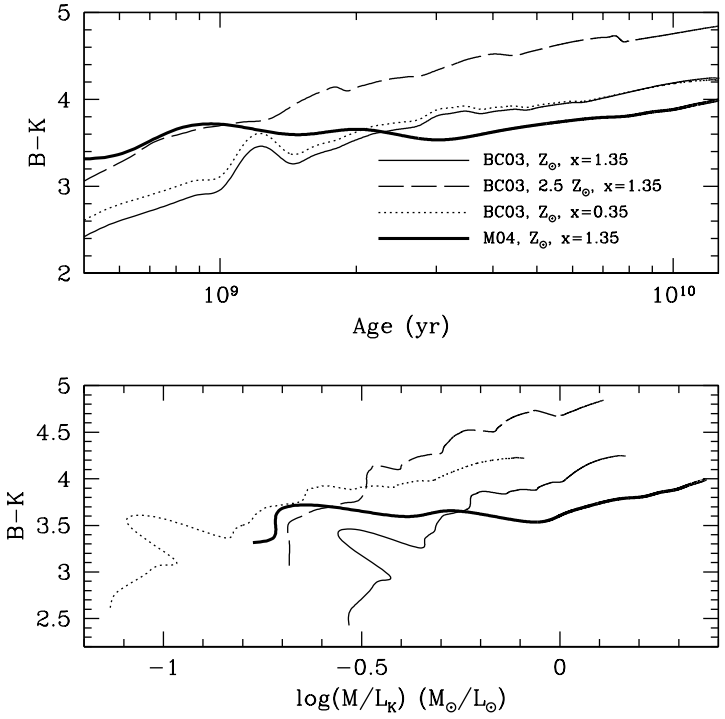

Figure 7.2: Evolution of $B-K$ with age for the models shown in Figure 7.1, which illustrates the differences in the evolution of the slope of the SED with age of a stellar population. *Bottom panel:* $B-K$ as a function of M/L_K, which illustrates that the conversion from $B-K$ colors to M/L ratios is strongly model-dependent. The age-range for the model tracks is the same as in the top panel, i.e., $0.5\ Gyr$ to $12.5\ Gyr$. Most notably are the different slopes of the lines of the BC03 models with $x = 1.35$ and $x = 0.35$ and the BC03 and M04 models. These differences have profound consequences for the interpretation of the SEDs of high-z galaxies.

lead to very large differences in the prediction of the evolution of K-band luminosity. This is caused by stars in the thermally pulsating AGB (TP-AGB) stage, which is very hard to model because of short time-scale variability of luminosity and color, and the scarcity of calibration spectra. BC03 and M04 use similar models to describe the properties of TP-AGB stars; the difference between the models is caused by the way the contribution of these stars to the total energy output of the stellar population is calculated. This particular evolutionary stage is extremely short-lived, and might therefore be hard to implement numerically with the isochrone synthesis technique, while the fuel consumption approach is a numerically more stable method for short-lived stages in general.

Of the M04 models we only consider the SSP model with solar metallicity and a Salpeter IMF. Of the BC03 models we consider various sets of parameters. First, we adopt the single stellar population (SSP) model with solar metallicity and a Salpeter

initial mass function (IMF). Second, we consider the BC03 model which is identical to the previous model but adopts a higher metallicity: $Z = 2.5Z_{\odot}$. Third, we consider the BC03 model with solar metallicity but which adopts a 'top-heavy' IMF with a slope of $x = 0.35$ (instead of $x = 1.35$, which is the Salpeter IMF), which has been shown to provide a better match to the evolution of M/L in the optical and in the near-infrared simultaneously (van der Wel et al., 2005a).

In Figure 7.1 we show the spectra of the three BC03 models and the M04 model for ages of 0.5, 1, 2, and 5 Gyr. The difference between the BC03 models with different metallicities, shown in the left-hand panel, is subtle, except for the longest wavelengths. The BC03 models with different IMF slopes (middle panel) show much larger variation. This is primarily a difference in overall energy output, which is simply due to the larger numbers of giants in the case of a flat IMF, especially at young ages. A secondary, but actually more interesting difference is the different evolution of the slope, i.e., color, of the SED in models with different IMFs. Such differences in color evolution are also apparent if the BC03 models are compared to those of M04, shown in the right-hand panel. For ages younger than $2.5\ Gyr$, the M04 model predicts much higher luminosities in the K-band than the BC03 model, whereas the optical luminosities are similar.

7.3.3 Fitting Method

We use redshifted model spectra to compute apparent magnitudes, $m_{\rm mod}$. We allow the age (and, optionally, the star-formation history (SFH) and the dust content) to vary, and normalize the calculated magnitudes to match the observed magnitudes, $m_{\rm obs}$, to obtain the photometric mass. $m_{\rm obs}$ are the color magnitudes given in Table 7.1, but including a correction from fixed aperture magnitudes to total magnitudes as measured by SExtractor in the K-band. The derived stellar mass includes the dark, compact remnants of massive stars, but not the gas lost due stellar winds and supernovae ejecta. The best-fitting model is selected on the basis of the root mean square of $m_{\rm mod} - m_{\rm obs}$ (RMS), weighing with the square of the inverse of the photometric errors, and adopting a minimum error of 0.10 mag. In practice this means that for the high-z galaxies the b_{435}, 5.8μ, and 8.0μ data points have lower weight than the other data points (see Table 7.1).

For the SSP models described in the previous section, there is a unique relation between color and age. Subsequently, age determines M/L, and thus $M_{\rm phot}$. The conversion from color to age, and from age to M/L is strongly model dependent, as was already suggested by the differences among the model spectra shown in Figure 7.1. This is further illustrated in Figure 7.2, where we show how the $B-K$ color varies with age, and how $B-K$ translates into M/L for the four different models. This figure clearly suggests that there will be systematic differences between the photometric masses obtained with different models. Furthermore, a certain change in color from low to high redshift, implies a certain change in M/L, which depends on the model. The comparison with the evolution of the dynamical M/L, thus puts constraints on the models. This will be investigated by comparing photometric masses of the low- and high-redshift galaxy samples described above, which have measured dynamical masses.

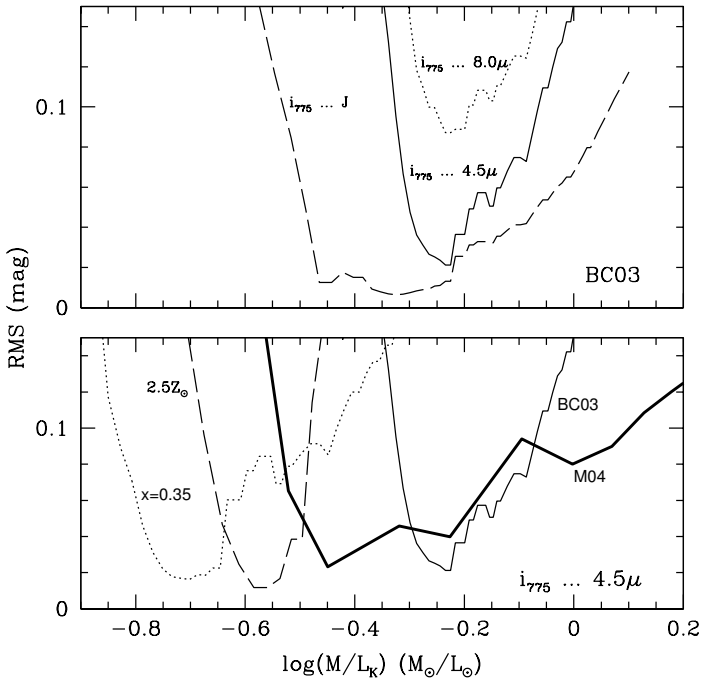

Figure 7.3: The quality of the SED fit, quantified by the root means square (RMS) of the difference between the calculated model magnitudes and the observed magnitudes, of object CDFS-2 at $z = 0.96$, as an illustration of the fitting method. The upper panel shows how the results vary by changing the wavelength range included in the fit, if we use the BC03 model with solar metallicity and a Salpeter IMF. *Dashed line:* result for fitting i_{775}, z_{850}, and J. *Solid line:* result for fitting i_{775}, z_{850}, J, K, 3.6μ and 4.5μ. *Dotted line:* result for fitting i_{775}, z_{850}, J, K, 3.6μ, 4.5μ, 5.8μ and 8.0μ. If we include the rest-frame near-infrared in the fit we find a somewhat higher M/L. The bottom panel shows how the results vary if we fit i_{775} through 4.5μ with different models. *Solid line:* result for the BC03 model with Solar metallicity and a Salpeter IMF. *Dashed line:* result for the BC03 model with super-solar metallicity. *Dotted line:* result for the BC03 model with a top-heavy IMF. *Solid thick line:* result for the M04 model with solar metallicity and a Salpeter IMF. Different models clearly yield different M/L ratios. The broad minimum obtained for the M04 model can be explained by the slow evolution of the optical-to-near-infrared color (see Figure 7.2), and the consequently poorly constrained age.

In Figure 7.3 we show, as an example, the fit results for object CDFS-2, if we use the SSP models. In the top panel we show how M/L_K of the best-fitting BC03 model (with solar metallicity and a Salpeter IMF) changes if different wavelength ranges are used in the fit. In the bottom panel we show how the results vary from model to model, if we fit the SEDs from i_{775} to 4.5μ. The M/L_K of the best-fitting models vary by a factor of 3, which indicates the level of the systematic uncertainty of photometric mass estimates. Note that the quality of the fits is generally good: the RMS of the best-fitting model is typically only ~ 0.02 mag.

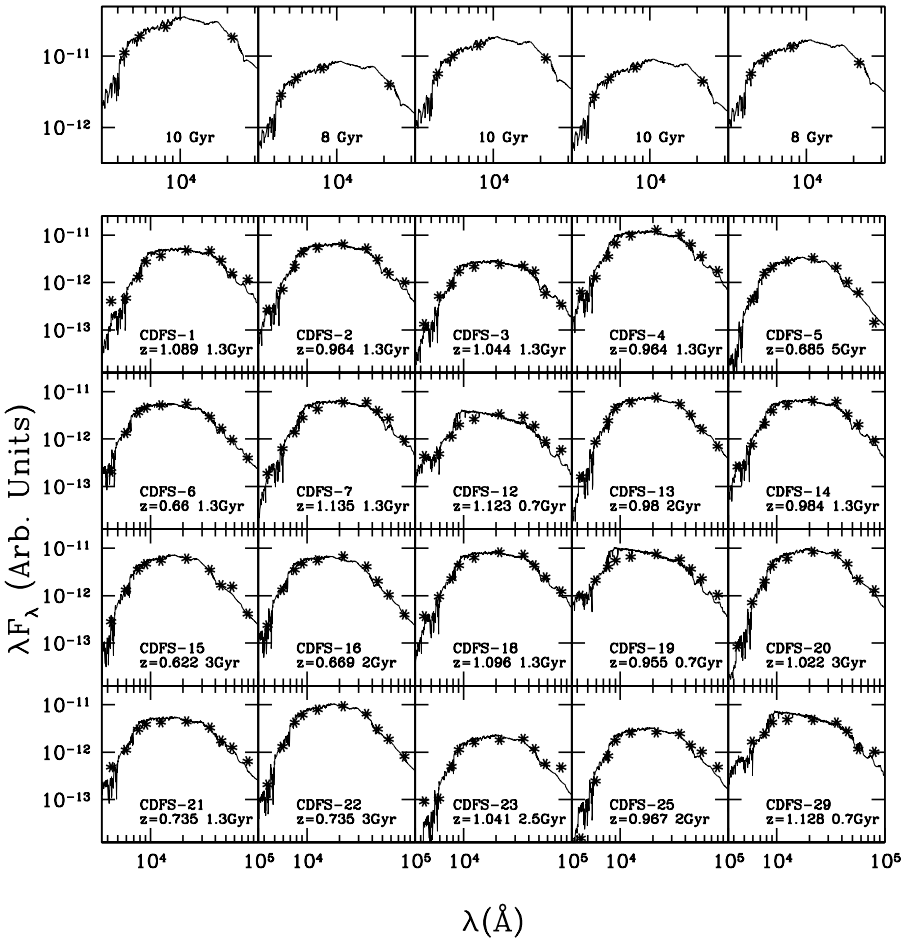

Figure 7.4: SEDs of all 20 high-redshift ($0.6 < z < 1.15$) early-type galaxies and 5 of the 23 low-redshift ($z = 0.024$) early-type galaxies (top row). The photometric data points in the top panels are B, V, I and K, and those in the other panels are b_{435}, v_{606}, i_{775}, z_{850}, J, K, 3.6μ, 4.5μ, 5.8μ, 8.0μ. The model spectra are the best-fitting SSP models of BC03 with solar metallicity and a Salpeter IMF (age is the only free parameter besides the mass normalization). IDs, redshifts, and ages of the best-fitting models are indicated. The majority of the SEDs is fitted very well with this simple model.

Not only object CDFS-2 is fitted well by a SSP model. In Figure 7.4 we show for five of the local galaxies, and all 20 high-z field galaxies, the photometric data points and the spectra of the best-fitting BC03 model with solar metallicity and a Salpeter IMF. In general, the photometric SEDs are fitted quite well by this simple model, with as most notable exceptions the objects CDFS-19 and CDFS-29.

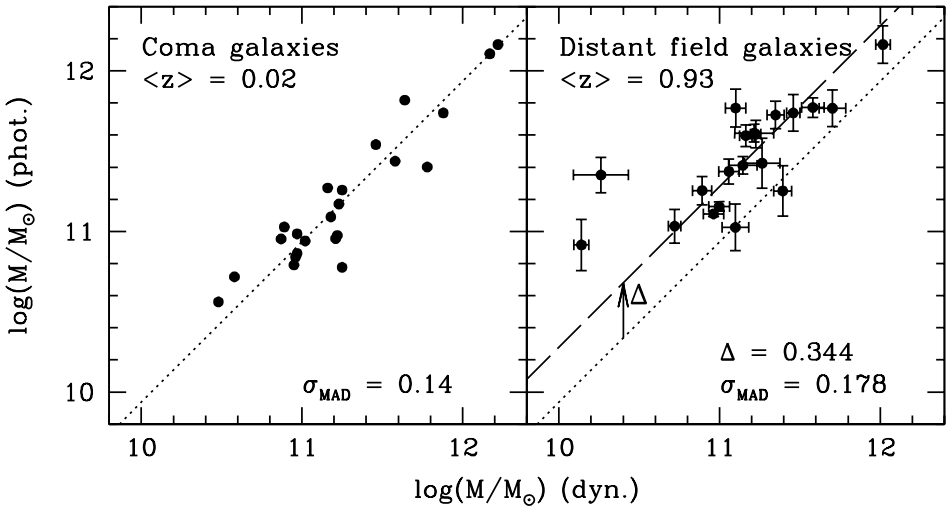

Figure 7.5: *Left:* Comparison between dynamical and photometric masses of early-type galaxies in the Coma cluster at $z = 0.024$. The photometric masses are obtained by fitting the photometric SEDs (B, V, I, and K) by model spectra from BC03 for a SSP with solar metallicity and a Salpeter IMF. Age and mass are the only free parameters. The dotted line indicates the best-fitting line with slope 1, minimizing the median absolute deviation. $\sigma_{\rm MAD}$ is the standard deviation from that line. *Right:* Comparison between dynamical and photometric masses of the distant field early-type galaxies. Photometric masses are obtained by fitting the photometric SEDs from i_{775} to 4.5μ by the same BC03 model as used for the local galaxies. The dotted line, the same as in the left panel, is shown as a reference. The dashed line is the best-fitting line with slope 1 to the distant field sample, excluding the galaxies with velocity dispersions lower than 100 km s^{-1}. The errors on the photometric masses are obtained through a Monte-Carlo simulation of the photometric data points. The typical error is $\sim 10\%$. As can be seen, there is a systematic offset between the local and distant sample, quantified by Δ. The fact that $\Delta \neq 0$, or, that the dashed and dotted lines do not coincide, shows that the evolution of M/L and the evolution of the shape of the SED (i.e., the color evolution) cannot be reproduced simultaneously by the BC03 model with solar metallicity and a Salpeter IMF.

7.4 Systematic and Random Uncertainties in Photometric Mass Estimates

7.4.1 Modeling Rest-Frame Optical and Near-Infrared SEDs

In this section we compare photometric and dynamical mass estimates. We begin by fitting the rest-frame optical and near-infrared SEDs. Thus, for the local sample we use the B-, V-, I-, and K-bands in the fit, and for the distant sample we use i_{775} through 4.5μ, excluding the rest-frame UV b_{435}- and v_{606}-bands. The rest-frame optical and near-infrared are less affected than the UV by young stars, and should therefore yield better mass estimates. We start with exploring the results obtained with the SSP model from BC03 with solar metallicity and a Salpeter IMF. The left-hand

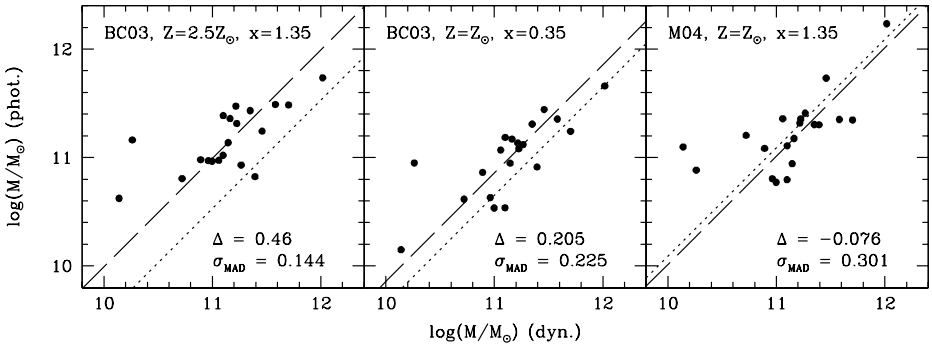

Figure 7.6: Comparison between dynamical and photometric masses of distant field early-type galaxies as in Figure 7.5, but for different models. Again, the SEDs are fitted from i_{775} to 4.5μ. The left panel shows the results for the BC03 model with super-solar metallicity and a Salpeter IMF. The middle panel shows the result for the BC03 model with solar metallicity and a top-heavy IMF. In the right-hand panel we show the results for the M04 model with solar metallicity and a Salpeter IMF. Remarkably, this model yields a value for Δ that is close to zero, i.e, M04 simultaneously reproduces color and M/L evolution from the optical to the near-infrared. On the other hand, the scatter is much larger.

panel of Figure 7.5 shows $M_{\rm dyn}$ vs. $M_{\rm phot}$ for the sample of local early-type galaxies. On the right-hand side we show the same relation for the distant galaxies. As can be seen, $M_{\rm phot}$ and $M_{\rm dyn}$ correlate well; the scatter around the median $M_{\rm phot}/M_{\rm dyn}$ is a factor of 1.38 for the local sample and a factor of 1.51 for the distant sample. Fitting a relation of the form $M_{\rm phot} \propto M_{\rm dyn}^{\alpha}$ gives $\alpha = 0.90 \pm 0.07$ for the local sample, and $\alpha = 0.98 \pm 0.21$ for the distant sample. Because α is close to 1, it is safe to conclude that there is one-to-one correspondence between photometric and dynamical masses, which is encouraging.

There are, however, systematic differences between $M_{\rm phot}$ and $M_{\rm dyn}$. The median $M_{\rm phot}/M_{\rm dyn}$ is 0.86 for the local sample, i.e., the photometric masses are slightly smaller than the dynamical masses. Such a difference is not unexpected, and might by due to the presence of non-baryonic or baryonic dark matter, and due to deviations from the Salpeter IMF at the low-mass end (see, e.g., Gerhard et al., 2001; Cappellari et al., 2005). However, for the distant sample this ratio is $M_{\rm phot}/M_{\rm dyn} = 1.90$. This implies that the ratio between the photometric and dynamical masses changes from the local to the distant sample by more than a factor of two. We quantify this by the parameter $\Delta = 0.344 \pm 0.075$, which is the change in $M_{\rm phot}/M_{\rm dyn}$ from $z = 0$ to $z \sim 1$ in logarithmic units. If we assume passive evolution, this BC03 model does not correctly predict color evolution and M/L evolution simultaneously. The implication is that derived photometric masses are a factor of 2.2 higher at $z \sim 1$ compared to $z = 0$. Hence, the mass-density at $z \sim 1$ would be overestimated by the same factor. This is a severe problem, since the mass-density is thought to evolve by about a factor of 2 (see, e.g.,. Bell et al., 2004). The systematic error is of the order of the measurement, which is obviously a serious limitation to the robustness of such results.

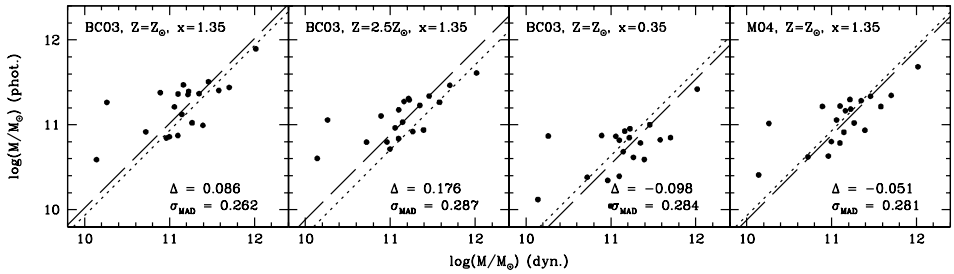

Figure 7.7: Comparison between dynamical and photometric masses of distant field early-type galaxies as in Figures 7.5 and 7.6, but if we only include i_{775}, z_{850}, and J in the fits. The models used in the different panels are the same as used in the right-hand side of Figure 7.5, and in Figure 7.6. The photometric masses of the local sample (represented by the dotted line) are derived by fitting the B, V, and I data-points. For all BC03 models Δ has a value close to zero, but the scatter increases with respect to the values obtained if we include the K, 3.6μ, and 4.5μ data-points in the fits. For the M04 model Δ is also close to zero, and the scatter close to a factor of 2, which is very similar to what was found if we include the K, 3.6μ, and 4.5μ data-points in the fits.

We now investigate by how much our results change if we adjust the model parameters. In Figure 7.6 we show, in the left-hand and middle panels, the results for the two BC03 models with super-solar metallicity and a top-heavy IMF, respectively. As can be seen, Δ is always positive for BC03 models, but its value varies if the model parameters are changed. For the model with the top-heavy IMF, the inconsistency is smallest ($\Delta = 0.205 \pm 0.08$). This is caused by the relatively fast evolution of the near-infrared M/L (see Figure 7.2). The BC03 model with a super-solar metallicity produces an even larger value of $\Delta = 0.46 \pm 0.08$, which is caused by the smaller relative age differences between the local and distant galaxies.

The right-hand panel of Figure 7.6 shows the result if we use the M04 model with solar metallicity and a Salpeter IMF. The M04 model yields $\Delta = -0.076 \pm 0.102$, albeit with a large scatter in $M_{\rm phot}/M_{\rm dyn}$ of a factor of ~ 2. The latter can be understood by the slow change of $B-K$ with age (see Figure 7.2): age and, thus, M/L are not well-constrained by the optical-to-near-infrared color, which leads to large random errors in $M_{\rm phot}$. This also manifests itself in Figure 7.3 by the broad minimum inferred from the M04 model. Nonetheless, the small value of Δ means that the M04 model successfully predicts the change in the shape of the SED, i.e., color, and the evolution of M/L from $z \sim 1$ to the present simultaneously. This can be compared to $\Delta = 0.344$ obtained for the BC03 model with solar metallicity and a Salpeter IMF. It is remarkable that the BC03 and M04 models with identical parameters yield such contrary results.

Table 7.2 lists average ages of the best-fitting models and the average $\rm RMS$ of the fits. As can be seen, the quality of the fits does not depend on the model used: the average $\rm RMS$ is ~ 0.09 magnitudes. The typical age at $z \sim 1$ inferred from any model with solar metallicity is $3-4\ Gyr$. For the super-solar metallicity BC03 model the typical age is 1.2 Gyr.

Table 7.2: SED fitting results

Model	Δ	$\sigma_{\rm MAD}$	δ	$<$ RMS $>$ mag	$<$ Age $>$ Gyr	$<\tau>$ Gyr	$<A_V>$ mag
$z=1$: i_{775} , z_{850} , J , K , 3.6μ , 4.5μ							
BC03, $Z_\odot$, $x=1.35$	0.344 ± 0.075	0.178 ± 0.040	0.279 ± 0.063	0.095	3.653	–	–
BC03, $2.5Z_\odot$, $x=1.35$	0.460 ± 0.080	0.144 ± 0.048	-0.008 ± 0.064	0.075	1.216	–	–
BC03, $Z_\odot$, $x=0.35$	0.205 ± 0.080	0.225 ± 0.045	-0.144 ± 0.069	0.088	3.284	–	–
M04, $Z_\odot$, $x=1.35$	-0.076 ± 0.102	0.301 ± 0.051	0.013 ± 0.090	0.095	3.258	–	–
$z=1$: i_{775} , z_{850} , J							
BC03, $Z_\odot$, $x=1.35$	0.086 ± 0.122	0.262 ± 0.051	0.019 ± 0.100	0.034	2.042	–	–
BC03, $2.5Z_\odot$, $x=1.35$	0.176 ± 0.107	0.287 ± 0.041	-0.118 ± 0.082	0.035	1.116	–	–
BC03, $Z_\odot$, $x=0.35$	-0.098 ± 0.123	0.284 ± 0.052	-0.462 ± 0.103	0.033	1.789	–	–
M04, $Z_\odot$, $x=1.35$	-0.051 ± 0.104	0.281 ± 0.046	-0.122 ± 0.081	0.037	1.542	–	–
$z=1$: i_{775} , z_{850} , J , K							
BC03, $Z_\odot$, $x=1.35$	0.250 ± 0.114	0.248 ± 0.043	0.183 ± 0.090	0.066	2.847	–	–
M04, $Z_\odot$, $x=1.35$	0.016 ± 0.112	0.263 ± 0.044	-0.054 ± 0.091	0.061	2.774	–	–
$z=1$: b_{435} , v_{606} , i_{775} , z_{850} , J , K , 3.6μ , 4.5μ							
BC03, $Z_\odot$, $x=1.35$	0.159 ± 0.093	0.289 ± 0.052	0.095 ± 0.084	0.282	2.158	–	–
BC03, τ	0.382 ± 0.074	0.215 ± 0.046	0.314 ± 0.065	0.193	4.684	0.721	–
BC03, τ, A_V	0.249 ± 0.086	0.232 ± 0.041	0.181 ± 0.078	0.161	2.316	0.342	0.432
M04, $Z_\odot$, $x=1.35$	-0.209 ± 0.134	0.339 ± 0.069	-0.119 ± 0.126	0.223	2.026	–	–
M04, τ	-0.085 ± 0.115	0.419 ± 0.073	0.013 ± 0.103	0.178	3.405	0.437	–
M04, τ, A_V	-0.129 ± 0.104	0.280 ± 0.060	-0.030 ± 0.091	0.188	2.247	0.347	0.284

The separation into four parts indicates the different filter combinations used for the fits. The first column shows the used model and the parameters. If τ or A_V are mentioned, these are free parameters in the fit. Δ and $\sigma_{\rm MAD}$ are defined in the caption of Figure 4. For the value Δ the photometric and dynamical masses the Coma sample are relevant. Photometric masses of the Coma galaxies are obtained by fitting the B-, V-, I-, and K-band data-points, except for the two middle sections, for which the K-band is omitted, in order to match the fitted wavelength range better. δ is the median $\log(M_{\rm phot}/M_{\rm dyn})$ for the distant field galaxy sample. $<$ RMS $>$ is the average standard deviation of the observed magnitudes minus the best-fitting model magnitudes, which indicates the quality of the SED fits. $<$ Age $>$ is the average age of the best-fitting models. $<\tau>$ is the average star formation timescale of the best-fitting model with an exponentially declining star formation rate. $<A_V>$ is the average dust extinction.

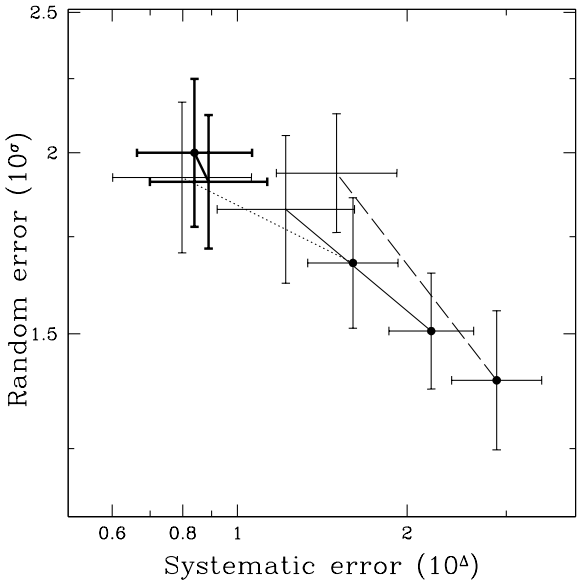

Figure 7.8: Summary of the fit results for the rest-frame optical and near-infrared. For each of the four models used in Figures 7.5, 7.6, and 7.7 we show the values of Δ and σ in linear units. The errorbars with a *filled circle* are the results if we fit the i_{775}, z_{850}, J, K, 3.6μ and 4.5μ data-points, i.e., the rest-frame optical and near-infrared. The errorbars without symbols are the results if we fit the i_{775}, z_{850}, and J data-points, i.e., the rest-frame optical. The results for every model are connected by lines with the same style as in Figure 7.2.

From the spread in the values of Δ in Figures 7.5 and 7.6, we conclude that the systematic uncertainty in photometric masses of high-z galaxies, if we model the rest-frame optical and near-infrared parts of the SEDs, is as large as a factor of 3.5. The M04 model is able to correctly predict the evolution of colors and M/L ratios, contrary to the BC03 models which always underpredict the M/L evolution by a factor of 1.6 to 3.

To test the effect of the rest-frame near-infrared data on the results of the SED fits, we have also preformed SED fits only to the filters sampling the rest-frame optical: i_{775}, z_{850}, and J for the distant galaxies, and B, V, and I for the local galaxies. We show the results for the four different models in Figure 7.7. As can be seen, BC03 models produce values of Δ that are consistent with zero, which implies that the systematic effects described above originate in the near-infrared part of the model spectra. The scatter in $M_{\rm phot}/M_{\rm dyn}$ is typically a factor of 1.9, compared to a factor of 1.5 when the near-infrared is included (see Table 7.2). Fits to the rest-frame optical SEDs of low- and high-redshift galaxies correctly reproduce the observed M/L evolution, albeit with a slightly larger scatter compared to what is produced if the infrared is included.

To test whether the discrepancy is due to a problem with the IRAC data, we fit also fitted the "standard" BC03 and M04 models to the i_{775}, z_{850}, J, and K filters. We find that Δ significantly deviates from zero (see Table 7.2). This shows that the

discrepancy is most likely not caused by a problem with the IRAC data, but by model problems in the near-infrared. Furthermore, this test demonstrates that interpreting K-band observations at $z = 1$ by comparing them to BC03 model predictions is hazardous: stellar masses of red galaxies at $z \sim 1$ (see, e.g., Fontana et al., 2004) are easily overestimated by a factor of 1.5.

For the M04 model the situation is different. Δ is close to zero, with and without the near-infrared, and the scatter, contrary to what happens if we use a BC03 model, is approximately the same (see Table 7.2). This is not surprising as in the M04 model changes with age in the near-infrared take place at the same rate as changes in the optical (see Figure 7.2).

Note that, if we omit the near-infrared, the average model ages of the distant galaxies decrease from $3 - 4$ to $1.5 - 2$ Gyr for the models with solar metallicity. This can be understood if one realizes that the near-infrared luminosity in the BC03 models is relatively low. Older model stellar populations are therefore required to explain the observed red optical-to-near-infrared colors. The model ages of the local galaxies, on the other hand, hardly change by including the K-band data in the fit. The inferred relative age difference between the local and distant galaxies is thus small we include the near-infrared in the fit, hence the slow M/L-evolution and the consequently large positive values of Δ.

The spread in Δ among the models corresponds to a factor of 1.8 if the near-infrared is excluded, compared to a factor of 3.5 if we include the near-infrared. This significant decrease indicates that the optical properties of the model spectra are more alike, and probably more robust, than their near-infrared properties. The quality of the SED fits is generally very good in the rest-frame optical ($\mathrm{RMS} \lesssim 0.04$ mag, see Table 7.2).

The fit results are summarized in Figure 7.8. The M04 models give small systematic errors but large random uncertainties, whereas the BC03 models, if we include the near-infrared, give small random uncertainties and large systematic errors. Irrespective of the model the uncertainty in the mass of an individual galaxy is always at least a factor of ~ 2.

7.4.2 Including the Rest-Frame UV: Constraining the Star-Formation History

The scatter in $M_{\rm phot}/M_{\rm dyn}$ and the systematic differences between the local and the distant samples may be caused by an over-simplification of the models. In this section we explore whether extending the analysis to the rest-frame UV part of the spectrum and allowing for more free parameters in the models (SFH and dust content) provides more accurate and consistent photometric mass estimates.

We first consider the BC03 and M04 SSP models with solar metallicity and a Salpeter IMF, but now we fit the b_{435}, v_{606}, i_{775}, z_{850}, J, K, 3.6μ and 4.5μ datapoints. The results are shown in the left-hand panel of Figure 7.9. As can be seen, the scatter in $M_{\rm phot}/M_{\rm dyn}$ is somewhat larger than the scatter obtained without the b_{435}- and v_{606}-bands: it increased from a factor of 1.5 to 1.9 for the BC03 model, and from 2.0 to 2.2 for the M04 model. The decrease in the quality of the fit is also clear, as can be seen in Table 7.2: for the BC03 model, the average RMS is now 0.282 mag (it is 0.095 mag without the two shortest-wavelength filters); for the M04 model this

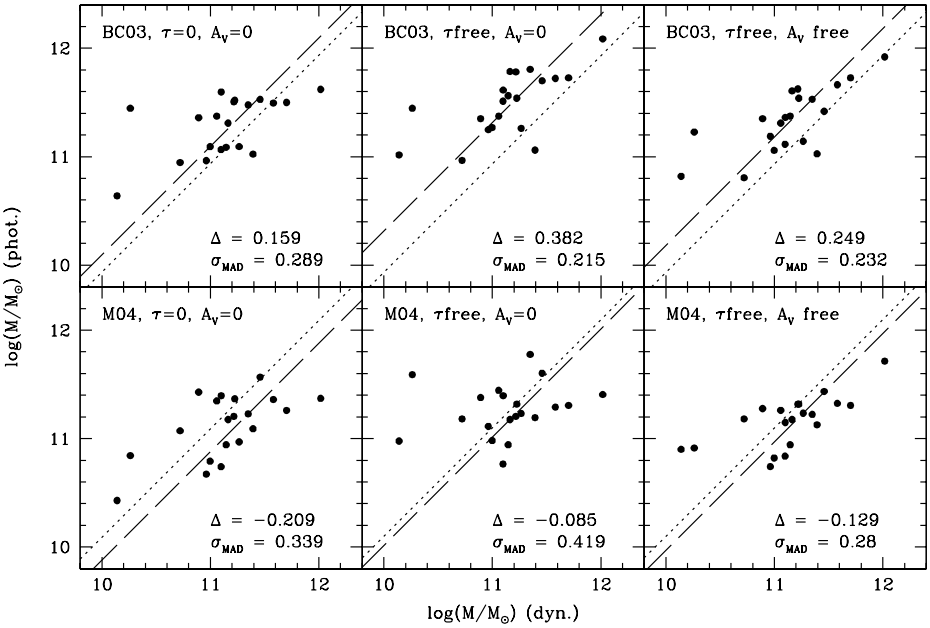

Figure 7.9: Comparison between dynamical and photometric masses of distant field early-type galaxies as in Figure 7.5, but now also including the rest-frame UV part of the SEDs: all photometric data points between b_{435} and 4.5μ are used in the fits. From left to right, we increase the numbers of degrees of freedom, first assuming a dust-free SSP (left-hand panel), then assuming an exponentially declining SFR with the time scale τ as a free parameter (middle panel), and finally we allow for dust-extinction as well (right-hand panel). The top row shows the results for the BC03 model with solar metallicity and a Salpeter IMF. The bottom row shows the results for the M04 model with solar metallicity and a Salpeter IMF. See Table 7.2 for the inferred ages, and average values of τ and A_V. Generally, modeling the rest-frame UV part of the spectrum does not improve on the quality of the SED fits, even if we allow for more free model parameters.

is 0.223 mag, instead of 0.095 mag.

Now we allow for an exponentially declining star-formation rate (SFR) with timescale τ, instead of assuming a single burst. Since star-formation is related to extinction by dust, we consequently adopt A_V as a free parameter as well. The results are shown in the middle and right-hand panels of Figure 7.9. With τ and A_V both as free parameters, the scatter in $M_{\rm phot}/M_{\rm dyn}$ becomes a factor of 1.7 for the BC03 model, and a factor of 1.9 for the M04 model. This is comparable to the numbers obtained if we exclude the rest-frame UV and use SSP models to fit the SEDs. The values of Δ are 0.25 and -0.13 for BC03 and M04, respectively, which implies that the systematic effects described in Section 7.4.1 are not removed by adopting more complicated models. The quality of the fits has improved with respect to restricting the fits to $\tau = 0$ (the average RMS values are 0.16 mag and 0.19 mag for BC03 and M04, respectively), but not quite to the level of the fits that ignored the rest-frame UV (0.10 for both models).

The large errors in the b_{435}-band photometry are likely responsible. We conclude that an SSP model is sufficient to model the rest-frame optical and near-infrared SEDs of early-type galaxies, but that this is not the case if the rest-frame UV is included.

In Table 7.2 we show the average values of age, τ, and A_V. Age and τ are very similar for both models: ~ 2.3 and $\sim 0.35\ Gyr$, respectively. This implies an average SFR of $\sim 1\ M_\odot\ yr^{-1}$. Assuming that this declines exponentially between the epoch of observation and the present, the average stellar mass increases by no more than $\sim 0.2\%$ after $z \sim 1$. The galaxy with the highest SFR would increase its stellar mass by 8.0%. We conclude that residual star-formation is not relevant for the galaxies in our sample, and, barring interactions or mergers, have assembled all of their stellar mass by $z \sim 1$.

The dust content inferred from the BC03 model is remarkably high: $A_V = 0.43$ on average. We interpret this as an artifact: the relatively red optical-to-near-infrared colors of the high-z galaxies can only be reproduced by the BC03 model we assume rather high values for the extinction. Recall that a similar argument was deployed to explain the relatively old ages inferred if we model the rest-frame near-infrared with a single burst. Because the M04 predicts higher near-infrared luminosities and redder optical-to-near-infrared colors, this model requires less dust to model the SEDs: we find $A_V = 0.28$ on average. Apparently, the model A_V is not determined by the UV-properties of a galaxy, which are most affected by extinction, but by the near-infrared properties of the model used for the SED fit.

We conclude that if we adopt τ and A_V parameters, modeling the rest-frame UV through near-infrared SED does not improve the results with respect to fitting the rest-frame optical and near-infrared only with dust-free SSP models. The systematic under-prediction of the M/L-evolution by the BC03 remains of the order of a factor of 2. The results obtained in this section are not shown in Figure 7.8, but from Table 7.2 it can be seen that these datapoints would not deviate by much from the other results obtained with the same models.

7.5 Summary and Discussion

In this paper we have compared photometric and dynamical masses of early-type galaxies at both high ($z \sim 1$) and low redshifts. The random and systematic uncertainties were analyzed quantitatively. We start this discussion with a summary our main conclusions.

1) The random uncertainty in photometric mass estimates of individual galaxies is a factor of 1.5 to 2. This depends on the choice of the stellar population model and the fitted wavelength range. If we use BC03 models the random uncertainty reduces from a factor of 2 to a factor of 1.5 if we model the rest-frame optical and near-infrared instead of the rest-frame optical alone. For the M04 model the scatter is roughly constant if we extend the SED fits to the near-infrared.

2) The spread of the average photometric masses as obtained we use different models and wavelength ranges is a factor of ~ 4. Differences between models are largest when rest-frame near-infrared data are included in the SED fits, which suggests that the main source of the systematic differences is the near-infrared part of the model spectra. This is not very surprising given the intrinsic uncertainty in modeling

the type of stars (TP-AGB stars) that contribute most to the luminosity at those wavelengths, certainly for the typical ages of $\sim 1-3\ Gyr$ inferred for the $z \sim 1$ early-type galaxies.

3) If we use "standard" BC03 models with a Salpeter IMF to fit the rest-frame optical and near-infrared SEDs, there is a large systematic difference between photometric masses of low- and high-redshift early-type galaxies with the same dynamical mass. This means that this model does not correctly infer the M/L-evolution from the observed evolution of optical-to-near-infrared colors. The discrepancy is in the order of a factor of $2-3$, depending on the assumed metallicity. If we adopt a top-heavy IMF (with slope $x = 0.35$ instead of $x = 1.35$), this systematic difference decreases somewhat, but it does not disappear. If we exclude the rest-frame near-infrared from the fits, the discrepancy disappears. This implies that the source of the systematic problems originate in the near-infrared, and that the models correctly predict the evolution of the optical M/L and colors. High-redshift galaxy masses can therefore be constrained better by rest-frame optical photometry than by rest-frame near-infrared photometry. Consequently, measurements of the evolution of the mass-density out to $z \sim 1$ based on the evolution of optical colors (e.g., Bell et al., 2004) are more robust and less biased than measurements based on rest-frame near-infrared photometry.

4) Contrary to the BC03 model, the M04 model with solar metallicity and a Salpeter IMF yields similar photometric masses for low- and high-redshift galaxies with the same dynamical mass. The model M/L-evolution as inferred from the colors, is thus consistent with the dynamically derived M/L-evolution. This is a consequence of the relatively fast evolution of M/L_K in the M04 model, with respect to the BC03 model. Using the M04 model to derive the evolution of the stellar mass density will provide a better estimate than using the BC03 model. However, the slow evolution of the $B-K$ color causes the age and M/L to be not well constrained, which results in the above mentioned relatively large random uncertainty of a factor of ~ 2. Therefore, in general, not much is gained by extending the fits to the rest-frame near-infrared.

5) If we adopt the SFH and dust-extinction as free parameters, and extend the SED fits to the rest-frame UV, we cannot remove the systematic uncertainties and offsets in the derived model M/L, nor increase the quality of the SED fits, nor decrease the random uncertainty in the photometric masses.

Problems with the BC03 model are the most straightforward interpretation of the overestimated photometric masses at $z \sim 1$ compared to $z = 0$. This interpretation relies on two assumptions. First, we assume that that local and distant galaxies have similar dynamical structures and dark matter fractions. However, it is unlikely that $z \sim 1$ early-type galaxies have anisotropies that are very different from local early-types, which would mean that the aperture correction applied to the velocity dispersions should be different, but this cannot strictly be ruled out. The same holds for the ratio between dark matter and stellar mass. Second, we assume that local and distant galaxies can directly compared. By that we ignore the possibility that the galaxies in our $z \sim 1$ sample merge between the redshift of observation and the present. Gas-rich mergers, supplying significant numbers of young stars, possibly changing the metal-content, would have an important impact on the photometric mass estimates. That this is a realistic concern is shown by Jørgensen et al. (2005), who find that cluster early-type galaxies cannot evolve passively from $z = 0.8$ to the present, but that the

metal-content has to increase over that time. We point out that, if this would affect our results, that our estimate of the discrepancy between the photometric masses of local and distant galaxies would be an underestimate. We also note that mergers between early-type galaxies, which are likely very important in shaping the mass-function of the early-type galaxy population (e.g., van Dokkum, 2005), do not affect our conclusions because the stellar populations themselves do not change.

IRAC data have been used to infer stellar masses and rest-frame near-infrared properties of samples of galaxies at $z \gtrsim 2$ (Shapley et al., 2005; Labbé et al., 2005), using BC03 models. It remains to be seen what the systematic effcts are for these much younger and dusty galaxies, which are actively forming stars. A comparison between masses derived from BC03 models and M04 models is required to constrain the uncertainties, and obviously, the next step is to obtain a dynamical calibration of the mass-scale at $z \sim 2$.

Furthermore, it is essential that the systematic differences among the models and between the models and the observations are reduced. Therefore, a better understanding of the near-infrared properties of stellar populations is required. Our work provides a new tool to verify the predictions of the models, a method that can be exploited more thoroughly by obtaining a large sample of early-type galaxies with a wide range in redshift, accurate dynamical masses and abundance measurements, and photometric masses derived from multi-wavelength imaging, including the rest-frame near-infrared. Only when the model discrepancies are resolved can the full potential of IRAC for measuring stellar masses of distant galaxies be realized.

References

Bell, E. F. & de Jong, R. S. 2001, *ApJ* **550**, 212

Bell, E. F. et al. 2004, *ApJ* **608**, 752

Bruzual, G. & Charlot, S. 2003, *MNRAS* **344**, 1000 (BC03)

Cappellari, M. et al. 2005, *MNRAS* submitted, astro-ph/0505042

Djorgovski, S. & Davis, M. 1987, *ApJ* **313**, 59

Dressler, A., Lynden-Bell, D., Burstein, D., Davies, R. L., Faber, S. M., Terlevich, R., & Wegner, G. 1987, *ApJ* **313**, 42

Drory, N., Bender, R., Feulner, G., Hopp, U., Maraston, C., Snigula, J., & Hill, G. J. 2004, *ApJ* **608**, 742

Förster Schreiber, N. M. et al. 2004, *ApJ* **616**, 40

Faber, S. M., Wegner, G., Burstein, D., Davies, R. L., Dressler, A., Lynden-Bell, D., & Terlevich, R. J. 1989, *ApJS* **69**, 763

Fazio, G. G. et al. 2004, *ApJS* **154**, 10

Fontana, A. et al. 2004, *A&A* **424**, 23

Franx, M. 1993, *PASP* **105**, 1058

Gerhard, O., Kronawitter, A., Saglia, R. P., & Bender, R. 2001, *AJ* **121**, 1936

Jørgensen, I., Franx, M., & Kjærgaard, P. 1996, *MNRAS* **280**, 167

Jørgensen, I., Bergmann, M., Davies, R., Barr, J., Takamiya, M., & Crampton, D. 2005, *AJ* **129**, 1249

Kochanek, C. S. 1994, *ApJ* **436**, 56

Labbé, I. et al. 2005, *ApJ* **624**, L81

Maraston, C. 2004, *MNRAS* submitted, astro-ph/0410207 (M04)

Pahre, M. A., Djorgovski, S. G., & de Carvalho, R. R. 1998, *AJ* **116**, 1591

Papovich, C., Giavalisco, M., Dickinson, M., Conselice, C. J., & Ferguson, H. C. 2003, *ApJ* **598**, 827

Scodeggio, M., Giovanelli, R., & Haynes, M. P. 1998, *AJ* **116**, 2728

Shapley, A. E., Steidel, C. C., Pettini, M., & Adelberger, K. L. 2003, *ApJ* **588**, 65

Shapley, A. E. et al. 2005, *ApJ* accepted, astro-ph/0503485

Tully, R. B. & Fisher, J. R. 1977, *A&A* **54**, 661

van der Wel, A., Franx, M., van Dokkum, P. G., Huang, J., Rix, H.-W., & Illingworth, G. 2005a, *ApJ* submitted (Chapter 6)

van der Wel, A., Franx, M., van Dokkum, P. G., Rix, H.-W., Illingworth, G., & Rosati, P. 2005b, *ApJ* in press, astro-ph/0502228 (Chapter 4)

van Dokkum, P. G. 2005, *AJ* submitted, astro-ph/0506661

van Dokkum, P. G. & Stanford, S. A. 2003, *ApJ* **585**, 78

Samenvatting

Sterrenstelsels

De Melkweg, waarin de Zon één van de circa 100 miljard sterren is, is slechts één van de vele sterrenstelsels in het Heelal. Sterrenstelsels, ook wel de bouwstenen van het heelal genoemd, bestaan in verschillende soorten.

Ten eerste zijn er spiraalstelsels (ook laat-type stelsels genoemd). De Melkweg behoort tot deze soort, waarvan het uiterlijk wordt gedomineerd door een schijf van sterren, stof en gas met spiraalarmen. In deze schijf worden tot op dit moment nog steeds nieuwe sterren gevormd. In het centrum bevindt zich een lensvormige verzameling sterren. Een voorbeeld hiervan is te zien in Figuur 1. Ten tweede zijn er de elliptische sterrenstelsels (ook vroeg-type stelsels genoemd). Bij deze soort ontbreekt de gas-rijke schijf en wordt de verschijning door een ronde of rugbybal-vormige verzameling sterren gedomineerd (zie Figuur 1). Er zijn nog andere soorten sterrenstelsels (bijvoorbeeld dwergstelsels en onregelmatige stelsels).

Spiraalstelsels komen het meest voor, maar elliptische stelsels zijn doorgaans groter. Volgens de laatste schattingen bevindt minstens de helft van alle sterren in het Heelal zich in een elliptisch stelsel. Tot aan jaren '70 dacht men dat elliptische stelsels heel lang geleden gevormd zouden zijn, terwijl spiraalstelsels in latere stadia nog zouden groeien via hun schijf.

Sterrenstelsels zijn niet willekeurig verspreid door het heelal, maar ze zijn verdeeld over structuren die we, met toenemende grootte, groepen, clusters en superclusters noemen. Andere gebieden van het heelal zijn juist vrijwel leeg. De eigenschappen van individuele sterrenstelsels hangen af van de omgeving waarin ze zich bevinden. In de centra van clusters, waar de stelsels dicht op elkaar staan, bevinden zich alleen maar elliptische stelsels, terwijl in de legere gebieden meer spiraalstelsels voorkomen. Dit leidde tot het idee dat elliptische stelsels bij nader inzien helemaal niet ouder zijn dan spiraalstelsels, maar dat ze juist gevormd worden door het samensmelten van spiraalstelsels. Spiraalstelsels komen elkaar het meest waarschijnlijk tegen in gebieden waar zijn dicht bij elkaar staan, dus in de centra van clusters. Dat het samensmelten van stelsels geen bizar idee of zeldzaam verschijnsel is, bleek uit de ontdekking dat de eerder genoemde onregelmatige stelsels veelal samensmeltende stelsels zijn.

De conclusie is gerechtvaardigd dat elliptische stelsels een cruciale rol spelen in het heelal: het zijn de grootste stelsels, ze domineren de centrale delen van clusters, zijn het einde van de "voedselketen" wat betreft sterrenstelsels, en bevatten het merendeel van de sterren. Daarom gaat dit proefschrift uitsluitend over elliptische sterrenstelsels.

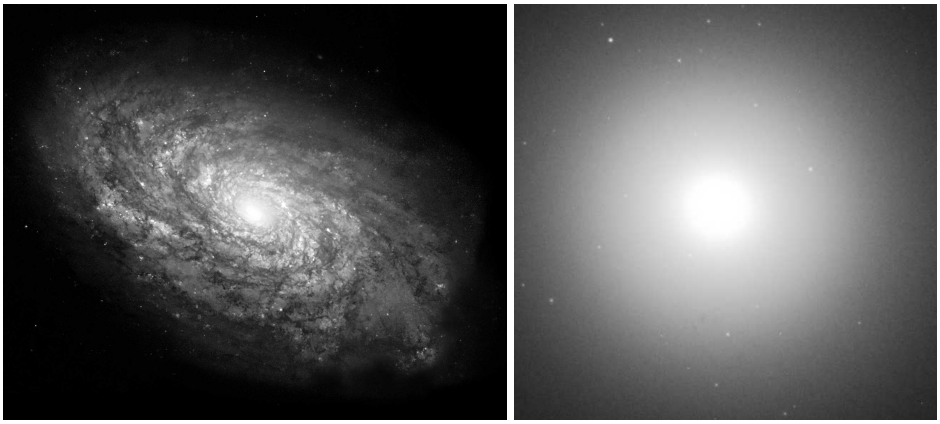

Figuur 1: *Links:* Voorbeeld van een spiraalstelsel (NGC 4414). *Rechts:* Voorbeeld van een elliptisch stelsel (NGC 4552).

Het Ontstaan van Structuur in het Heelal

Via samensmelting hangt de levensloop van sterrenstelsels, ofwel hun evolutie, samen met de vorming van clusters en andere grote-schaal structuren. De vorming van structuur wordt op zijn beurt weer beïnvloed door de uitdijing en "vorm" van het heelal. Een theorie voor de vorming van sterrenstelsels moet dus worden opgesteld binnen de theorie voor de evolutie van het heelal zelf.

Het heelal is 13.7 miljard geleden begonnen met de Big Bang. 300.000 jaar daarna was alle materie vrijwel perfect egaal verdeeld. Er was geen sprake van structuur, behalve minieme afwijkingen in dichtheid. Die zijn als gevolg van de zwaartekracht gegroeid, waardoor gebieden die een iets hogere dichtheid hadden steeds voller werden, en gebieden die een iets lagere dichtheid hadden steeds leger.

Volgens de modernste theorieën werden eerst kleine "units" van gas en sterren gevormd die in de loop van de tijd samensmolten tot steeds grotere sterrenstelsels. Het samensmelten van verschillende stelsels is dus een vanzelfsprekende eigenschap van deze theorie.

De grote-schaal structuur in het heelal, clusters en super-clusters, kan goed verklaard worden met de huidige modellen. De theorie wordt betrouwbaar geacht, want er is slechts een klein aantal ingrediënten nodig, met als belangrijkste de zwaartekracht.

De vorming van individuele sterren en sterrenstelsels is echter een veel gecompliceerder proces, waaraan veel meer facetten zitten waarvan de kennis beperkt is. Zo is er geen goede theorie voor de vorming van sterren. De modellen voor de vorming van sterrenstelsels zijn dus heel flexibel. Er wordt dikwijls opgemerkt dat de theoretici alles voor elkaar kunnen krijgen door 'aan de knoppen te draaien'. Om de voorspellingen van de modellen te controleren, moet er dus voortdurend vergeleken worden met waarnemingen.

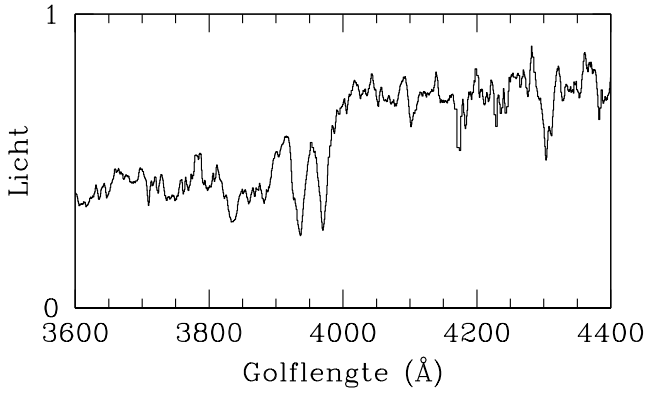

Figuur 2: Voorbeeld van een spectrum. Langs de horizontale as staat de golflengte. Naar rechts toe wordt de golflengte langer, en heeft het licht dus een rodere kleur. De smalle "dallen" zijn de spectraallijnen. Aan de hand van de precieze positie van deze lijnen kan de roodverschuiving bepaald worden. Dit spectrum is het resultaat van 24 uur lang waarnemen met de VLT.

Roodverschuiving

In een laboratorium, of op wat voor wijze dan ook, kun je geen experimenten met sterren of sterrenstelsels doen. Je kunt ook niet wachten tot een sterrenstelsel verandert in de loop van de tijd, want die veranderingen treden niet op in de loop van het schrijven van een proefschrift, maar in de loop van op z'n snelst tientallen miljoenen, en meestal miljarden jaren.

Niettemin is er een directe methode om de evolutie van sterrenstelsels te bestuderen. De basis daarvan is het feit dat licht tijd nodig heeft om van de ene naar de andere plek te komen, net als geluid. In tegenstelling tot de snelheid van geluid, is de snelheid van licht zo groot dat we er in het dagelijks leven niets van merken. Op de schaal van ons zonnestelsel is het al wel merkbaar: het licht van de Zon zien wij 8 minuten nadat de Zon het heeft uitgestraald. Het licht van de dichtstbijzijnde ster behalve de Zon heeft er 4 jaar over gedaan (zijn afstand is dus 4 lichtjaar), en de afstand van het dichtstbijzijnde grote sterrenstelsel buiten de Melkweg is zo'n 2 miljoen lichtjaar. Als je nu sterrenstelsels bestudeert die miljarden lichtjaren ver weg staan, zie je ze dus zoals ze er miljarden jaren geleden uitzagen. Op die tijdschaal, een behoorlijk deel van de leeftijd van het heelal, treden er veranderingen op.

Licht bestaat uit elektro-magnetische golven. Hoe langer de golflengte (de afstand tussen twee toppen van de golf), hoe roder het licht. Het licht van een veraf gelegen sterrenstelsel is zó lang geleden uitgezonden dat het heelal sindsdien een flink stuk is uitgedijt. Nu is het licht, zeg maar, mee uitgedijt, waardoor de golflengte langer is geworden en het licht dientengevolge roder. We zeggen dat het sterrenstelsel een *roodverschuiving* heeft. Hoe groter de roodverschuiving, hoe meer het heelal is uitgedijt sinds het licht werd uitgezonden, hoe langer geleden dat is gebeurd, en hoe verder weg het sterrenstelsel staat. Roodverschuiving is dus een maat voor afstand en tijd.

Roodverschuiving kan gemeten worden aan de hand van een zogeheten spectrum. Je maakt een spectrum door het licht dat je waarneemt te sorteren naar kleur, ofwel golflengte. Dit kun je doen met behulp van een prisma of, zoals gebeurt in de praktijk, met een ingewikkelder apparaat dat onder een telescoop hangt. Sterren zenden bij de ene golflengte meer licht uit dan bij de andere. Dit komt ten eerste door de temperatuur. Een koele ster zendt bij lange golflengten meer licht uit dan bij korte, en krijgt daardoor een rode kleur. Een hete ster is blauw. Ten tweede absorberen atomen in de sterren licht bij bepaalde golflengten. Hierdoor ontstaan zogenaamde spectraallijnen.

Figuur 2 laat een voorbeeld van een spectrum van een sterrenstelsel zien. Dit spectrum bevat het licht van alle sterren in het stelsel bij elkaar. Je kunt zien dat er meer licht bij lange golflengtes is dan bij korte. Het is dus een stelsel waarin zich veel rode sterren bevinden. De smalle "dalen" waarbij minder licht waargenomen wordt, zijn de spectraallijnen. Voor een sterrenstelsel op *hoge* roodverschuiving zijn zulke lijnen meer naar rechts verschoven dan voor een stelsel op *lage* roodverschuiving. Een dergelijke waarneming wordt tegenwoordig routinematig gedaan voor stelsels tot 10 miljard lichtjaar ver weg.

De vraag die astronomen via waarnemingen van sterrenstelsels op hoge roodverschuiving proberen te beantwoorden, kan als volgt geformuleerd worden: *Hoe veranderen de aantallen van verschillende types sterrenstelsels en de sterren daarin met roodverschuiving?* De kunst is om eigenschappen van sterrenstelsels op verschillende roodverschuivingen met elkaar te vergelijken, en zodoende de evolutie in kaart te brengen.

Massa's van Sterrenstelsels

Een belangrijke eigenschap is het gewicht, of de massa, van een sterrenstelsel. Hier zijn twee redenen voor. Ten eerste wordt massa voorspeld door de modellen voor de vorming van sterrenstelsels. Ten tweede is massa een eigenschap die niet verandert, tenminste als een sterrenstelsel niet samensmelt met een ander stelsel. Dit laatste stelt je in staat om stelsels op verschillende roodverschuivingen maar met dezelfde massa direct met elkaar te vergelijken, en de evolutie van andere eigenschappen te meten.

Hoe meet je een massa zonder weegschaal? De zwaartekrachtswet van Newton zegt dat de kracht die een object op een ander object uitoefent slechts afhangt van de massa's van de objecten en de afstand tussen de objecten. De bewegingen van sterren in een sterrenstelsel worden uitsluitend door de zwaartekracht bepaald.

Een meer alledaags voorbeeld is de beweging van de Aarde rond de Zon. De snelheid van de Aarde in zijn baan rond de Zon is zo'n 30 km/s, met een gemiddelde afstand tot de Zon van 150 miljoen km. Stel dat die snelheid tweemaal zo groot was geweest. Dat zou betekenen dat de Zon $4\times$ zwaarder is. Ook als de snelheid hetzelfde was, maar de afstand tweemaal zo groot, zou de Zon $2\times$ zwaarder zijn.

Wat voor de Zon geldt, geldt ook voor sterrenstelsels: hoe sneller de bewegingen van de sterren, hoe groter de massa, en hoe groter het stelsel, hoe groter de massa. Om een sterrenstelsel te wegen, moet je dus zijn grootte meten en hoe snel de sterren in het stelsel bewegen.

Om de grootte van een sterrenstelsel te meten, moet je zijn afstand weten (via de roodverschuiving). Iets dat ver weg staat lijkt immers kleiner dan iets dat dichtbij staat.

Het meten van snelheden binnen een stelsel is lastiger. Hiervoor gebruiken we ook het spectrum en de spectraallijnen daarin. De ene ster beweegt in een andere richting dan de andere ster, waardoor de roodverschuiving van een spectraallijn varieert van ster tot ster. Aangezien het miljarden sterren betreft, uit die snelheidsvariatie zich in een verbreding van de spectraallijn van een sterrenstelsel. Hoe groter die verbreding, hoe groter de snelheden.

Een dergelijke verbreding is meetbaar, maar dit is niet eenvoudig, zeker niet voor zeer ver weg gelegen sterrenstelsels. Het vereist een veel hogere kwaliteit van het spectrum dan het bepalen van een roodverschuiving, want daarvoor hoef je een spectraallijn alleen maar te kunnen zien. Zelfs als je de grootste telescopen ter wereld gebruikt, is het nodig om vele uren te besteden aan het verzamelen van het licht van een sterrenstelsel.

Toch is het zeer de moeite waard om veel tijd te besteden aan dit soort waarnemingen. Als het éénmaal is gelukt om de massa van een veraf gelegen stelsel te meten, kun je de eigenschappen van dat stelsel vergelijken met een nabij gelegen stelsel met dezelfde massa. Op deze manier kun je bijvoorbeeld op directe wijze de evolutie van de helderheid van zo'n stelsel bepalen. Dat geeft op zijn beurt weer een indicatie van leeftijd en het moment van vorming van het stelsel. Dit zou niet mogelijk zijn zonder de massa van veraf gelegen stelsels te kennen.

Dergelijke leeftijdsbepalingen hebben geleid tot de conclusie dat de sterren in elliptische sterrenstelsels in clusters relatief kort na de Big Bang zijn gevormd. De modellen voor de vorming van sterrenstelsels voorspellen dat sterren in elliptische stelsels die zich niet in clusters bevinden, de zogenaamde veldstelsels, jonger zijn. De eerste centrale vraag die in dit proefschrift aan de orde komt is: **Zijn veldstelsels jonger dan clusterstelsels?**.

Kennis van het moment van vorming van individuele stelsels is zeer interessant. Maar om de vorming van de hele verzameling sterrenstelsels te begrijpen, moeten we achterhalen hoe de hele populatie van sterrenstelsels evolueert. Het is ondoenlijk om massa's te meten voor alle stelsels omdat dat het een tijdrovend proces is. Verder is het ook niet mogelijk voor zeer zwakke en de verst weg gelegen stelsels massa's te meten. Het zou te lang duren om goede spectra te meten met de huidige telescopen.

Om deze redenen moet men vaak terugvallen op minder nauwkeurige schattingen van de massa. Deze schattingen zijn gebaseerd op de helderheid en de kleur van sterrenstelsels die relatief makkelijk te meten zijn. Met kleur wordt de verhouding tussen de hoeveelheid licht bij twee verschillende golflengtes bedoeld. Figuur 2 laat een voorbeeld van een rood stelsel zien: er is meer licht bij lange golflengtes dan bij korte.

Voor sterren geldt dat de zwaarsten en heldersten het kortste leven. Ook zijn de zwaarste sterren het heetst en hebben daardoor een blauwe kleur. In de loop van het leven van een sterrenstelsel, verdwijnen de heldere, blauwe sterren, en blijven alleen de zwakke, rode sterren over. Door de kleur van een sterrenstelsel te meten, kan dus een schatting worden gemaakt van de soort sterren die het bevat. Dit geeft een schatting voor de leeftijd van het sterrenstelsel. De helderheid van het stelsel zegt

dan hoeveel sterren er zijn, en dus hoe zwaar het stelsel is: de zogenaamde “kleur” massa.

Voor het omrekenen van kleur naar leeftijd en massa zijn modellen gemaakt. Het probleem is dat de omrekeningsfactor verandert als je de eigenschappen van de sterren verandert. Sterker nog, als je modellen gemaakt door verschillende mensen met elkaar vergelijkt, blijken er verschillen te bestaan, zelfs als de eigenschappen van de sterren hetzelfde zijn. Door de verschillende uitkomsten te vergelijken met de “echte” massa’s die zijn gemeten aan de hand van de verbreding van spectraallijnen, kan de betrouwbaarheid van de indirecte methode getest worden. Eventuele problemen komen op deze manier aan het licht.

Dit is het onderwerp van de hoofdstukken 6 en 7. De tweede centrale vraag die in dit proefschrift behandeld wordt is de volgende: **Hoe nauwkeurig en betrouwbaar is de indirecte methode om de massa van een sterrenstelsel te bepalen aan de hand van zijn kleur?**

Dit Proefschrift

Hoofdstuk 2 In dit hoofstuk beschrijven we waarnemingen van 4 sterrenstelsels in één van de meest veraf gelegen bekende clusters (afstand ca. 8.5 miljard lichtjaar). Met de *Very Large Telescope* (VLT) in de Atacama woestijn Chili hebben we de beste spectra ooit gemaakt van zulke veraf gelegen stelsels. Een voorbeeld is te zien in Figuur 2. De “sluitertijd” van deze waarnemingen met de VLT, de beste telescoop ter wereld voor dit soort werk, was 24 uur. Met beelden van de *Hubble Space Telescope* (HST) hebben we de grootte en de helderheid van de stelsels gemeten. Deze sterrenstelsels behoren tot de meest massieve stelsels in het heelal: ze zijn wel 1000 miljard maal zo zwaar als de Zon (zo’n stelsel bevat dus ruwweg 1000 miljard sterren).

Door deze stelsels te vergelijken met nabije stelsels met dezelfde massa, hebben we bepaald dat dit soort stelsels 8.5 miljard jaar geleden circa 2.5 maal helderder waren dan ze nu zijn. Deze evolutie in lichtkracht impliceert dat de sterren in dit type stelsel momenteel 11.5 miljard oud zijn, en dus al 2 miljard jaar na de Big Bang zijn ontstaan. De resultaten in dit hoofdstuk zijn consistent met eerder uitgevoerd werk aan clusterstelsels op lagere roodverschuiving, of met spectra van mindere kwaliteit.

Hoofstukken 3 en 4 In deze twee hoofdstukken stappen we over naar veldstelsels. Met dezelfde technieken (spectra van de VLT; beelden van de HST) bepalen we de massa’s van enkele tientallen elliptische veldstelsels op een afstand van zo’n 8 miljard lichtjaar. Nooit eerder werd van een dergelijk groot aantal veldstelsels op deze afstand de massa gemeten. De kwaliteit van de data is ook nog eens bijzonder goed.

Dit stelt ons in staat om de evolutie van de veld- en clusterstelsels met elkaar te vergelijken. In antwoord op de eerste centrale vraag van dit proefschrift: **De sterren in massieve elliptische veld- en clusterstelsels vertonen geen leeftijdsverschil.** Dit is dus in tegenspraak met de theorie die voorspelt dat er wel een verschil is. Ook de sterren in zware veldstelsels waren 8 miljard jaar geleden al een paar miljard jaar oud.

Andere projecten die poogden een verschil te vinden tussen veld- en clusterstelsels hebben steeds tegenstrijdige resultaten opgeleverd. We verklaren deze resultaten

door verschillen in methoden, te kleine aantallen sterrenstelsels, te magere kwaliteit van de data, en te kleine afstand van de stelsels.

We vinden dus geen verschil tussen vergelijkbare sterrenstelsels in verschillende omgevingen. Aan de andere kant vinden we wel een leeftijdsverschil tussen sterrenstelsels met een grote en een kleine massa: zware sterrenstelsels lijken ouder te zijn dan lichte sterrenstelsels. Een complicatie in de interpretatie van deze ontdekking is dat oude, weinig massieve sterrenstelsels niet erg helder zijn. Daarom kan er geen spectrum worden gemeten dat goed genoeg is voor het bepalen van de massa. Echter, zelfs als we dit zogenaamde selectie effect meenemen in de analyse, dan vinden we nog steeds een leeftijdsverschil tussen zware en lichte stelsels. Hoe groot dit verschil is, kunnen we met deze resultaten niet bepalen.

Hoofdstuk 5 In dit hoofdstuk bestuderen we de kleuren van elliptische veldstelsels op een afstand van 8 miljard lichtjaar. Omdat stelsels met oude sterren een rodere kleur hebben dan stelsels met jonge sterren, zou het leeftijdsverschil tussen zware en lichte sterrenstelsels (ontdekt in Hoofdstuk 4) ook tot uiting moeten komen in hun kleuren. Bovendien zijn kleuren veel gemakkelijker te meten dan massa's.

Uit de kleuren van 90 elliptische stelsels met afstanden tot 8 miljard lichtjaar leiden we af dat de kleuren van heldere en zwakke stelsels nauwelijks verschillen. Hieruit concluderen we dat het in Hoofdstuk 4 beschreven leeftijdsverschil tussen zware en lichte stelsels inderdaad in eerste instantie veroorzaakt wordt door het eveneens in Hoofdstuk 4 beschreven selectie effect.

Het mogelijke leeftijdsverschil tussen zware en lichte stelsels is vermoedelijk erg klein. De enige methode om de precieze grootte van dit verschil te achterhalen, is het direct meten van massa's van lichte stelsels. Dit vereist waarnemingen die op het moment niet uitvoerbaar zijn.

Hoofdstuk 6 In dit hoofdstuk worden infrarode waarnemingen geanalyseerd van de in Hoofdstuk 4 beschreven objecten. Deze waarnemingen zijn gedaan met de nieuwe *Spitzer Space Telescope* (SST). Met deze data meten we de evolutie van de infrarode lichtkracht van elliptische sterrenstelsels gedurende de afgelopen 8 miljard jaar. Deze vergelijken we met de evolutie bij visuele golflengtes (zie de Hoofdstukken 3 and 4).

De evolutie van de lichtkracht in het infrarood is 30% langzamer dan bij visuele golflengtes. Dit klopt niet met de meeste modellen: deze voorspellen dat de lichtkracht evolutie in het infrarood wel tweemaal zo langzaam is dan bij visuele golflengtes. Met andere woorden, de kleur (ofwel, de verhouding van de hoeveelheden licht gemeten bij visuele en infrarode golflengtes) van elliptische sterrenstelsels evolueert anders dan verwacht. Dit heeft consequenties voor de interpretatie van infrarode waarnemingen die in Hoofdstuk 7 aan bod zullen komen.

Hoofdstuk 7 In dit hoofdstuk verzamelen we waarnemingen van de helderheid van de in Hoofdstuk 4 beschreven sterrenstelsels bij 10 verschillende golflengtes. Deze lopen uiteen van het ultra-violet, via visuele golflengtes tot het infrarood. Deze waarnemingen zijn gedaan met drie verschillende telescopen: HST, VLT en SST.

We vergelijken de waargenomen kleuren met modellen voor de evolutie van kleur en lichtkracht. Dit levert een bepaling van de leeftijd en de massa van de stelsels op.

We hebben dan twee verschillende massa bepalingen: de “kleur” massa en de “echte” massa uit Hoofdstuk 4. Door deze met elkaar te vergelijken, krijgen we een indruk van de betrouwbaarheid van de “kleur” massa en de toepasbaarheid van de modellen.

We vinden dat voor het meest gangbare model de twee verschillende massa bepalingen sterk uiteen lopen: de “kleur” massa van de sterrenstelsels is wel driemaal groter dan de “echte” massa. Dit is het gevolg van het probleem dat in Hoofdstuk 6 al werd geconstateerd: de kleur evolutie is anders dan de modellen voorspellen. De leeftijd en de massa van de sterren in een stelsel worden dus verkeerd bepaald.

Als de infrarode waarnemingen worden weggelaten bij de bepaling van de “kleur” massa, blijkt dat de “kleur” massa wel klopt met de “echte” massa. Dit toont aan dat de fout in de modellen in het infrarood zit, en dat je beter visuele waarnemingen kunt gebruiken.

Het antwoord op de tweede vraag centrale vraag gesteld in dit proefschrift is: **de “kleur” massa van sterrenstelsels zoals bepaald met infrarode waarnemingen is onbetrouwbaar doordat de modellen voor de evolutie van kleur en lichtkracht niet kloppen. De visuele kleuren van een sterrenstelsel geven een betere indicatie van de massa.**

Met de SST kun je gemakkelijk verre sterrenstelsels waarnemen. De hoop was dat de gemeten lichtkracht in het infrarood de massa van een stelsel zou geven, en dat de moeizame meting van “echte” massa’s, het onderwerp van dit proefschrift, overbodig zou worden. De resultaten van de Hoofdstukken 6 en 7 tonen aan dat mensen die “echte” massa’s kunnen meten, onmisbaar zijn.

Curriculum Vitae

Van 1996 tot en met 2001 studeerde ik sterrenkunde aan de Universiteit Leiden. Tijdens mijn eerste onderzoeksproject werkte ik samen met Peter Katgert aan dynamische modellen van clusters van sterrenstelsels om te bepalen wat de invloed is van radiële bewegingen van sterrenstelsels op massa-bepalingen van clusters. Mijn tweede onderzoeksproject deed ik onder begeleiding van Marijn Franx. In het kader van het *FIRES* project, wat diepe waarnemingen in het infrarood omvat, heb ik simulaties van deze waarnemingen gedaan die duidelijk moesten maken hoe zwak de zwakste sterrenstelsels zijn die nog detecteerbaar zijn, hoeveel licht er wordt gemist door achtergrondruis, en hoe dit afhangt van het soort sterrenstelsel.

In September 2001 studeerde ik af, en begon ik met mijn promotie onderzoek bij Marijn Franx, waarvan dit proefschrift het resultaat is. Tussen september 2002 en oktober 2003 ben ik viermaal naar ESO's *Very Large Telescope* in Chili gereisd, om spectroscopische waarnemingen te doen van veraf gelegen sterrenstelsels. Daarnaast heb ik aan conferenties in Leiden, Dalfsen, Vlieland, Durham (UK), Tegernsee (D) en Baltimore (USA) deelgenomen en presentaties gegeven in Leiden (Sterrewacht Science Day), Dalfsen en Vlieland (Nederlandse Astronomen Conferentie), Pasadena (Caltech and Carnegie Observatories), Santa Cruz (UCSC) en Baltimore (STScI en Johns Hopkins University).

Op de Sterrewacht was ik werkgroep assistent bij Pierre van Baal (Speciale Relativiteitstheorie) en Frank Israël (De Melkweg). Ik was lid van de Instituutsraad en de Commissie Publiekscontact, waarvoor ik regelmatig radio, televisie en kranten interviews gegeven heb.

Vanaf november 2005 zal ik mijn sterrenkundig onderzoek voortzetten als *Assistent Research Scientist* aan de Johns Hopkins University in Baltimore, Maryland, USA.

Arjen van der Wel
Geboren op 12 september 1978, te Benthuizen

Nawoord

De Sterrewacht is gedurende het afgelopen decennium steeds meer een tweede thuis voor mij geworden; de laatste maanden het eerste. Het is tijd om te vertrekken. Zonder het secretariaat en de computergroep was mijn verblijf hier uiteraard niet mogelijk geweest.

Dit dankwoord zou ik vooral willen besteden aan iedereen die in mijn sterrenkunde-leven een belangrijke rol speelt en dus betrokken is bij het tot stand komen van dit proefschrift: Lottie en Sirach, m'n eerste echte vrienden; Jean-Paul en Rogier, dank voor mijn muzikale opvoeding; Glenn en Roderik, jaar- en lotgenoten, hopelijk blijven we elkaar tegenkomen; Elise, als ik geen zin had om te werken, was jij de reden om toch te gaan; Inti, als kamergenoten nou mee konden verhuizen...; Ivo, Mariska, Ned, Stijn, dank voor de motivatie en belangstelling als groepsgenoten; Andrew, je bent nog niet van me af!; Jeanne en Frans, dank voor de hoognodige cafeïne; Bram, Leonie, Mariska, dank voor de gezelligheid tijdens de vele lunches.

Ik wil de volgende mensen van harte bedanken voor hun bijdragen aan het ontwerp van de omslag: Alex te Pas en mevr. H. te Pas - Snijders voor het verzorgen van de foto's van de weegschaal; Maaike Damen voor het ter beschikking stellen van materiaal van NGC 4552; Inti Pelupessy voor fotomateriaal voor de achterzijde; en hem en Ned Taylor voor tips voor het werken met *GIMP*. Andrew, Inti, Lottie, Paul, Thijs: dank voor het lezen van Hoofdstuk 1 en de Samenvatting.

Ik wil mijn lieve ouders en zusje bedanken voor hun geduld en de acceptatie van mijn soms egocentrische gedrag. Tot slot: Anke, Carolien, Maaike, Marc, Sabine, Thijs; zonder jullie had het voor mij niet gehoeven.